INVESTIGATIONS ON THE DIRECT CONVERSION OF NUCLEAR FISSION ENERGY TO ELECTRICAL ENERGY IN A PLASMA DIODE

ANNUAL REPORT

FOR

NONR - 3109(00)

OCTOBER 31, 1962

GENERAL MOTORS RESEARCH LABORATORIES

WARREN, MICHIGAN

OFFICE OF NAVAL RESEARCH

Contract Nonr-3109(00)

Investigations on the Direct Conversion of Nuclear Fission Energy to Electrical Energy in a Plasma Diode

Frank E. Jamerson
Editor

Contributors
Robert J. Donohue
Fay E. Gifford
Robert F. Hill
Frank E. Jamerson
Charles B. Leffert
Richard F. Majkowski

Report for Period February 1, 1962 to October 31, 1962

General Motors Research Laboratories
Warren, Michigan

TABLE OF CONTENTS

		Page
Abstract		i
Introduction		1
Objectives		1
Summary of Results		2
Conclusions		4
Future Plans		4
References		5
Acknowledgments		5
Section		
A	Inpile Ion Chamber Experiment - Theory and Tube Design, F. E. Jamerson, C. B. Leffert, and R. F. Hill	19 pages
B	Pulsed Noble Gas Plasma Diode Experiments	
	(1) A System for the Study of Pulsed Discharge Ionization of Noble Gases, C. B. Leffert	29 pages
	(2) Ion Decay Rate in the Pulsed Discharge Ionization of Xenon, C. B. Leffert and J. F. Walkup	20 pages
C	Electron Mobility in Gases, W. P. Allis and F. E. Jamerson	19 pages
D	Spectroscopic Measurements in a Cesium Low Voltage Arc Converter, R. J. Donohue and R. F. Majkowski	14 pages
E	Uranium Carbide-Rhenium Cermet Emitter R. F. Hill and F. E. Gifford	6 pages
Publications		1 page
Distribution		5 pages

ABSTRACT

Results of experimental and theoretical investigations are presented on the use of a nuclear generated plasma in a noble gas plasma diode thermionic converter. Related programs of emitter materials development and plasma measurements are described. These are presented in the following individual reports.

A. Inpile Ion Chamber Experiment - Theory and Tube Design

B. Pulsed Noble Gas Plasma Diode Experiments

C. Electron Mobility in Gases

D. Spectroscopic Measurements in a Cesium Low Voltage Arc Converter

E. Uranium Carbide-Rhenium Cermet Emitter

Investigations on the Direct Conversion of Nuclear Fission Energy to Electrical Energy in a Plasma Diode

Introduction

This report for the period February 1, 1962 to October 31, 1962 covers the research programs related to the conversion of nuclear heat to electricity in a noble gas filled thermionic converter. It consists of individual reports presented on various phases of the problem. The following sections on Objectives, Summary, Conclusions and Future Plans give the substance of the main body of the report in condensed form.

Previous inpile experiments on a plasma generated by fission fragment penetration of a noble gas[1, 2] were performed using a diode arrangement with a hot emitter. Data were obtained for xenon at 8 Torr and for a Penning mixture of neon:argon (1000:1) at 20 Torr. From saturated voltage-current characteristics an ion number density of 1.5×10^9 cm^{-3} was observed for xenon and 1.3×10^{10} cm^{-3} for the Penning mixture. A value of 9×10^{10} cm^{-3} was observed for a particular 'ion trapping' configuration[2] for the Penning mixture. These number densities were observed for a neutron flux of about 5×10^{12} n sec^{-1} cm^{-2} incident on the enriched uranium fission fragment source.

This report is concerned with studies related to a nuclear generated plasma and in particular to the problem of extending measurements over a wider range of gas pressure and number density. Progress in other areas such as plasma spectroscopy and electron emitters related to program objectives are also presented.

Objectives

The primary objective for investigating a nuclear generated plasma in a noble gas is to determine the feasibility of using a plasma of this type in a thermionic converter employing nuclear heating of the emitter. A noble gas filled converter would have an advantage from the point of view of eliminating the corrosion problems associated with an initially filled cesium converter.

The objectives of the research reported under this contract period are the following:

1. Inpile experiments on noble gas filled diodes with uranium bearing emitters are to be continued to determine the maximum attainable plasma density in a given neutron flux using fission fragment ionization of the gas.

2. Experiments are to continue on noble gas filled diodes using electrically heated emitters wherein a plasma will be generated by auxiliary discharge means both pulsed and dc. Measurements as a function of pressure and electrode spacing will be made to determine conditions for achieving high plasma densities.

3. Techniques previously developed for spectroscopic investigation of cesium plasmas are to be continued on diodes that operate as thermionic converters.

4. Theoretical studies of the plasma physics of thermionic conversion is to continue.

5. An analysis is to be made of the noble gas plasma diode converter using fission fragment ionization from the standpoint of performance that would be predicted on the basis of the experimental data obtained.

Summary of Results

A brief summary of results is given for the individual reports contained herein:

A. Inpile Ion Chamber Experiment - Theory and Tube Design

Plasma density is sensitive to gas pressure since ion loss mechanisms are density dependent. Thus it is desirable to extend plasma density measurements over a wide pressure range. This can be done by using a tube with cold electrodes in which ion current only is measured. An analysis has been developed for the various plasmas modes in an ion chamber of this type. A measurement of ion density as well as source rate appears feasible from the analysis. Several development problems have been solved in the fabrication of tubes for inpile experiments. Four tubes have been completed and filled to 21, 61 and 220 Torr of neon:argon (1000:1) and one tube was processed as a vacuum tube. The inpile operation of these tubes has been delayed pending an AEC approval of an amendment to the University of Michigan operating license.

B. Pulsed Noble Gas Plasma Diode Experiments

Electrically generated plasmas are used as a diagnostic tool for investigating the controlling ion loss mechanism under given gas conditions. Studies of a pulsed discharge plasma are to be related to inpile ion chamber measurements. This might allow more detailed studies of plasma parameters to be made in the laboratory on a variable pressure tube rather than inpile at fixed tube pressure. These data are also of interest in correlating with sheath theory developed for the noble gas plasma diode.[3] Two variable pressure diodes have been fabricated and circuits developed for these pulsed studies.

Pulsed discharge data have been taken in xenon at 0.25, 2, 20 and 100 Torr. At the high pressures, ion number densities of 10^{11} to 10^{12} cm^{-3} are observed and the rate of plasma decay is indicated to be controlled by recombination initially, and diffusion at the end of the decay period. The data in the recombination regime were correlated with the dissociative recombination coefficient for xenon. Plasma lifetime increases up to 20 Torr and decreases at 100 Torr indicating that an optimum plasma density exists between these two pressure limits.

C. Electron Mobility in Gases

In the investigation of a mobility limited space charge theory, it became evident that literature does not contain all the electron mobility data of interest for the noble gases. A method has been developed for converting collision probability data, which are available in certain cases, into mobility.

The analysis is given for converting collision probability versus voltage data to a drift velocity versus E/p_o. Computations for $E/p_o > 10^{-2}$ volt cm^{-1} $Torr^{-1}$ show good agreement with recent data of drift velocuty for helium and neon whereas poor agreement is exhibited for argon, krypton and xenon. For small values of E/p_o the lack of collision probability data precludes making direct comparisons to drift velocity data.

D. Spectroscopic Measurements in a Cesium Low Voltage Arc Converter

The cesium plasma spectroscopy techniques previously developed have been employed in plasma studies of a cesium low voltage arc converter. The unique feature of the low voltage arc converter is that emitter temperatures below that normally required for sustained cesium ion generation by surface ionization can be used. Impact ionization due to electron acceleration at a positive emitter sheath is possible. Electron temperature data taken in a low voltage arc converter substantiate this since an electron temperature of 2700°K has been observed for an emitter temperature of 1400°K for a diode operated as a converter. This high electron temperature is also measured in the accelerating voltage regime indicating the relative constancy of the emitter sheath potential once the arc is initiated.

E. Uranium Carbide-Rhenium Cermet Emitter

Data have been previously published[1,4] on the metallurgical development of a uranium carbide-rhenium emitter. A summary of this work is given here. More recent thermionic emission data are given for this emitter under rather low 'high field' conditions. Using an extrapolation technique as employed previously with UC-Nb,[1] the saturated emission current is in the range of UC-Nb emission. Current densities of order amps/cm^2 from this emitter require temperatures greater than 2000°K.

Other Results

An analysis has been made of the electronic efficiency of a noble gas plasma diode converter. The electronic efficiency includes all terms except thermal losses. The calculations were made using the computer developed voltage current characteristic for the noble gas diode sheath theory. This work will be extended and reported when additional noble gas plasma data become available for inclusion in the calculations.

An auxiliary dc discharge tube with a grid collector was operated in xenon at variable pressure. The objective was to study the voltage current characteristic of a Gabor mode triode to correlate with sheath theory results. The results from this tube were inconclusive and are not reported here.

Conclusions

A new method has been developed for obtaining inpile data on ion density caused by fission fragment ionization of a noble gas. This method uses tubes of an ion chamber type design in which electrode surfaces are cold. Analysis shows that ion density and ion generation rate can be measured from this type of tube. Measurements are to be made as a function of pressure using a series of identical tubes filled to various gas pressures. This method should provide the data necessary to determine a) which gas (xenon or neon:argon) and gas pressure provides the highest ion density for a clean tube condition and b) whether diffusion or volume recombination is the dominant ion loss mechanism.

Observations on the decay characteristic of a xenon plasma created by pulse discharge techniques indicate a maximum ion density in the range 20 to 100 Torr. This is a pressure region considerably higher than used in previous inpile tubes. The techniques for obtaining pulsed data have been developed and are being used to accumulate additional data for comparison to inpile studies and for sheath theory analysis.

Future Plans

Experiments will be continued inpile to measure ion number density generated by fission fragments as a function of gas pressure and neutron flux. Diodes (ion chambers) with uranium coated electrodes and negligible thermionic emission (operating at low temperature) and planar guard ring geometry will be used. Several identical ion chambers will be filled to varying gas pressures of neon:argon (1000:1) and xenon.

Studies will be continued on the pulsed discharge of noble gases in order to guide and complement the inpile noble gas fission fragment ionization studies. From the time rate of decay of the ion density, the controlling decay mechanism (diffusion or volume recombination) will be determined as a function of (1) type of gas, (2) gas pressure, (3) diode spacing, and (4) ion number density.

An anomalous low voltage arc discovered[1] in the operation of a noble gas diode inpile with a uranium bearing emitter and barium coated collector will be studied by operating a noble gas diode inpile with a uranium bearing emitter and a bare collector in order to determine whether the arc characteristic observed was due to the presence of barium vapor from the collector or fission product vapor from the emitter.

Theoretical studies of the plasma physics of thermionic conversion in noble gas diodes will be continued.

References

1. Investigations on the Direct Conversion of Nuclear Fission Energy to Electrical Energy in a Plasma Diode, 1960 Annual Report ASTIA AD No. 250 673; ibid, R. H. Abrams, Jr., R. J. Donohue, R. F. Hill, F. E. Jamerson (Editor), C. B. Leffert, R. Silver, 1961 Annual Report ASTIA AD No. 273 067

2. F. E. Jamerson, R. H. Abrams, Jr., C. B. Leffert, R. Silver, "Nuclear Generated Plasmas in Noble Gas Thermionic Converters", to be published in Journal of Advanced Energy Conversion.

3. C. B. Leffert, "A Plasma-Sheath Theory for Noble Gas Thermionic Converters", to be published in Journal of Advanced Energy Conversion.

4. R. F. Hill, "The Development of Emitter Materials for Use in the Noble Gas Plasma Diode", to be published in Journal of Advanced Energy Conversion.

Acknowledgments

Professor W. P. Allis of Massachusetts Institute of Technology, consultant, has made significant contributions to plasma studies.

Professor H. Griem of University of Maryland has consulted on plasma spectroscopy analysis.

The contributions of Mr. R. H. Abrams, Jr. to the ion chamber experiment prior to his taking educational leave are gratefully acknowledged.

Mr. J. F. Walkup, a summer employee, performed the measurements on the pulsed discharge xenon plasma.

Technical assistance in the design and fabrication of experimental systems has been given by Messrs. R. Aikin, A. Dolenga, R. Dusman, R. Knoll, J. Palazzolo, and C. Williams.

SECTION A

INPILE ION CHAMBER EXPERIMENT - THEORY AND TUBE DESIGN

F. E. Jamerson, C. B. Leffert and R. F. Hill

ABSTRACT

A theory is presented for the measurement of ion density and ion generation rate from a cold fissioning source in a noble gas. The design and fabrication details of a tube to be used for inpile experiments is given.

CONTENTS

		Page No.
	ABSTRACT	1
I	INTRODUCTION	2
II	THEORY	2
	A. High Plasma Density	2
	B. Intermediate Plasma Density	6
	C. Space Charge Limited Plasma Density	7
	D. Pressure Dependence of Ion Current	8
	E. Ion Generation Rate	9
III	TUBE DESIGN AND FABRICATION	10
	A. Electrodes	10
	1. Geometry	10
	2. Materials	11
	3. Uranium Bonding Technique	11
	4. Uranium Brazing Procedure	14
	5. Temperature Calculations	14
	B. Tube Details	15
	C. Fabrication	17
IV	REFERENCES	17

I INTRODUCTION

The inpile experiments on the ionization of a noble gas by fission fragments have previously used hot emitters in diodes operated at a fixed gas pressure. Plasma generation and subsequent increased electron carrying capability of the diode has been demonstrated.[1] Ion number density has been inferred from the forward saturated current and from the reverse saturated current when collector electron emission is sufficiently low. The ion density is related to electron current density J by $J \sim n/10^{12}$ where J is in amp cm^{-2} and n in cm^{-3}. An ion density measurement thus determines what electron current carrying capability is available in a gas ionized by fission fragments. An experiment has been designed to measure ion density and ion generation rate. The measurement of the plasma density under minimum contamination of the gas and as a function of gas pressure and type was desired. This experiment uses an ion chamber type tube in which the uranium coated electrodes are cold, thus eliminating thermionic electron contribution to the current.

The spatial potential distribution between two cold electrodes immersed in a plasma is a function of plasma density. Analyses are presented for several plasma density modes. For the expected predominant mode, that of high plasma density, a voltage current characteristic is derived along with a method of obtaining electron temperature. The ion source rate can also be determined by operating the ion chamber in a low ion density mode.

A number of considerations in the design and fabrication of the tube for making these measurements is given. Several development problems had to be solved and one of the most important, the uranium foil coating problem, is discussed in detail.

II THEORY

The details of the ionization process by fission fragment penetration of a noble gas has been discussed previously.[1] It is assumed that the gas is ionized uniformly between two cold electrodes (fragment range is greater than interelectrode gap). The voltage current characteristic is dependent on the plasma density and the maximum saturated ion current is a measure of plasma density. The analysis for the high plasma density condition is discussed first. The intermediate and low plasma density cases are also discussed and the pressure dependence of the ion current is shown to give information on the predominant ion loss mechanism.

A. High Plasma Density

The analysis and notation will closely follow that of a previously developed plasma sheath theory.[2] The following assumptions are made:

(1) The electrodes are sufficiently cold so that thermionic emission is negligible.
(2) The interelectrode plasma is neutral and spatially uniform.
(3) The plasma resistivity is negligible.
(4) The work functions of the electrode surfaces are the same.
(5) A uniform ion temperature ($T_2^+ = T_1^+ = T^+$) and a uniform electron temperature ($T_2^- = T_1^- = T^-$) is assumed in the interelectrode plasma although T^+ may not equal T^- (T is used in units of volts).
(6) Parallel plane geometry is assumed with equal electrode areas.
(7) The ion source strength and electron source strength are equal.

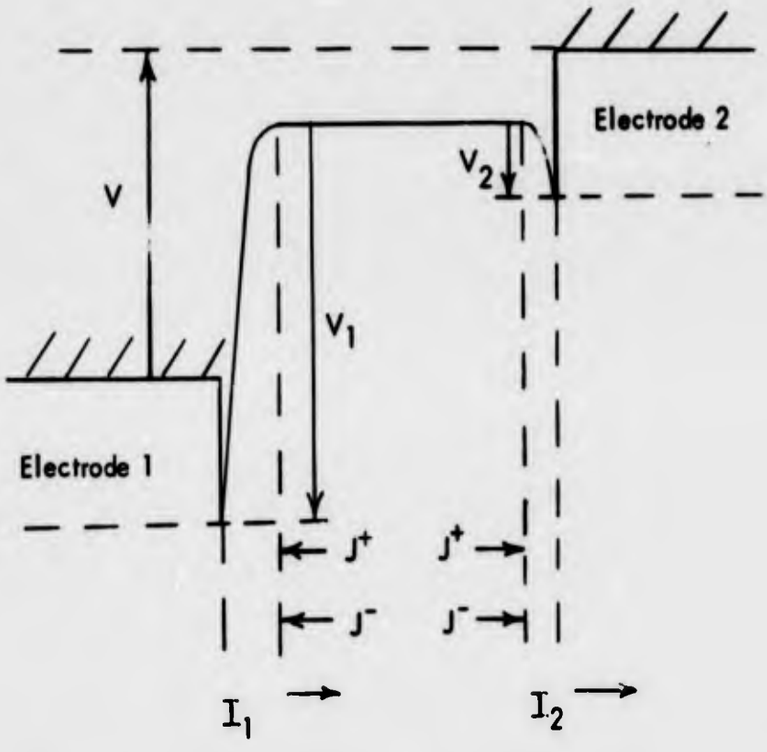

Figure 1 - Motive diagram for high plasma density.

The motive diagram for operation with negligible thermionic emission is presented in Figure 1. Random ion and electron current densities (J^+ and J^-) incident on the sheaths are assumed to be the same at both electrodes. It can be shown (since $J^- >> J^+$) that the net currents through the sheaths are equal ($I_1 = I_2$) only for the case where plasma potential is higher than either electrode potential ($V_1 < 0$, $V_2 < 0$).

The basic equations are as follows:

Voltage Balance,

$$V = V_2 - V_1 ; \tag{1}$$

Net Current Balance using assumption (6)

$$I = I_1 = I_2 = J^- A_1 - J^- A_1 e^{V_1/T^-} = J^- A_2 e^{V_2/T^-} - J^+ A_2 ; \tag{2}$$

Ion Balance,

$$S = (J^+ A_1 + J^+ A_2)\, U^{-1} q^{-1} + \alpha N^2 + \frac{D_a}{\Lambda^2} N ; \tag{3}$$

Electron Balance,

$$S = (J^- A_1 e^{V_1/T^-} + J^- A_2 e^{V_2/T^-})\, U^{-1} q^{-1} + \alpha N^2 + \frac{D_a}{\Lambda^2} N . \tag{4}$$

I is measured positive for electron flow from A_1 to A_2 and the symbols are defined as follows:

J^+ and J^- = ion and electron random current density (amps cm^{-2})

I_1 and I_2 = net current at electrodes 1 and 2 (amps)

V_1 and V_2 = sheath potentials at electrodes 1 and 2 (volts)

A_1 and A_2 = electrode areas (cm^2)

S = ion or electron source strength (cm^{-3} sec^{-1})

U = interelectrode volume (cm^{-3})

d = interelectrode spacing (cm)

N = ion or electron density (cm^{-3})

D_a = ambipolar diffusion coefficient (cm^2 sec^{-1})

Λ = diffusion length (cm)

α = recombination coefficient (cm^3 sec^{-1})

q = electronic charge

Combining equations (1) and (2) and solving for net current gives:

$$I = J^+ A_2 \left[\frac{1 - e^{-V/T^-}}{(A_2/A_1) + e^{-V/T^-}} \right] \tag{5}$$

In the limit as $V \rightarrow \infty$, I approaches a saturated current level, I_s,

$$I \rightarrow I_s = J^+ A_1 \tag{6}$$

which is equal to the random ion current into electrode 1. Thus equation (5) can be written in terms of this measurable saturated current, I_s

$$I = I_s \left[\frac{1 - e^{-V/T^-}}{1 + A_1/A_2 \, e^{-V/T^-}} \right] \tag{7}$$

In terms of saturated current equations (3) and (4) reduce to:

$$I_s = J^+ A = \left(\frac{A_1}{A_1 + A_2} \right) \left[SqU - qU\alpha N^2 - \frac{D_a N q U}{\Lambda^2} \right] \tag{8}$$

which shows that in the limit as $V \longrightarrow \infty$ the saturated current, I_s, measures the difference between the ion source and loss terms. For parallel plane geometry ($A_2 = A_1$) and one half of the ions flow to each electrode.

Since $J^+ = \frac{N^+ q \bar{v}+}{4}$ where N^+ is ion density and average ion velocity $\bar{v}+ = 100\sqrt{\frac{8qT^+}{\pi M}}$

equation (6) can be rewritten:

$$N^+ = \left[\frac{(2\pi M)^{1/2}}{100\, q^{3/2}}\right] \frac{I_s}{A_1 \sqrt{T^+}} \tag{9}$$

This expression provides a means of computing the ion number density from the measured saturated current, the ion collector area and the ion temperature. An estimate of the ion temperature, T^+, is needed which for the gas pressures considered here can be taken the same as gas temperature which will be close to electrode temperature and can be monitored.

A measure of the electron temperature, T^-, can be obtained from the theory and the experimental V-I curve. For equal electrode areas equation (7) becomes

$$I = I_s \tanh\left(\frac{V}{2T^-}\right) \tag{10}$$

Differentiating with respect to V yields the electron temperature, T^-. Thus from the slope of the V-I curve at V = 0.

$$T^- = \frac{I_s}{2\left.\frac{dI}{dV}\right|_{V=0}} \tag{11}$$

An estimate of sheath potential V_2 can be made when drawing saturated current from (2) by taking $I = J^+ A_1$. For equal electrode areas this results in:

$$V_2 = -T^- \ln\left(\frac{1}{2}\sqrt{\frac{M}{m}\frac{T^-}{T^+}}\right) \tag{12}$$

For $T^- = T^+ = 0.1$ ev and neon this yields -0.43 volts for V_2. Thus as V is made more positive, V_2 remains fixed and V_1 follows the increase in V.

It is expected that secondary ionization, by electron impact, would not be important until some potential beyond the first ionization potential of the gas would be reached. The voltage-current characteristic is expected to follow the shape shown in Figure 2 with equal area electrodes.

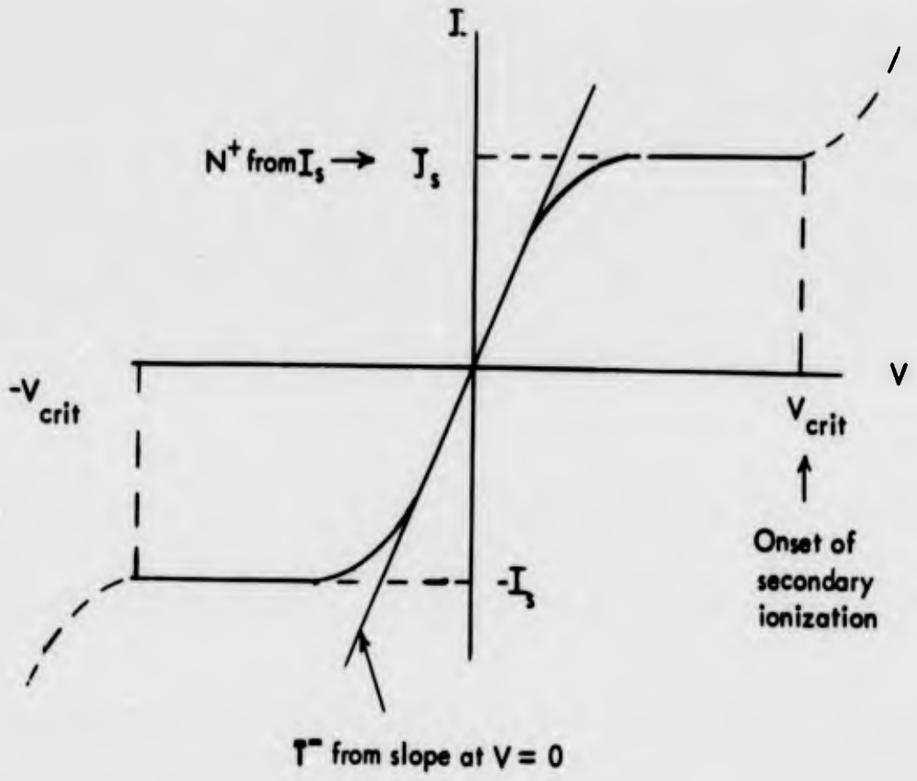

Figure 2 - Expected shape of V-I curve.

B. Intermediate Plasma Density

Figure 3 depicts a potential diagram for the case of intermediate plasma density where the sheath thickness is not small compared to the interelectrode spacing d.

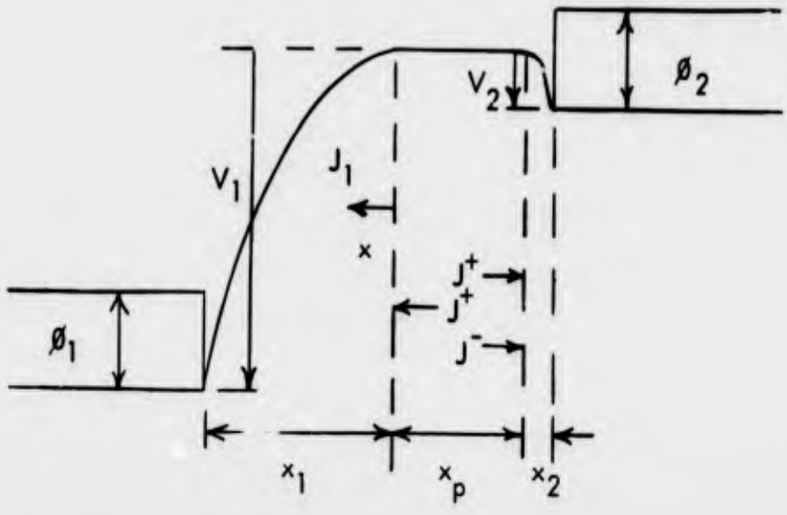

Figure 3 - Intermediate plasma density motive diagram.

In the sheath at electrode 1, the potential is derived using Poisson's equation. Since this sheath potential is retarding for electrons, the problem can be simplified by neglecting the electron number density in this equation.

$$\frac{dE}{dx} = \frac{q}{\epsilon_o} N^+ \tag{13}$$

The current in electrode 1 sheath is taken as ion current only and is given as a function of position x from the plasma-sheath boundary:

$$J_1 = J^+ + Sqx = N^+ q \mu^+ E \tag{14}$$

where μ = ion mobility ($cm^2\ sec^{-1}\ volt^{-1}$) and E = field ($volts\ cm^{-1}$). Combining (13) and (14) and integrating with the boundary condition of E = 0 at x = 0 and $J = J^+ + Sqx_1$ yields:

$$V_1 = \left(\frac{x_1}{2\beta}\right)^2 \sqrt{\frac{S}{\epsilon_o \mu^+}} \left[(1+2\beta)\sqrt{\beta(1+2\beta)} - \ln\left(\sqrt{1+\beta} + \sqrt{\beta}\right)\right] \tag{15}$$

where

$$\beta = \frac{Sqx_1}{2(J - Sqx_1)}$$

The voltage current characteristic makes use of $V = V_2 - V_1$ where V_2 is given by (12). To calculate a characteristic the quantities S and x_1 can be estimated and V_1 computed for a range of J. Parametric fitting to an experimental curve should yield source strength and sheath distance x_1.

When x_1 extends across the complete interelectrode space $\beta >> 1$ since $J = Sqx_1$ and (15) reduces to

$$V_1 = \frac{d^2}{2} \sqrt{\frac{Sq}{\epsilon_o \mu^+}} \tag{16}$$

C. Space Charge Limited Plasma Density

Figure 4 shows the potential diagram for the case where the field is not constant in the interelectrode gap and in particular goes to zero at electrode 2.

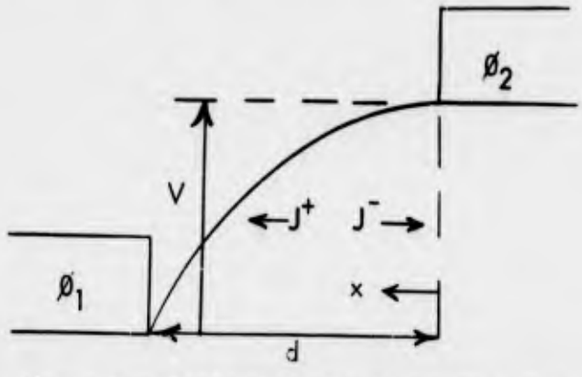

Figure 4 - Space charge limited motive diagram.

$$J^- = S q (d - x) = N^- q \mu^- E \tag{17}$$

$$J^+ = S q x = N^+ q \mu^+ E \tag{18}$$

$$\rho = (N^+ - N^-) q \tag{19}$$

Using (17), (18) and (19) with Poisson's equation $\frac{dE}{dx} = \rho/\epsilon_o$ yields:

$$V = \frac{d^2}{2} \sqrt{\frac{Sq}{\epsilon_o \mu^+}} \tag{20}$$

This agrees with (16) which was obtained in the limit of x_1 equal to d corresponding to the space charge problem of this section. From (18) in the limit J = Sqd so that (20) can be written:

$$J = 2 \epsilon_o \mu^+ \frac{V^2}{d^3} \tag{21}$$

D. Pressure Dependence of Ion Current

The previous analyses have given the results of the theoretical voltage current characteristics to be observed under given plasma density conditions. For the high plasma density case, additional information can be obtained from the pressure dependence of the saturated ion current.

For equal area electrodes, and since U/A = d then from (3):

$$S = \frac{2 J^+}{q d} + \alpha N^2 + \frac{D_a}{\Lambda^2} N \tag{22}$$

Since $J^+ = \frac{N q \bar{v}^+}{4} = a N$ where N = ion or electron density, including the pressure dependence of each of the terms in (22), it can be rewritten:

$$Sp = \frac{2 J^+}{q d} + J^+ \left(\frac{D_a}{p a \Lambda^2} \right) + J^{+2} \left(\frac{\alpha_2 + \alpha_3 p}{a^2} \right) \tag{23}$$

where the recombination coefficient is given as the two body (α_2) and three body (α_3) recombination terms.

At low pressure the terms linear in J^+ are controlling.

$$J^+ = \frac{S p^2}{2 p/d + D_a/a \Lambda^2} \tag{24}$$

at high pressure the J^{+2} term is controlling.

$$J^{+2} = \frac{\alpha^2 S p}{\alpha_2 + \alpha_3 p} \tag{25}$$

Thus the saturated ion current for the high plasma density regime will follow a pressure dependence similar to Figure 5 where loss by diffusion is controlling at low pressure and recombination is controlling at high pressure.

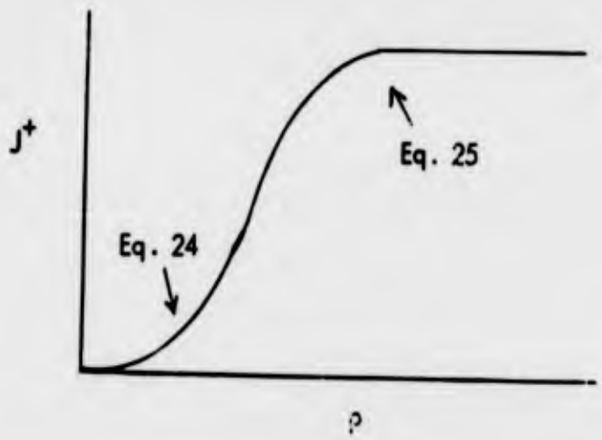

Figure 5 - Pressure dependence of saturated ion current.

E. Ion Generation Rate

An important quantity to be measured is the ion generation rate since it can be compared to earlier calculations of ion generation by fission fragments in noble gases.[1] This quantity can be deduced from experimental data taken at low number densities, i.e., low power level or low neutron flux on the fissioning source. In this case no sheaths are formed and all the ions are swept out by the field.

An estimate of expected currents can be made by using Poisson's equation and approximating $\nabla^2 V$ by $2V/d^2$ which gives the maximum number density that will be supported by a potential V.

$$N = \frac{2V}{d^2} \quad \frac{\epsilon_o}{q} \tag{26}$$

An ion chamber spacing of 3 mm is to be used and for 15 volts across the tube (below secondary ionization effects in argon) the computation using (26) gives $N = 1.8 \times 10^8$ ions cm^{-3}. A current density can be computed from $J^+ = Nq\mu^+N$ using $\mu^+ = 3.5$ cm^2 $volt^{-1}$ sec^{-1} (for A^+ in Ne) and $E = V/d$. For a pressure of 20 Torr ($\mu^+ = 3.5 \frac{760}{20}$) the current density is computed to be 2×10^{-7} amps cm^{-2}. Since collector area is 5 cm^2 this corresponds to a current of 1 μa.

The ion source rate is given by

$$S = \frac{2 J^+}{q d} \tag{27}$$

A J^+ of 2×10^{-7} corresponds to an ion generation rate of 4×10^{12} ions cm^{-3} sec^{-1} and an ion density in the order of 10^8 cm^{-3}. A density of order 10^{10} cm^{-3} has been measured at maximum neutron flux inpile so that from the above estimates the ion source rate may be measured at 10^{-2} of the maximum flux.

III TUBE DESIGN AND FABRICATION

The following criteria were set for the design of the tube for measuring ion density and ion generation rate.

1. Collector area should be large enough to give measurable ion currents.
2. Guard rings should be provided to eliminate the effect of fringing fields.
3. Uranium-235 should be applied to collector surfaces uniformly so as to produce equal and uniform work functions.
4. Uranium thickness and radiant heat transfer area should be adjusted to produce a maximum temperature below that required for negligible thermionic emission.
5. Thermocouples should be provided on the electrode surfaces.

A. Electrodes

1. Geometry

Collector area requirements were determined by available tube diameter and current measuring capability. A 2 inch diameter glass tube envelope was selected which provides space for a collector of 1 inch diameter with a guard ring of 1-1/2 inch diameter. For an ion density of 10^{10} cm^{-3} a current of 1.85×10^{-4} amps would be collected for this size electrode (area of 5 cm^2). This is considerably above the circuit leakage current of 10^{-8} amps* so the collector area of 5 cm^2 was considered adequate. The electrode gap of 3 mm is comparable to previous inpile and laboratory tubes to which subsequent inpile data will be compared.

The melting point of uranium is 1133°C and at 1300°C the vapor pressure is 10^{-6} mm Hg. The upper limit on the temperature as set by the thermionic emission is obtained from Richardson's equation

$$I = JA = A\ 120\ T^2 \exp(-\phi/T) \tag{28}$$

If the maximum allowable electron emission is set to 1×10^{-7} amp (10 times circuit leakage) and ϕ for uranium is taken to be 3 ev, then T_{max} = 1050°K = 777°C for A = 5 cm^2.

---

* As measured for a dc measuring circuit using dc meters, battery power supply and a shielded cabinet for circuit components.

2. Materials

To satisfy the criterion that the work function be uniform over the surface, the uranium should completely cover the inner electrode surfaces. To derive full benefit from the fission fragments the minimum thickness should be at least the range of the fission fragments in uranium which is 6.7×10^{-4} cm.

Zirconium was selected as the base material for the electrodes for the following reasons. Zirconium has a melting temperature of 1852°C which is well above the 1133°C melting temperature of uranium and thus should remain integral during the uranium bonding process. Also zirconium is machinable, has reasonable strength, and has a low neutron cross section.

The enriched uranium was available from Battelle Memorial Institute in the form of 3.8×10^{-3} cm thick foil. Attempts were made to reduce the foil thickness to 1×10^{-3} cm but after several passes through the rolling mill and successive anneals the foil was only reduced to 1.9×10^{-3} cm. It was decided at this point that the excess uranium could be removed easier and faster by an acid wash and polish than by continuing the rolling operation.

3. Uranium Bonding Technique

The initial bonding tests involved the melting of the uranium foil directly onto the zirconium electrodes. The results of this procedure were very unsatisfactory. During the melting process, the uranium foil would not melt uniformly across the surface of the electrode but rather would start melting at specific points. Once this took place the remaining uranium foil would melt and flow to the initial melting points thus causing the uranium to "bead up" at various points on the surface of the zirconium. This produced patchy areas on the surface of the electrodes.

Various other tests were also conducted which involved the addition of nickel and tantalum foils to the brazing process. Finally a process was developed whereby a relatively uniform layer of uranium was obtained on the surface of the electrodes. This process involved the formation of a nickel-uranium alloy that contained 19.5 a/o Ni bonded to a 1.27×10^{-2} cm tantalum foil. From the phase diagram of the nickel-uranium system [3] as shown in Figure 6 it can be seen that the 19.5 a/o Ni - 80.5 a/o U alloy has a melting point below that of pure uranium.

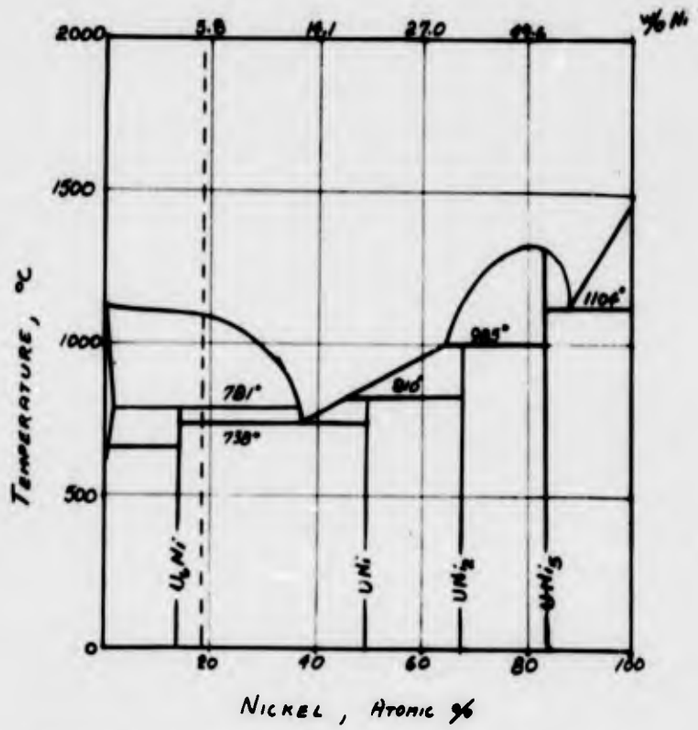

Figure 6 - Constitution diagram of the Ni-U system.

This alloy was obtained by melting together a 2.5×10^{-4} cm nickel foil with the 1.9×10^{-3} cm uranium foil onto the surface of a 1.27×10^{-2} cm tantalum foil. The tantalum foil was then joined to the zirconium electrode by means of a nickel foil braze. The phase diagram of the nickel-zirconium system[4] is shown in Figure 7.

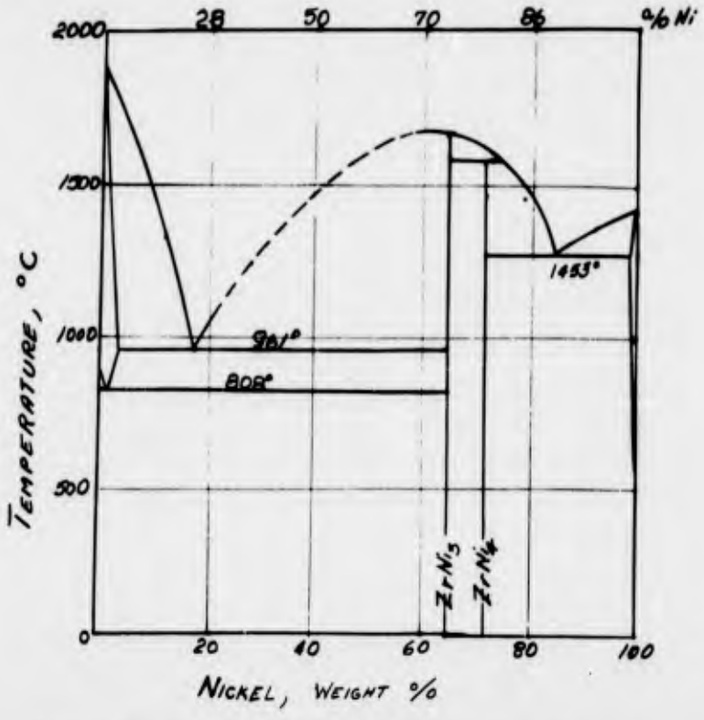

Figure 7 - Constitution diagram of the Ni-Zr system.

A photograph of a completed electrode is shown in Figure 8. A photomicrograph showing the uranium-tantalum-zirconium bonds is shown in Figure 9.

Figure 8 - Zirconium electrode with a 1.4×10^{-3} cm thick uranium surface.

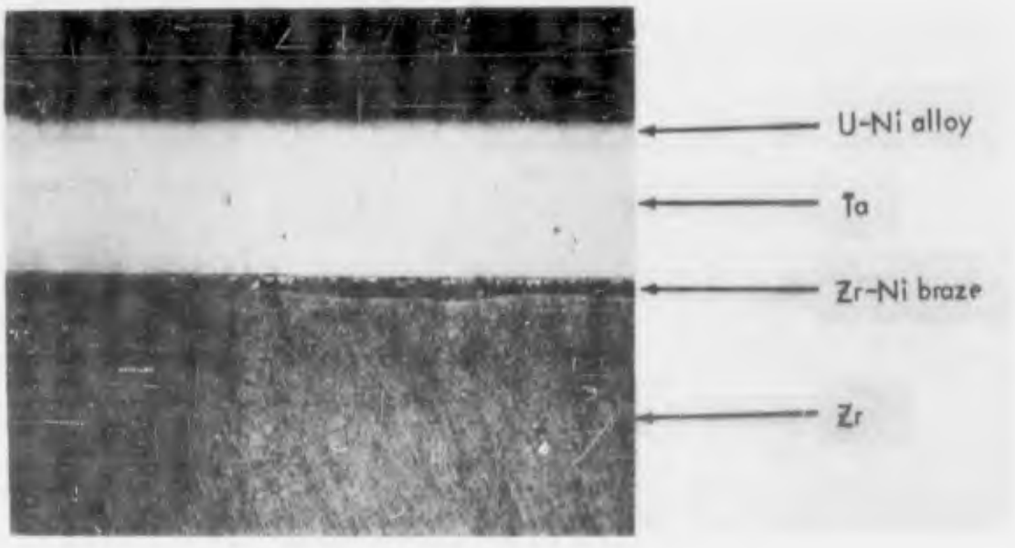

Figure 9 - Photomicrograph of the U-Ta-Zr braze. 150X

From the photomicrograph shown in Figure 9 it can be seen that the U-Ni alloy wetted the tantalum satisfactorily. Neither the uranium nor the nickel appeared to alloy with the tantalum. The reaction zone at the nickel-zirconium interface can also be seen. The uranium foil thickness after the acid wash was approximately 1.6×10^{-3} cm thick. Subsequent polishing after making the U-Ta-Zr braze is estimated to yield an equivalent uranium thickness of 1.4×10^{-3} cm.

4. Uranium Brazing Procedure

The brazing process was done in an 18 inch bell jar vacuum system. The heat was supplied by a 15 kw 450 kc frequency induction heater. The various steps in the brazing process were as follows:

1. The zirconium, nickel and tantalum components were cleaned in an ultra sonic cleaner through the following three solutions in the order given.
   a) trichloroethylene
   b) acetone
   c) methyl alcohol (2 changes)
   The zirconium components were then vacuum fired ($\sim 4 \times 10^{-5}$ Torr) at 1200°C for 30 minutes. The tantalum was vacuum fired ($\sim 4 \times 10^{-5}$ Torr) at 1500°C for 15 minutes. The uranium foil pieces were cleaned in dilute nitric acid (50 v/o HNO_3 - 50 v/o H_2O) followed by a water rinse and a methyl alcohol rinse in the ultrasonic cleaner. Since the uranium foil oxidizes very rapidly, it was cleaned just prior to using.

2. The tantalum, nickel and uranium foils were sandwiched together in that order and then spot welded together. This sandwich arrangement was then placed over a RF "pancake" coil and heated to approximately 1000°C under a vacuum. This caused the nickel and uranium to alloy and flow over the surface of the tantalum foil.

3. The tantalum foil, with the nickel-uranium surface exposed, was then spot welded to the zirconium electrode structure. A piece of 2.5×10^{-4} cm nickel foil was placed between the tantalum and zirconium pieces prior to the spot welding. This structure was then heated in the vacuum system to approximately 965°C. Under these conditions the nickel alloyed with the zirconium thus forming a braze between the tantalum and zirconium components.

This brazing process which involved the formation of nickel-uranium and nickel-zirconium alloys around 1.27×10^{-2} cm tantalum foil layer resulted in a satisfactory method for bonding the enriched uranium foils to the zirconium electrodes.

5. Temperature Calculations

Initial heat generation and loss calculations indicated that the foil thickness required to provide a temperature of 727°C was 9.4×10^{-4} cm. These calculations were made under the following assumptions:

1. Nuclear heat is lost only by radiation.
2. Assume heat radiating area = 2 x heat generation area.
3. Emissivity of electrodes is 0.2 radiating to a black body.
4. Neutron absorption of tantalum and self absorption of uranium is included.

The final foil configuration consisted of a 14.3×10^{-4} cm thickness of uranium on a 12.7×10^{-3} cm foil of tantalum. The calculation of the final electrode temperature using the previous assumptions follows.

The power density generated for a neutron flux incident on one side of a fissioning source including self absorption and attenuation and for the parallel plate geometry considered is:[5]

$$P = \frac{f}{3.1 \times 10^{10}} \left(\frac{\Sigma_f}{\Sigma_t}\right) \frac{F}{4} e^{-2\Sigma_a d} \quad \text{watts/cm}^2$$

where f = fraction of neutrons entering the uranium foil that are absorbed; Σ_f and Σ_t are fission and total absorption cross sections for uranium; F = neutron flux = 5×10^{12} n sec^{-1} cm^{-2}; $\Sigma_a d$ = absorption coefficient x absorber thickness. For the above uranium foil thickness f = 0.0815. The calculation was made for the geometry indicated in Figure 10.

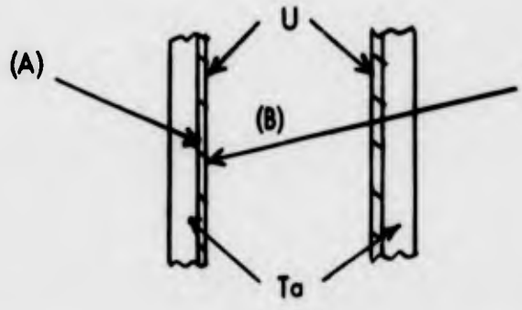

Figure 10 - Schematic for fission power calculation.

For the flux incident from A, a power density of 2.73 watts cm^{-2} is calculated while 2.57 watts cm^{-2} is calculated from B for a total of 5.3 watts/cm^2. The electrode radiating area was designed to be twice the collector area so that an effective 2.65 watts/cm^2 needs to be dissipated. For an electrode emissivity of 0.2 radiating to a black body, this power density corresponds to an electrode temperature of 1230°K. This value is 180°K higher than originally considered acceptable. However, this calculated value is an upper limit since heat conduction through electrode supports and the noble gas filling will reduce this temperature.

B. Tube Details

Figure 11 illustrates the final tube structure, glass envelope and containment can details.

The electrodes are assembled as a unit on three sapphire rods and mounted to a 9 pin Corning 1720 aluminosilicate glass press. The electrodes are reactor grade zirconium with the uranium-tantalum foil combination bonded to the planar surfaces. Thermocouples of Ni-Mo are spot welded to each of the three electrodes. The cold junction of these thermocouples is at the glass press. This is monitored by a Kulgrid-Constantan thermocouple where the Kulgrid lead to a molybdenum feed through wire is used as one leg of this thermocouple. A calibration of this cold junction thermocouple has been made so that the electrode thermocouples can be appropriately corrected for this cold junction.[6]

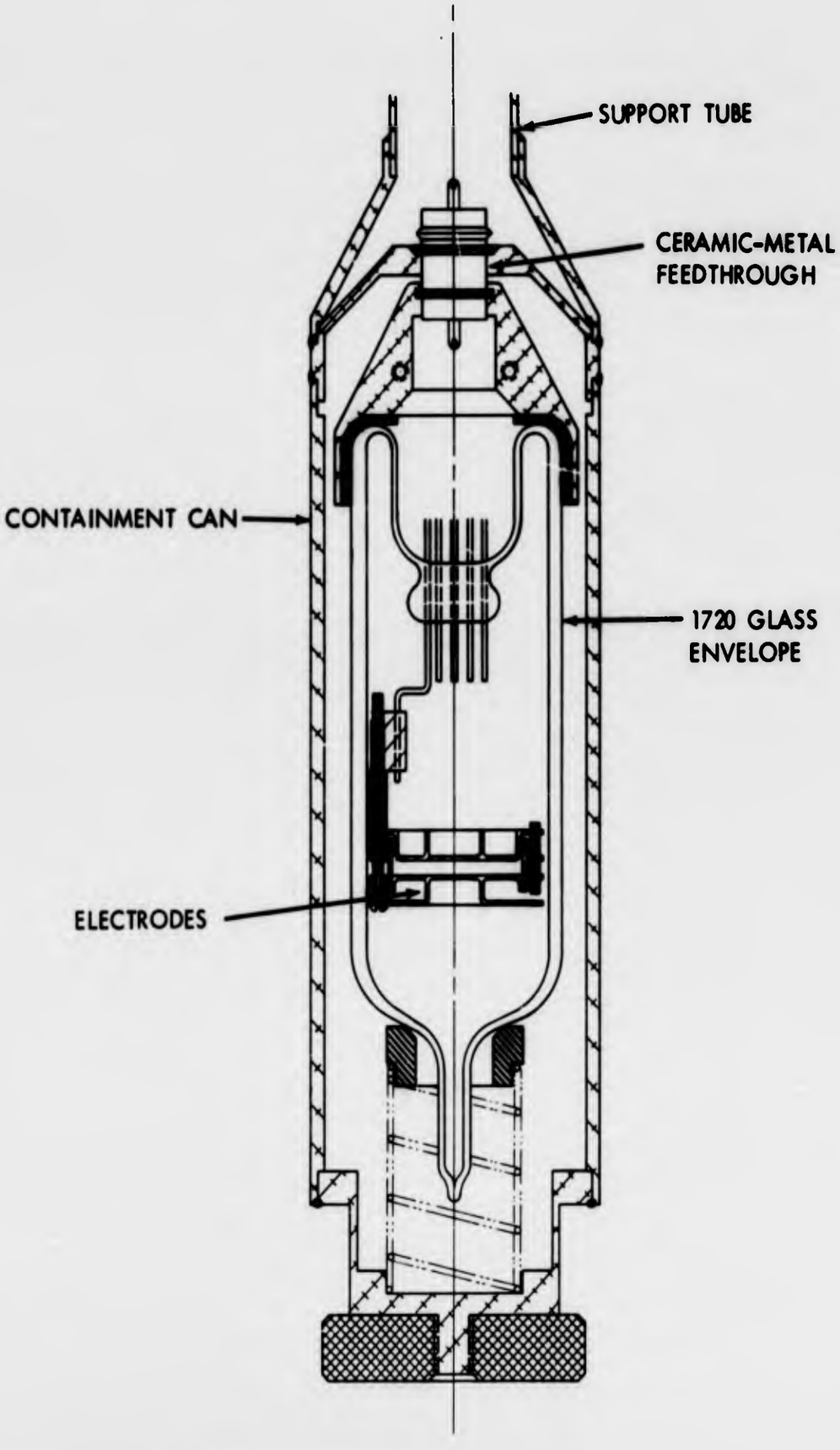

Figure 11 - Details of inpile ion chamber G12x-R.

The containment can is an all heliarc welded aluminum assembly with a ceramic-metal feed through soldered to the aluminum flange. The flange was copper plated to provide a good soldering surface. The containment can is heliarc welded to a 4 foot section of aluminum tubing which is connected to the 20 foot support tube by a gasketed flange (located 2 feet above the core and water shielded). This support tube carries all the electrical wiring and is pressurized with nitrogen gas to prevent water leakage.

C. Fabrication

Steps in the fabrication and processing of these ion chamber tubes (G12x-R) are seen in Figure 12. The final glass seal was made with open tubulation at both ends of the tube and dry argon flowing during the sealing operation. The tube was then annealed at 715°C within a susceptor heated by induction heating in a bell jar system at 10^{-6} Torr. Subsequently a series of four annealed tubes were attached to an ultra high vacuum station.

One tube was processed by usual means as a vacuum tube. The remaining tubes and manifold volume had been previously calibrated by a 'Wet Test Meter'. A bakeable valve between the gas flask and one between the manifold and diffusion pump isolated the system for gas filling. A one liter, one atmosphere flask of Airco reagent grade neon:argon (1000:1) was opened and expanded into the tubes and manifold. Isolating the gas flask at its new pressure and pumping out the manifold and tubes allowed for repeated gas expansions while still maintaining good 'vacuum' conditions in the system. After expansion to a selected pressure, one tube was sealed off and additional expansions continued until a lower desired pressure was reached and another tube sealed off. In this way final tube pressures of 21, 61 and 220 Torr were achieved.

A ceramic-metal connector is mounted to the tube leads which is used to connect to the feed through of the containment can as seen in Figure 13. The inside of the containment can was darkened by evaporating a layer of titanium in order to insure a high thermal emissivity. Final heliarc welding of the can is done in a helium atmosphere. The can is subsequently placed in a vacuum system and the system tested for helium which might arise from a bad seal. This assures seal integrity and double containment of the uranium.

IV REFERENCES

1. F. E. Jamerson, R. H Abrams, Jr., C. B. Leffert, and R. Silver, "Nuclear Generated Plasmas in Noble Gas Thermionic Converters", to be published in Journal of Advanced Energy Conversion.
2. C. B. Leffert, "A Plasma-Sheath Theory for Noble Gas Thermionic Converters" to be published in Journal of Advanced Energy Conversion.
3. The Reactor Handbook, Volume 3, Section 1, Atomic Energy Commission Report AECD-3647, March 1955, page 425.
4. Ibid, page 498.
5. C. B. Leffert, internal report.
6. J. F. Walkup, internal report.

CONSTRUCTION OF GAS FILLED TUBE FOR PLASMA STUDIES

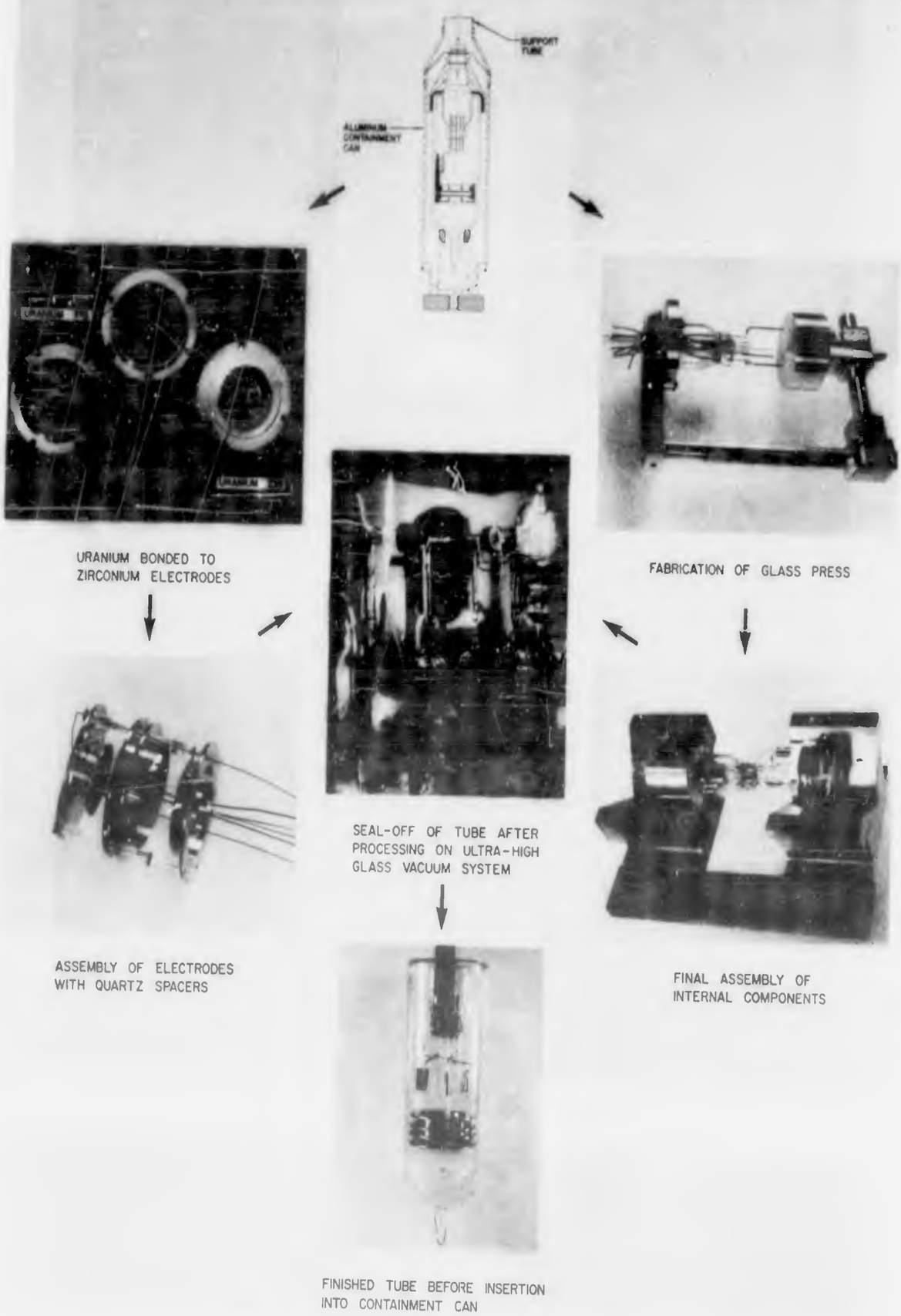

Figure 12 - Fabrication of G12x-R tubes.

Figure 13 - Completed G12x-R tube with special base.

SECTION B (1)

A SYSTEM FOR THE STUDY OF PULSED DISCHARGE IONIZATION OF NOBLE GASES

C. B. Leffert

ABSTRACT

The design, construction and processing of a system for studying the pulsed discharge operation of noble gas filled diodes is described. A variable pressure system with two diodes was constructed. One of the diodes, G7x, had planar geometry with guard rings and the other, G11x, had cylindrical geometry. A cold cathode, gas discharge getter ion vacuum station and a portable bakeout oven and power supply were constructed to process the variable pressure system. The design details are presented and the construction and processing steps are described. The electronic equipment and electrical circuits developed for these studies are also described.

TABLE OF CONTENTS

		Page No.
I	INTRODUCTION	2
II	VACUUM STATION AND BAKEOUT OVEN	3
	A. Vacuum Station	3
	B. Portable Bakeout Oven and Power Supply	5
III	VARIABLE PRESSURE SYSTEM	7
	A. G7x Pulsed Diode with Planar Geometry	10
	B. G11x Pulsed Diode with Cylindrical Geometry	14
	C. Vacuum Equipment	14
	D. Pressure Equipment	14
	E. Provisions for Freeze-out of Gas	18
IV	PROCESSING OF SYSTEM	18
	A. Construction Problems	18
	B. Bakeout and Processing of System	18
V	ELECTRICAL CIRCUIT	21
	A. Electronic Instruments	21
	B. Electrical Circuist	23
	C. Double Pulsing Circuit	27
VI	REFERENCES	27

I INTRODUCTION

The construction and tube processing phase has been completed for the variable pressure pulsed discharge system. Considerable experimental data have already been obtained. One of these studies has already been reported[1] and the other studies are in progress. The variable pressure pulsed discharge system was built to study the transient characteristics of electrically generated plasmas in noble gases. The objectives for the pulsed diode project are threefold: (1) to guide and complement the inpile noble gas fission fragment studies, (2) to provide experimental data for development of the plasma sheath theory, and (3) to evaluate the capabilities of this ion generating scheme for thermionic energy conversion. Many gaseous discharge phenomena can be studied with this system and the mode of operation and variables studied will depend upon which objective is being pursued.

In the ionization scheme employed here a low density plasma (10^9 - 10^{13} ions/cm^3) is created in a noble gas filled diode by applying a short (few μ sec) voltage pulse (10 - 100 v) between a plate and a hot electron emitter. The plasma is established in a few microseconds by inelastic collisions between the electrons and the gas atoms and the degree of ionization is determined by the power added during the pulse, the tube geometry and the type and pressure of the gas. At the end of pulse when the plate voltage is removed, the ion density decays (few millisec) at a rate depending upon the predominant ion loss mechanisms which in turn depend upon the applied fields, the tube geometry and the type and pressure of the gas. This pulsed discharge ion generating scheme is altogether different from the fission fragment ionization scheme in a nuclear reactor, however, the ion loss mechanisms are common to both the laboratory and reactor environments. By studying the ion decay rate following the pulse as a function of the tube geometry and the type and pressure of the gas it is planned to guide the optimization of these parameters for the nuclear generated plasma studies.

During the decay of the ion density following the ionization pulse it is expected that the plasma will be in a quasi-steady state, that is, the electrons will have reached a Boltzmann distribution of velocities even though they are not in thermal equilibrium with the ions or gas atoms. By obtaining the voltage current characteristics at predetermined time delays following the ionization pulse, data will be obtained for the development of the plasma sheath theory.[2]

Since the ion lifetime can be considerably longer than the ionization pulse it is conceivable that this pulsed discharge ionization scheme could be used to eliminate the space charge for the direct conversion of heat to electricity. For such an application the power output during the decay period must be an appreciable portion of the total heat plus pulse power input.

The apparatus that has been assembled for these studies will be described according to the function performed by the three main components: (1) a vacuum station and bakeout oven for processing the variable pressure system (2) the variable pressure system consisting of the pulsed diode tubes and the attendant values and gauges for changing the gas pressure and (3) the electrical circuit for supplying the pulse and measuring the transient electrical characteristics of the plasma.

II VACUUM STATION AND BAKEOUT OVEN

A. Vacuum Station

A new type of vacuum station was constructed to process the variable pressure glass system. A sketch of this station is shown in Figure 1 (see also the photograph in Figure 12). This station incorporates a 5 liter/sec cold-cathode gas discharge getter-ion ('Vaclon') pump manufactured by Varian Associates. Ultimate vacuums below 10^{-10} Torr are advertised and the pumping speed does not tail off at lower pressures as it does for oil diffusion pumps.

As shown in Figure 1, the vacuum station also includes a Varian "Vacsorb" forepump. This is simply a stainless steel tank filled with a molecular sieve (Linde, type 5-A) and cooled by liquid nitrogen. Pressure reduction from 1 atmosphere to about 20 microns Hg (about 1 hour) occurs by adsorption on the molecular sieve. When the entire system reaches this reduced pressure the Vaclon pump is started and the valve is closed to isolate the Vaclon-test chamber section. Since the Vaclon pump retains all the gases pumped, the pump-test chamber system can remain completely isolated from the atmosphere. Stainless steel plumbing and OFHC copper gaskets are used throughout the system.

The pumping system was mounted below the transite top of a portable cart and connection was made to the variable pressure system through a copper pinch off tube that extended through the transite top. The variable pressure system was placed on top of the transite and the portable bakeout oven was placed over it. The Vaclon station pumped continuously while the variable pressure system was baked out and the tubes processed.

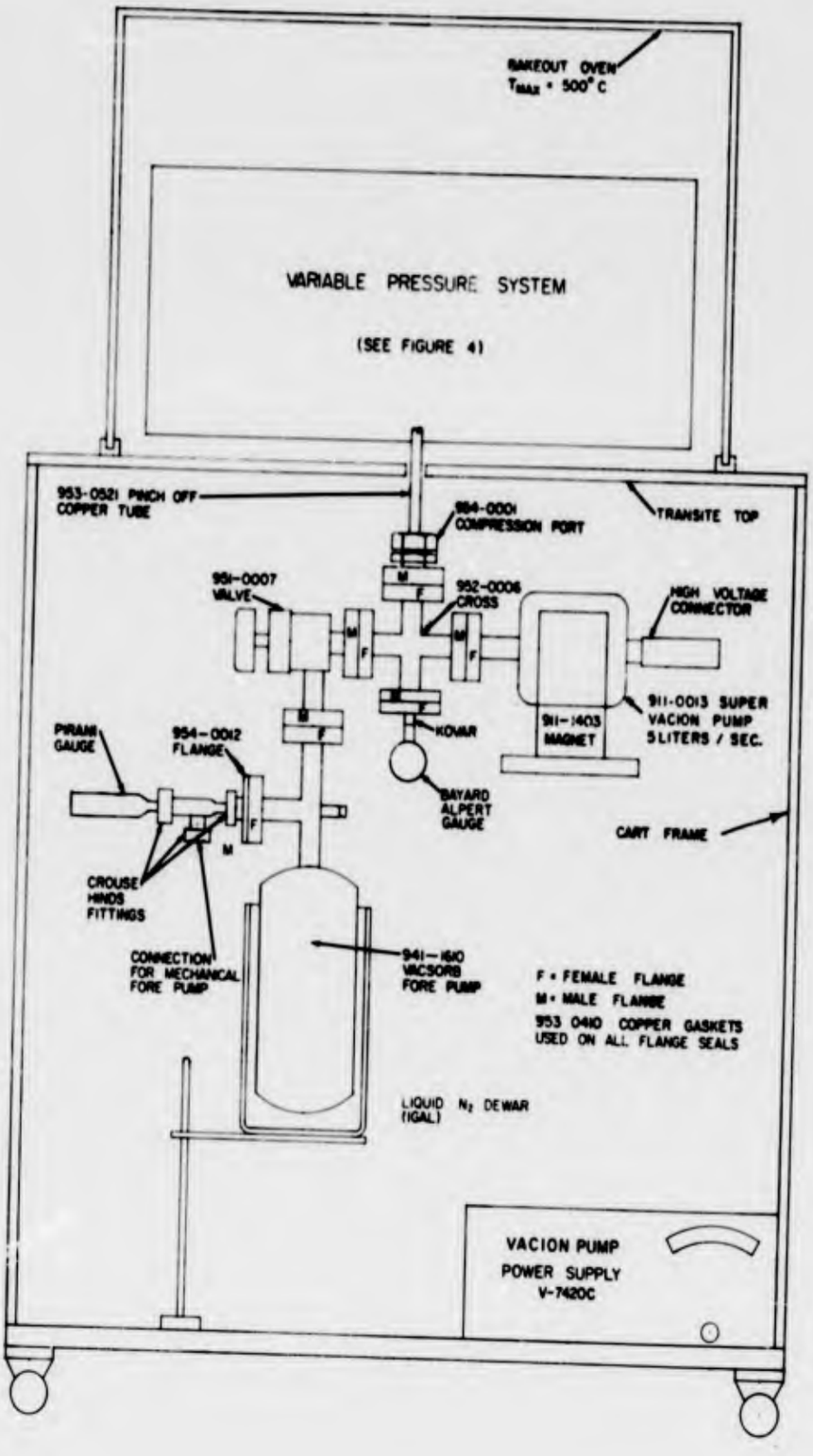

Figure 1 - Vacuum station for processing the variable pressure pulsed-discharge system.

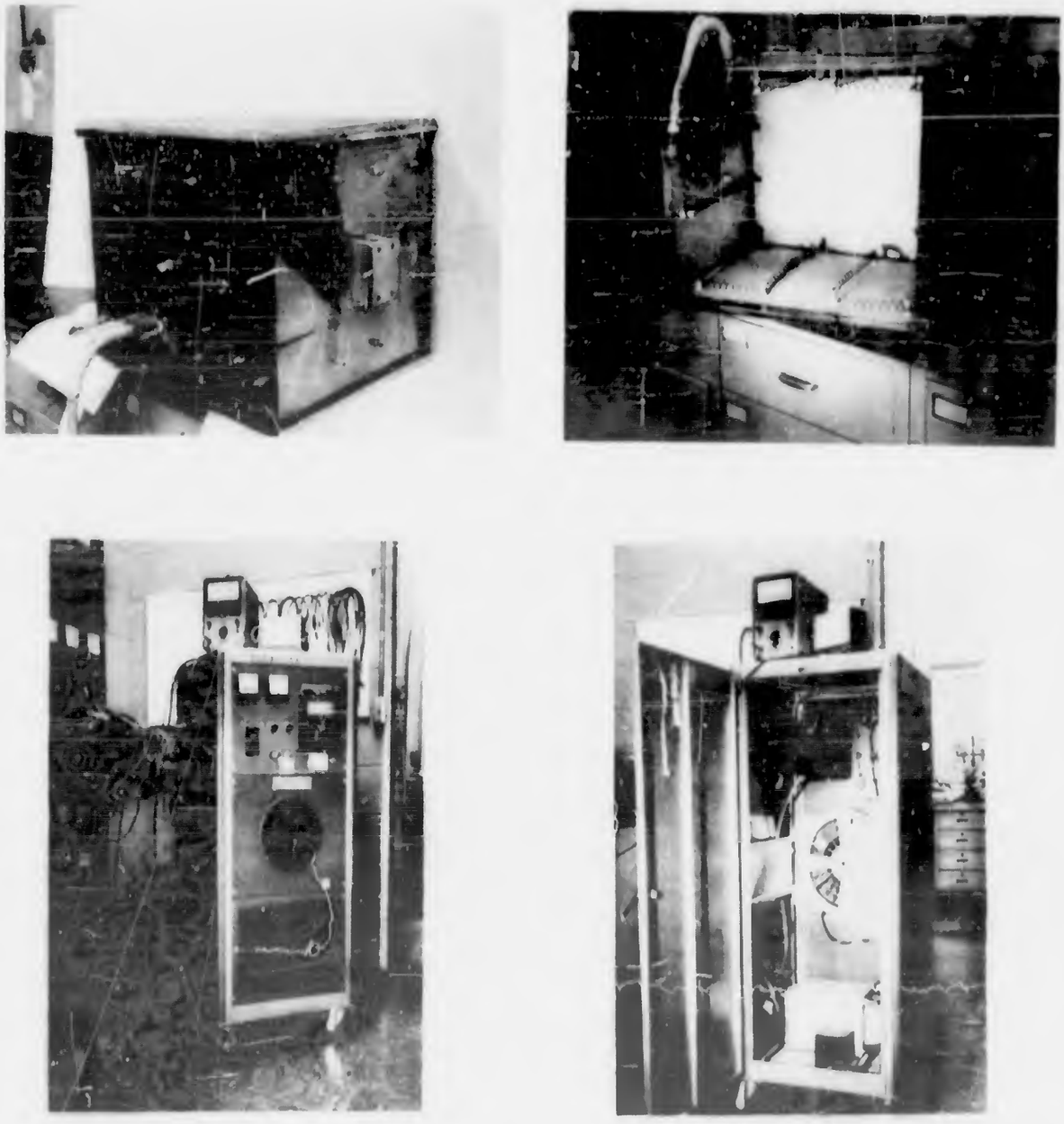

Figure 2 - Portable bakeout oven and power supply.

B. Portable Bakeout Oven and Power Supply

In order to outgas the variable pressure system it was necessary to bake out the entire system at 450°C. The design of a very light portable oven was obtained from F. E. Gifford in which a thin (0.016 in.) highly polished, chrome plated, stainless steel sheet was used as the heat barrier. The detailed design was completed by the Energy Converters and Plasmas Group and the power supply was built by the Electronics and Instrumentation Department. Photographs of the oven and power supply are shown in Figure 2 and a circuit diagram of the power supply is shown in Figure 3.

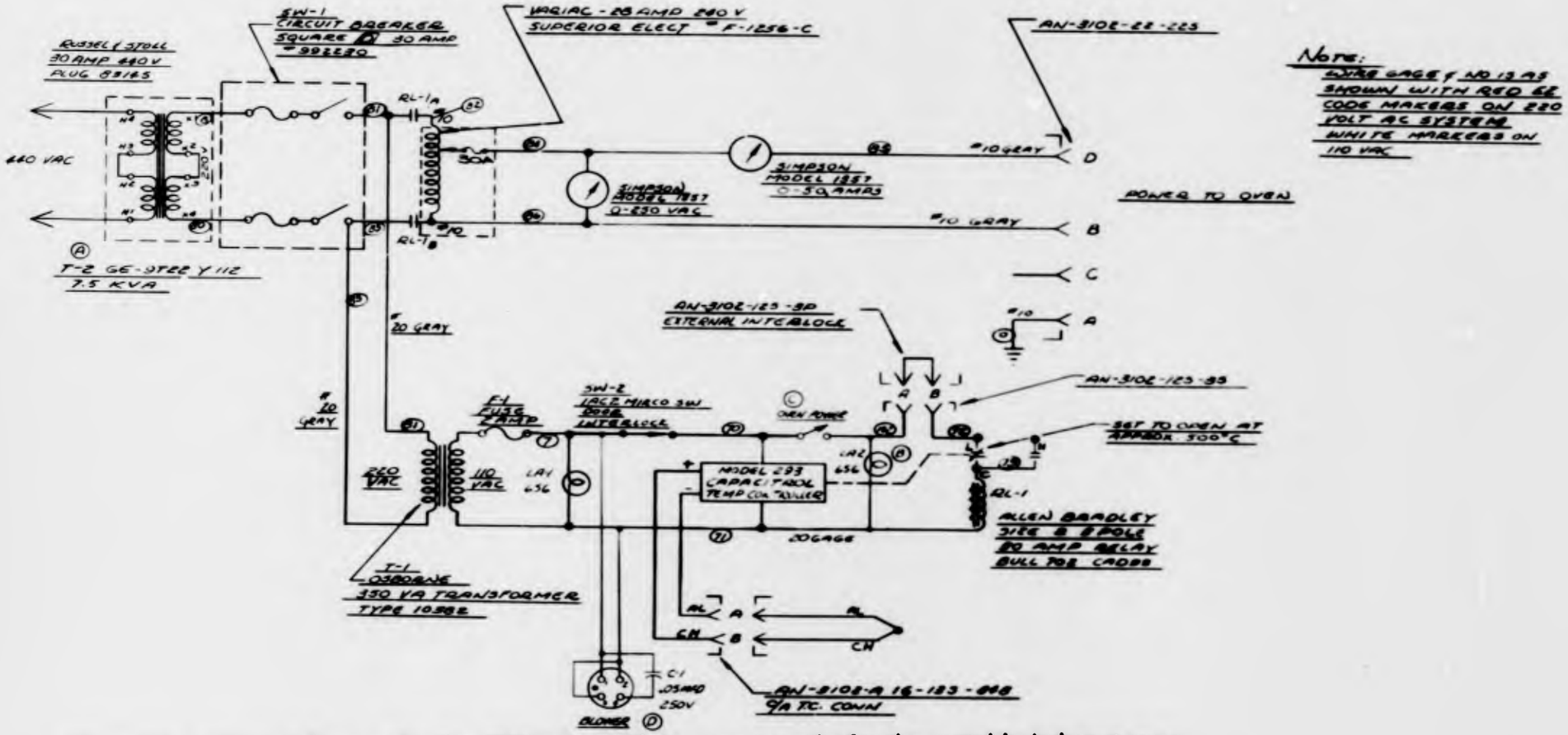

Figure 3 - Circuit diagram for the 220VAC, 6600VA power supply for the portable bakeout oven.

III VARIABLE PRESSURE SYSTEM

The glass manifold system that was constructed to vary the pressure in the pulsed diode tubes is shown schematically in Figure 4 and in the photograph in Figure 5. This system was constructed from the following components:

1. Pulsed Diodes
    a. G7x - planar geometry
    b. G11x - cylindrical geometry
2. Pressure Gauges
    a. Hastings thermocouple gauges
        DV - 16M (two) 0-20 Torr
        DV - 17M (one) 0-1 Torr
    b. Veeco RG-75 vacuum ion gauge
3. Granville Phillips bakeable valve
4. One liter flask of reagent grade noble gas (Air Reduction Sales Company)
5. One glass liquid nitrogen freeze out bulb.
6. One 5L/sec Super Vaclon pump (type 911-0013)
7. Stainless steel to Kovar to pyrex glass transition tee.
8. Pyrex manifold.

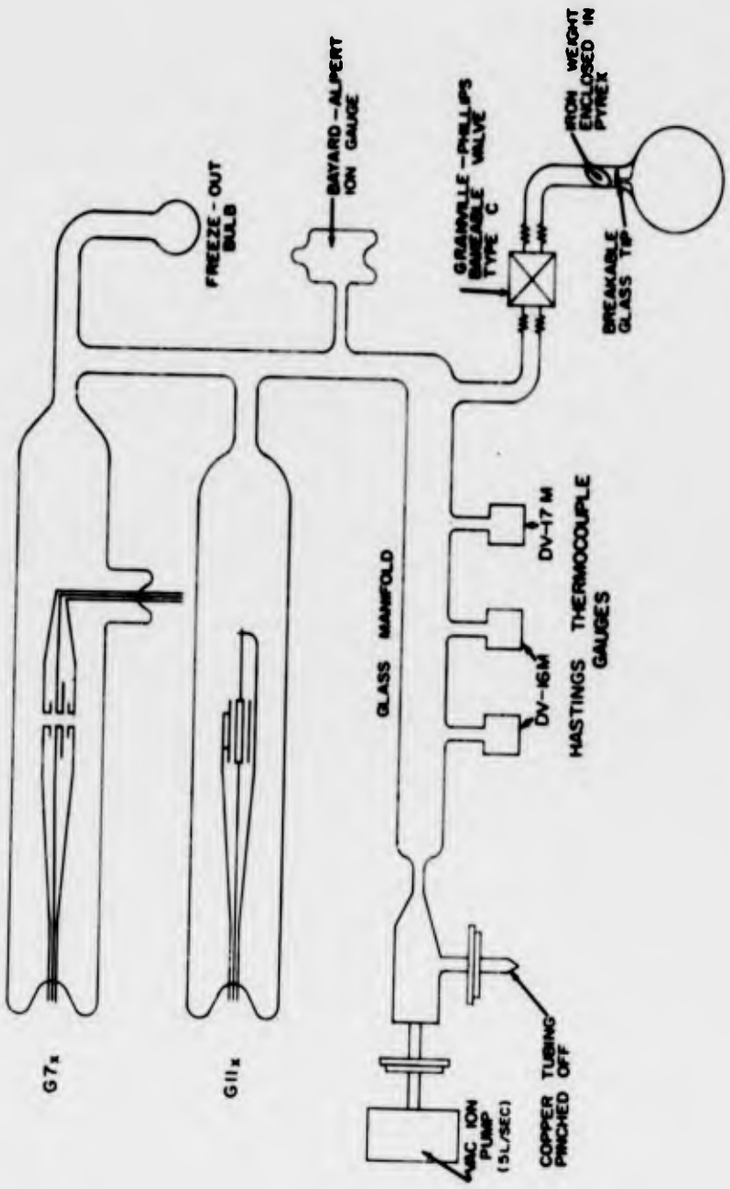

Figure 4 - Variable pressure pulsed discharge system showing the two pulsed diode tubes G7x and G11x together with the valves, gauges and manifold used to vary the gas pressure.

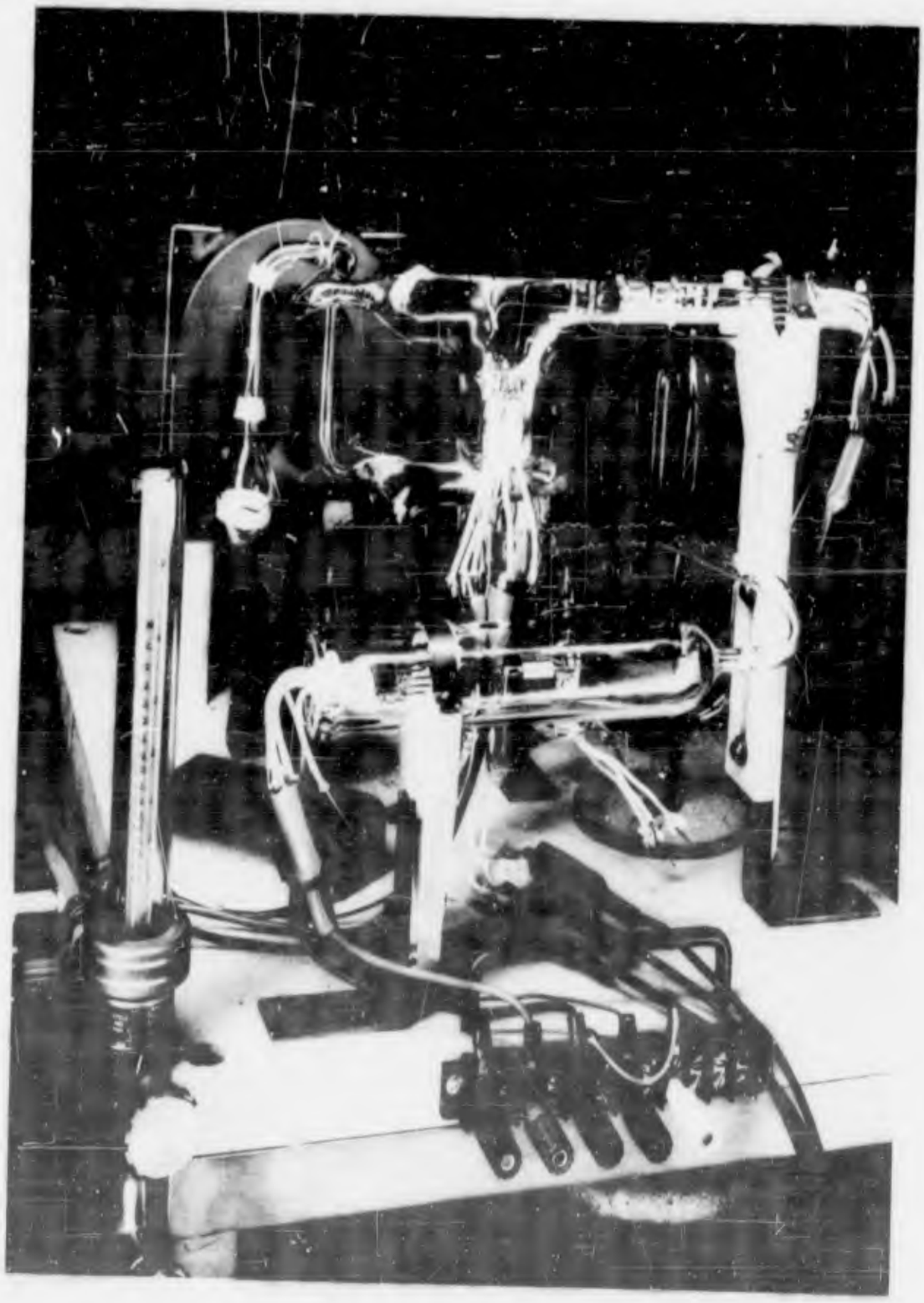

Figure 5 - Photograph of the variable pressure pulsed discharge system. The planar diode with guard rings (G7x) is shown at the top and the cylindrical diode (G11x) is shown in the middle of the photograph.

A. G7x Pulsed Diode with Planar Geometry

Details of the design of the G7x pulsed diode are shown in the assembly drawing in Figure 6. The finished tube is shown at the top of the photograph in Figure 7. A photograph of the internals before assembly is shown in Figure 8.

Parallel plane geometry with guard rings was desired for this tube with nickel-molybdenum thermocouples on the two barium impregnated tungsten emitters (Philips Type B). In order to be able to H_2 fire the tube components after assembly these components were mounted individually to two sapphire rods. This entire subassembly was then H_2 fired and then connected to one glass stem.

As shown in Figure 6 each 3 mm o.d. Type B emitter is supported by 3 sapphire balls mounted in the molybdenum guard ring and attached to a nickel strap by a 0.040 in. molybdenum wire. The nickel-molybdenum thermocouple is spotted to the side of the molybdenum cylinder of the Type B emitter and each wire is spotted to a nickel strap attached to the two sapphire rods. The two ends of the heating filament are attached to similar nickel straps. One of these straps also supports the Type B emitter. The 2 mm spacing between the two guard rings is maintained by two smaller sapphire rods mounted in the guard rings. The two larger sapphire rods are held in two slots on each guard ring. This design prevents distortion of the assembly due to cocking or twisting.

The entire assembly was hydrogen fired and then mounted to one 5-lead pyrex glass stem by nickel straps from the ends of the sapphire rods to the 0.040 in. molybdenum wires of the press. The significant details of the glass assembly are shown in Figures 6 and 8. A 5 lead glass stem was attached to the side of an open ended glass tube and then annealed. After cleaning the annealed tube the end stem plus internals was sealed to the end of the tube with the small side tubulation. This tubulation was used to blow dried argon gas over the internals during the glass blowing step. The connecting wires were spot welded to the molybdenum wires of the side stem by introducing special welding jaws through the one end of the tube that was still open. After this step the open end of the tube was drawn down to tubulation size and the side tubulation at the other end was tipped off to complete the tube.

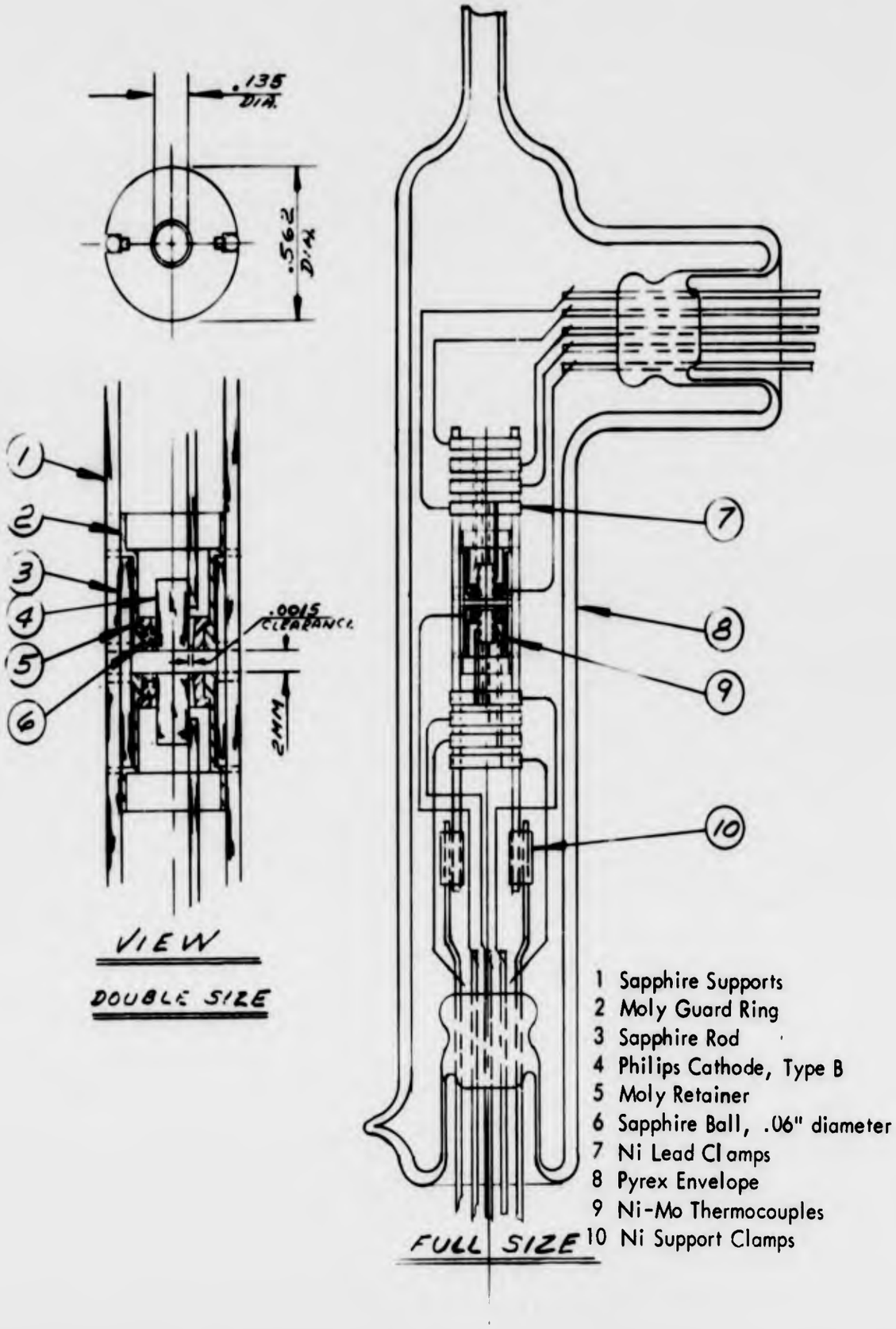

Figure 6 - Assembly drawing of the G7x pulsed diode.

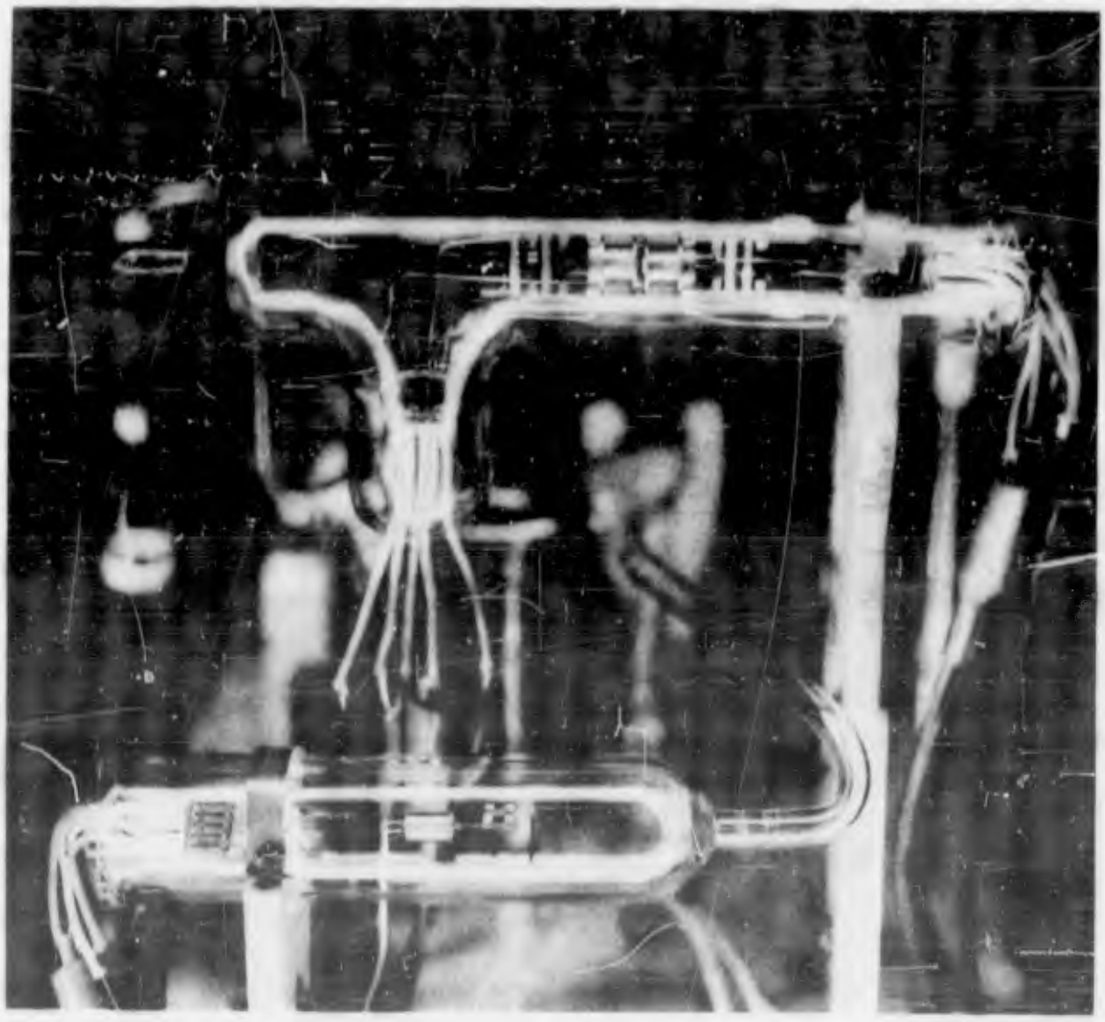

Figure 7 - Photograph showing the G7x pulsed diode at the top and the G11x pulsed diode at the bottom.

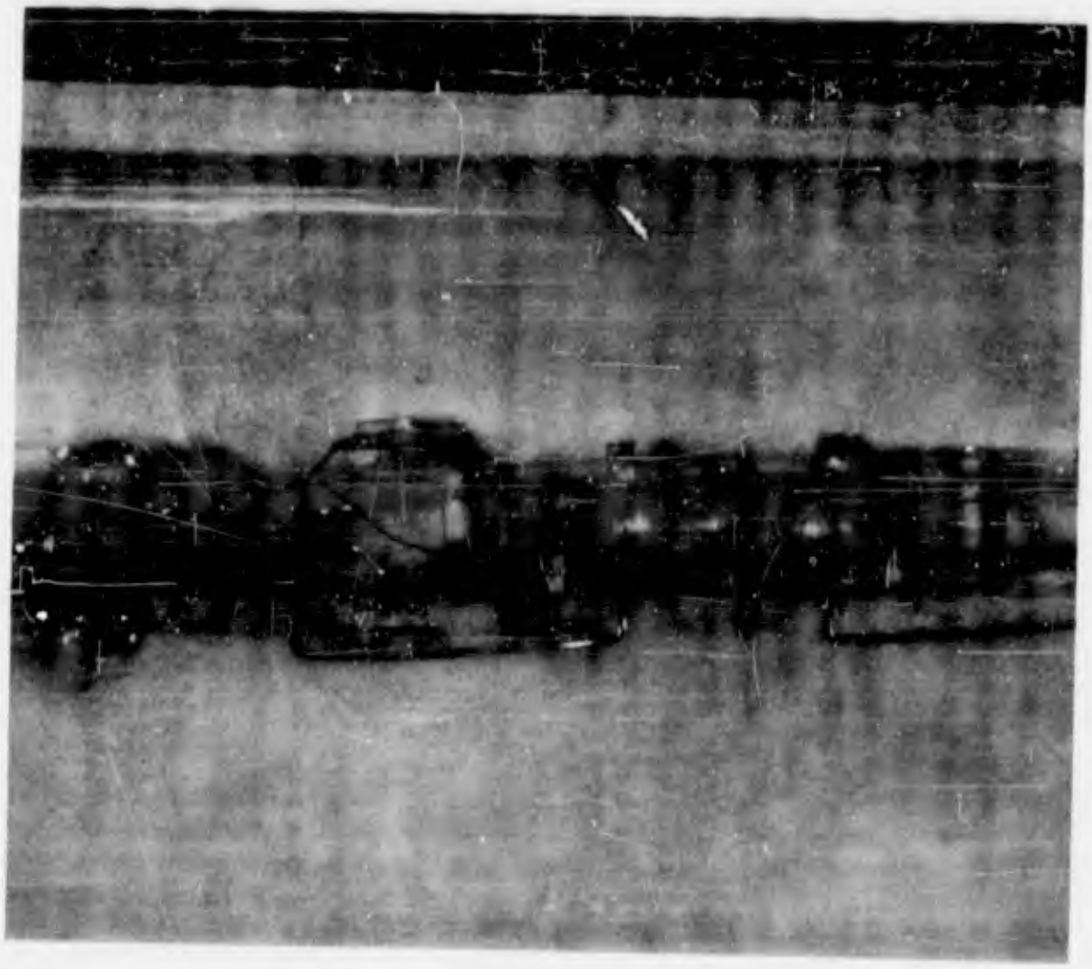

Figure 8 - Photograph showing the internal components of G7x mounted to the two sapphire rods.

B. G11x Pulsed Diode with Cylindrical Geometry

Details of the design of the G11x pulsed diode are shown in the assembly drawing in Figure 9. The finished tube is shown at the bottom of the photograph in Figure 7. Two views of the internals of this tube are shown in the photograph in Figure 10.

A cylindrical diode is of interest since it presents a collector to emitter area ratio greater than unity and also with an L/D considerably larger than unity a simple diode geometry can be used. Tube G11x was designed with these considerations in mind.

The cylindrical Type B emitter is suspended between two molybdenum end caps. One end cap is attached to a molybdenum lead wire from the stem and supports the filament and the other end cap is attached to a sapphire rod. The emitter-collector spacing is shown in Figure 9. The collector is a molybdenum cylinder with a horizontal slit to permit viewing of the emitter surface with an optical pyrometer. A nickel wire plus the molybdenum support wire serves as the thermocouple for the collector.

C. Vacuum Equipment

A 5-liter/sec Vaclon pump was attached to the system (see Figure 4) to check the performance of the pump after bakeout on a closed system. After removal of the magnet from the outside case these pump bodies can be baked out at 450°C. The stainless steel-kovar-glass transition piece is joined to the Vaclon pump and to the copper tubing pinch off tube by Varian stainless steel flanges with OFHC annealed copper gaskets. These flanges can also be baked out at 450°C. An RG75 Veeco ion gauge was also attached to the manifold to check the vacuum reading of the Vaclon pump.

D. Pressure Equipment

A one liter flask of reagent grade xenon at one atmosphere pressure was obtained from Air Reduction Sales Company and attached to the system (see Figure 4) below the transite plate. These flasks are sealed by a very small breakable glass tip in the outlet tubulation. A small piece of iron was sealed in a glass envelope and placed in the tubulation for breaking the tip after bakeout.

A Granville-Phillips type C valve with monel bellows was mounted in the glass tubulation between the 1 liter flask and the main manifold. This valve, when held open, is also bakeable to 450°C and is used to bleed the noble gas from the 1 liter flask to the main manifold after the flask tip is broken.

Three Hastings-Raydist glass thermocouple gauges were attached to the main manifold to measure the gas pressure. These gauges have a limited pressure range: DV-17M, 0-1 Torr and DV-16M, 0-20 Torr. Two DV-16M tubes and one DV-17M tube were attached to the manifold. The instruments are calibrated for air. Hastings-Raydist Company furnished calibration curves for argon, CO_2, $Freon_{22}$, helium, hydrogen and oxygen. Calibration curves for neon, argon and xenon were obtained by S. Stachnik of the Electronics and Instrumentation Department using a McLeod absolute pressure gauge. A calibration curve is shown in Figure 11.

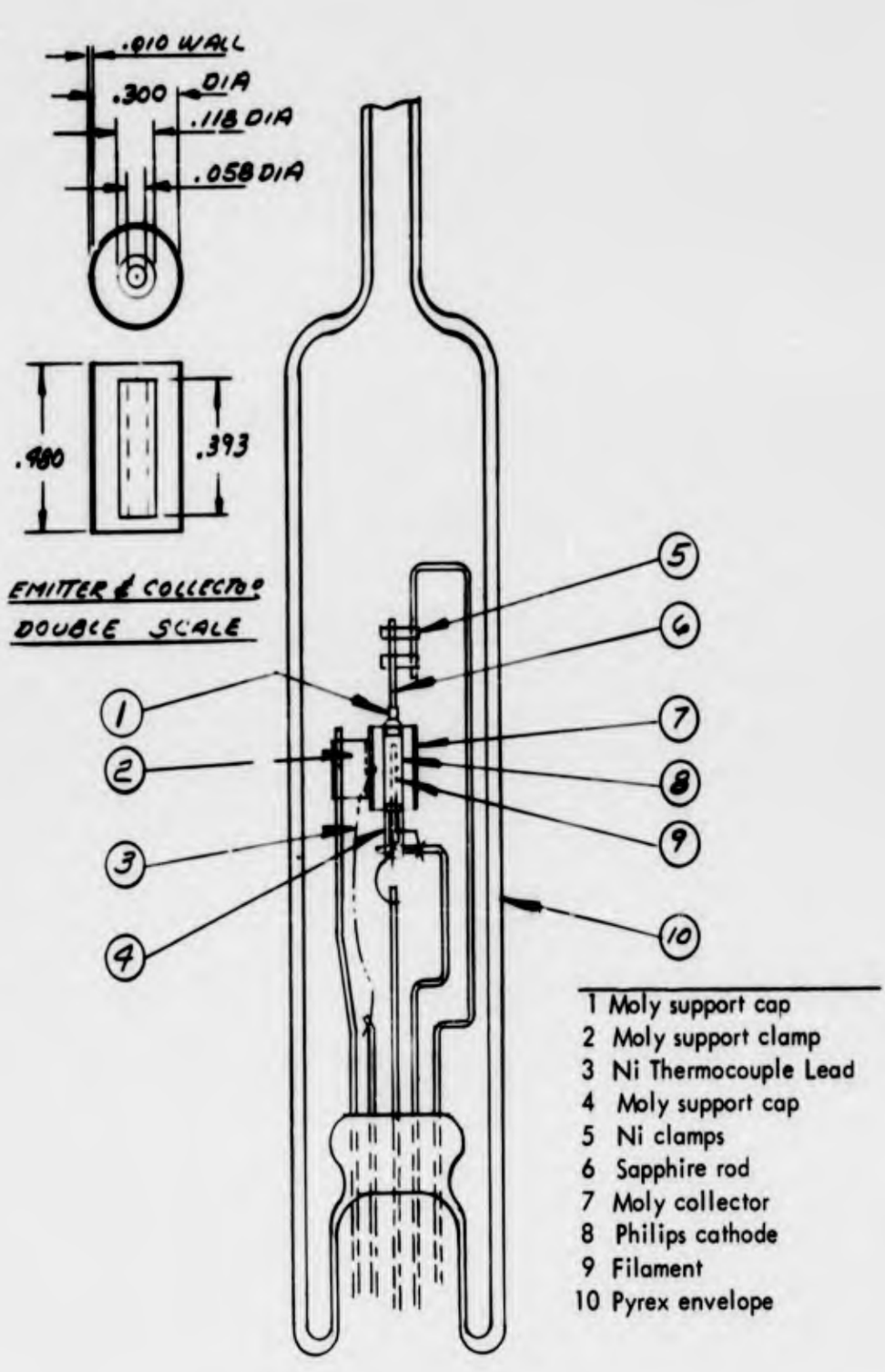

Figure 9 - Assembly drawing of the G11x pulsed diode.

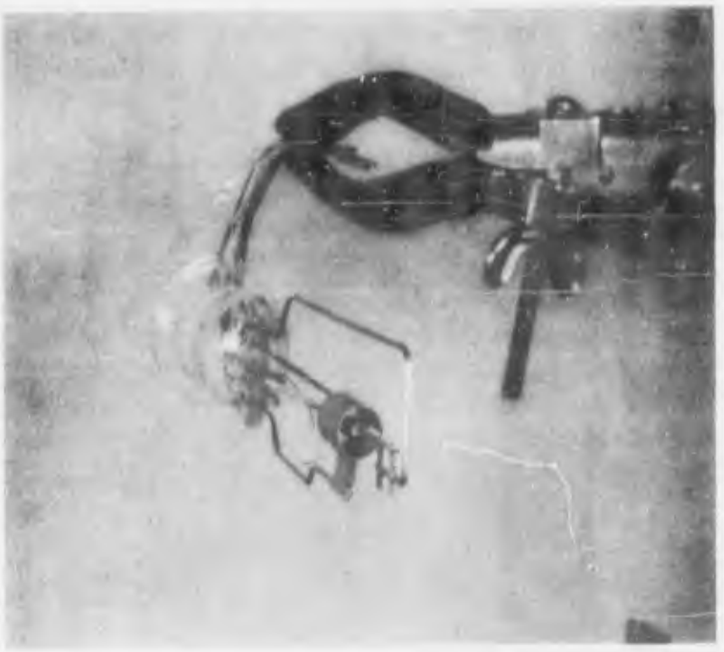

Figure 10 - Photographs showing the internal components of G11x mounted to the glass stem.

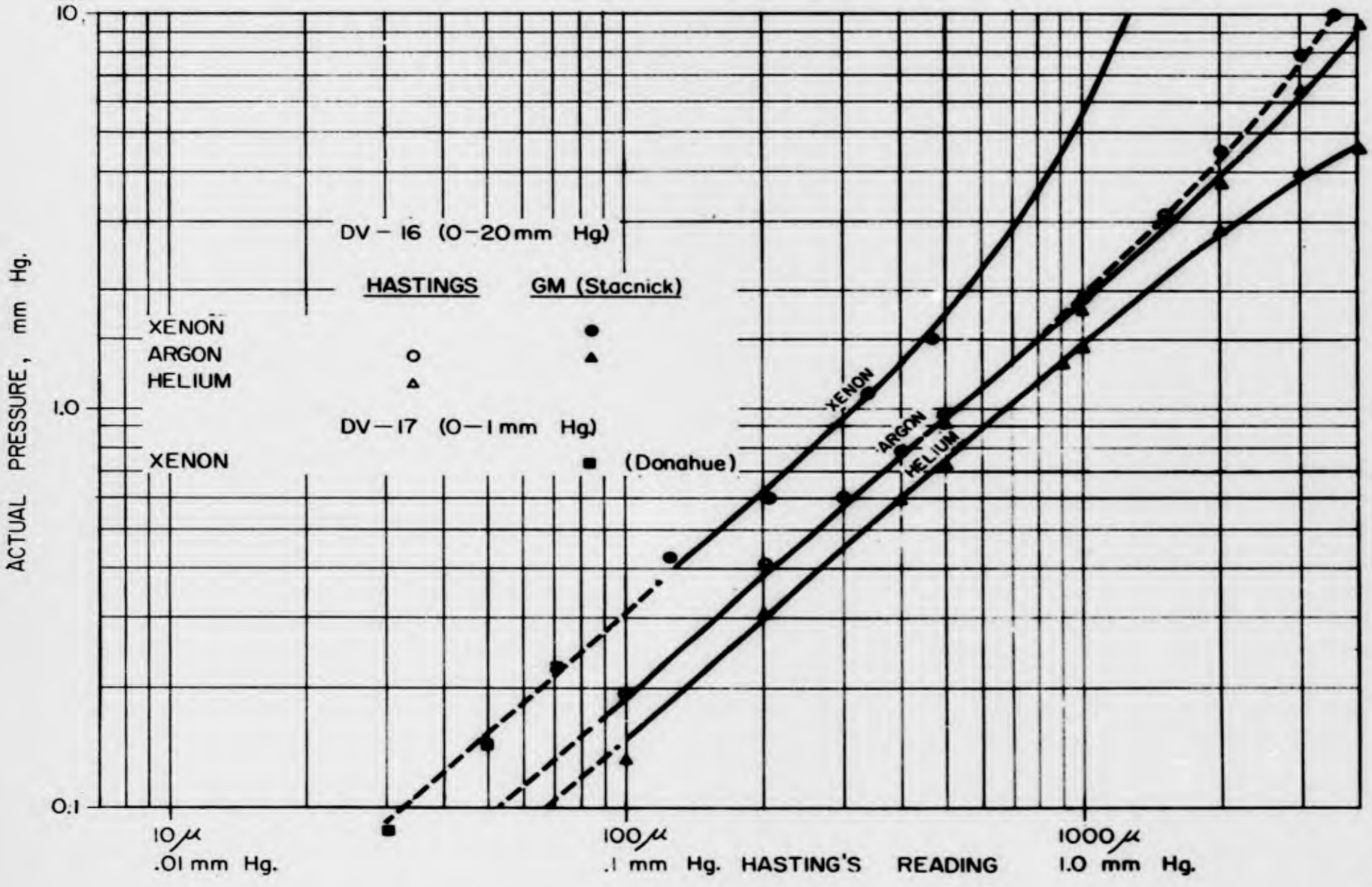

Figure 11 – Calibration of Hasting-Raydist thermocouple gauges.

E. Provision for Freeze-Out of Gas

The 1 liter flask of gas at one atmosphere pressure and the Granville Phillips valve provide a means for varying the pressure in the manifold in one direction only. In order to be able to lower the pressure a freeze out bulb was attached to the manifold so that it could be cooled using either liquid N_2 (for condensing Xe) or liquid He (for condensing the Ne:A, 1000:1 Penning mixture).

IV PROCESSING OF SYSTEM

A. Construction Problems

There were no major problems encountered in the construction and assembly of the two pulsed diode tubes, G7x and G11x. The glass blowing steps were also successful on the first attempt. There was no visible evidence of deposits on the inside of the tubes and the interelectrode resistance checks also showed no evidence of deposits. In view of previous problems with contamination during the glass blowing steps the success of this operation was attributed to the argon purging procedure adopted.

The kovar-glass seal broke in the first two attempts to heliarc weld the kovar to the stainless steel transition piece. This problem was solved by making a thin tight fit between the kovar and stainless steel.

B. Bakeout and Processing of System

The Varian (Vaclon) vacuum system and the new portable bakeout oven worked well for the first bakeout of the system. After the bakeout considerable trouble was experienced with the DV-16M Hastings-Raydist thermocouple gauges. A leak was found in the press of the first gauge. This gauge was replaced with a second but subsequent checking showed that an internal thermocouple element had broken during installation. Two new gauges were ordered and installed after delivery from the factory. Subsequent use of these gauges has shown that the calibration is subject to drift or contamination and a more reliable pressure measuring device is needed. The pressure during the second bakeout at 450°C was 5×10^{-6} Torr.

An interesting phenomenon was observed during bombardment of the molybdenum guard rings during the activation step. In order to outgas these guard rings it was decided to heat them to 1000°C by electron bombardment using the Type B emitters as the electron source. For the first attempt the circuit and deduced current path are shown below:

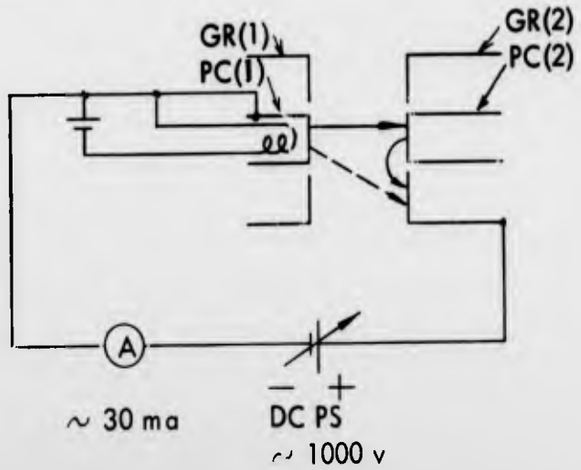

With this circuit the guard ring (2) started to heat correctly (dashed arrow) but as soon as PC(2) heated to emission temperature from thermal radiation from GR(2) the electron path changed to that depicted by the solid arrows--even though PC(2) was floating--and runaway bombardment of PC(2) occurred.

It was decided to try to bombard each guard ring with its own Type B emitter so for the second attempt the circuit and deduced current paths are shown below:

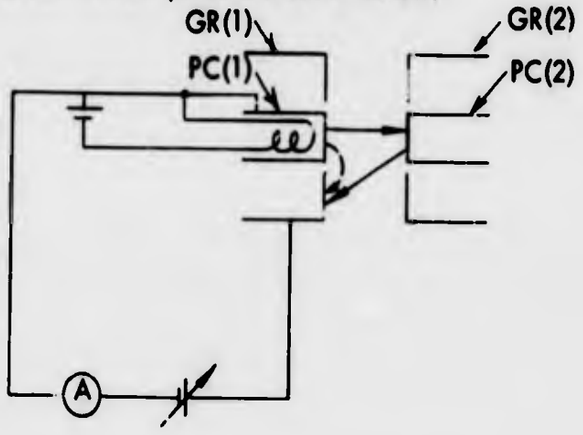

Again the guard ring started to heat correctly but suddenly--even though it was floating--PC(2) would heat rapidly and the power would have to be shut off. The problem was solved by holding GR(2) and PC(2) at the emitter potential as follows:

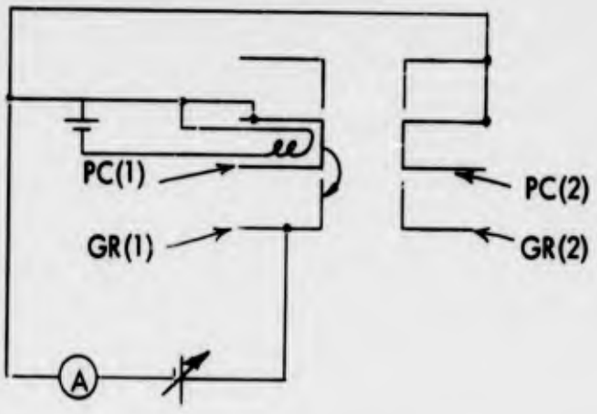

After activation of the cathodes and outgassing of the guard rings by electron bombardment, the copper tubing joining the variable pressure system to the vacuum station was pinched off with the pneumatic cutoff tool. The system pressure was 9×10^{-9} Torr during pinch off. After 12 hours without pumping the pressure in the variable pressure system had increased to only 3×10^{-8} Torr. The Vaclon pump was turned on to lower the pressure to 9×10^{-9} Torr, the Granville Phillips valve was closed and the tip was broken on the 1 liter flask of xenon. The Granville Phillips valve was opened slightly to bring the pressure in the system slowly up to 0.25 Torr of xenon for the first experimental study.

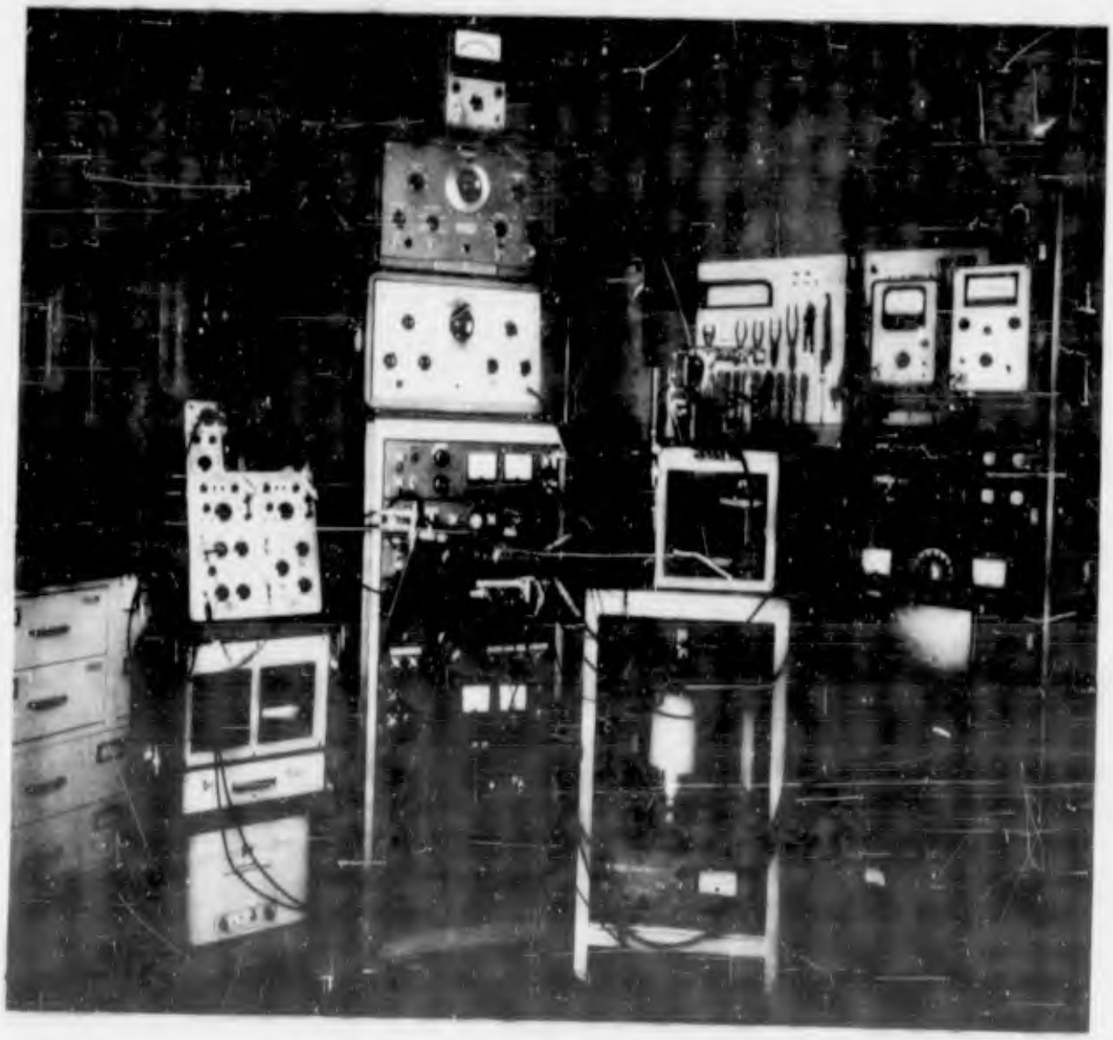

Figure 12 - Photograph showing the variable pressure system, the vacuum station and the instrumentation for the pulsed discharge project.

V ELECTRICAL CIRCUIT

During the construction and processing of the variable pressure system the electronic instruments were collected for the pulsed discharge project and a number of electrical circuits were studied in order to obtain the best circuit for the type of data desired. The various instruments are shown together with the variable pressure system and the vacuum station in the photograph in Figure 12. In this section the major specifications for the electronic instruments are presented, the final electrical circuits are shown, and some of the tests on the electrical circuits are described.

A. Electronic Instruments

The major specifications for the electronic instruments assembled for the pulsed discharge studies are presented below. The symbols used in the circuit diagrams are shown in parentheses immediately preceding the name.

(PG) Pulse Generator

Manufacturer	Hewlett Packard Company
Model No.	212 A
Pulse Length	0 .7 to 10 microseconds
Pulse Amplitude	To 50 volts peak into 50 ohm load (50 watts peak)
Pulse Polarity	Positive or Negative
Rise and Decay Time	.02 microseconds
Internal Impedance	50 ohms
Repetition Rate	50 to 5,000 pps

(CRO) Oscilloscope

Manufacturer	Tektronix, Inc.
Model No.	555 Dual Beam
Vertical Deflection System	
Bandpass	D.C. to 30 mc
Rise time	. 012 microseconds
External Horizontal Input	
Bandpass	D.C. to 240 kc

(E) Electrometer

Manufacturer	Keithley Instruments, Inc.
Model No.	610A
Voltage Ranges	.01, .03, .1, .3, 1,3,10,30 and 100
Input Impedance	10^{14} ohms
Recorder Output	1 mamp or 10 volts for end scale reading
Frequency Response	D.C. to 500 c to D.C. to 10 kc

(A1) Milli-Microammeter

Manufacturer	Hewlett Packard Company
Model No.	425A
Current Range	10 micromicroamperes end scale to 3 milliamperes end scale in an eighteen step 1, 3, 10 sequence.
Input Impedance	1 megohm to 0.33 ohm
Recorder Output	0 to 1 volt for end scale reading

(A2) Clip-on Milliammeter

Manufacturer	Hewlett Packard Company
Model No.	428A
Current Range	3 milliampere to 1 ampere full scale. Six ranges in a 3, 10, 30 ... sequence.
Inductance	Less than 0.5 μh introduced into measured circuit.

(LC) Logarithmic Converter

Manufacturer	F. L. Moseley Company
Model No.	60 B
Input Voltage	
A.C. Mode	.001 to 1 volt
D.C. Mode	.00316 to 3.16 volt
Frequency Range	20 cps to 20,000 cps (A.C. Input)
Dynamic Range	60 dB (1000 to 1)
Input Impedance	2 megohms, 35 mmf
Output	0 to -60 mv for 20,000 ohm load

(PS1) D.C. Power Supply

Manufacturer	General Motors Research Laboratories
Output	
Voltage	0 - 150 v
Current	0 - 4 amp

(PS2) D.C. Power Supply

Type	Battery supply to resistance bridge
Output	
Voltage	-12 to +12 v
Current	1 amp

(PS3) D.C. Filament Power Supply

Type	Battery supply

(T) Potentiometer

Manufacturer	Technique Associates
Model No.	9 B

(OP) Optical Pyrometer

Manufacturer	Leeds and Northrup Company
Model No.	8621-C

(D) Silicon Rectifier (4 in parallel)

Manufacturer	Sarkes - Tarzian
Type	40 - LF

B. Electrical Circuits

The various electrical circuits used in the pulsed discharge studies will now be described. The H.P. 212A pulse generator has one side of the signal output grounded and this greatly restricted the design of the electrical circuits.

1. Circuit for Pulsing an Auxiliary Electrode

During the construction and processing of the variable pressure system a number of circuits were tried for the pulse discharge operation on tube G1x. This tube had been constructed for dc auxiliary discharge studies and contained a Ne:A(1000:1) noble gas mixture at 20 Torr. The tube and some of the experimental data obtained during the pulsed discharge operation were described in another report.[1] The circuit used for these studies is shown in Figure 13. In this circuit the pulsed discharge was formed between the emitter (a) and electrodes (c) and (d). The converter circuit was completed between the emitter (a) and collector (b).

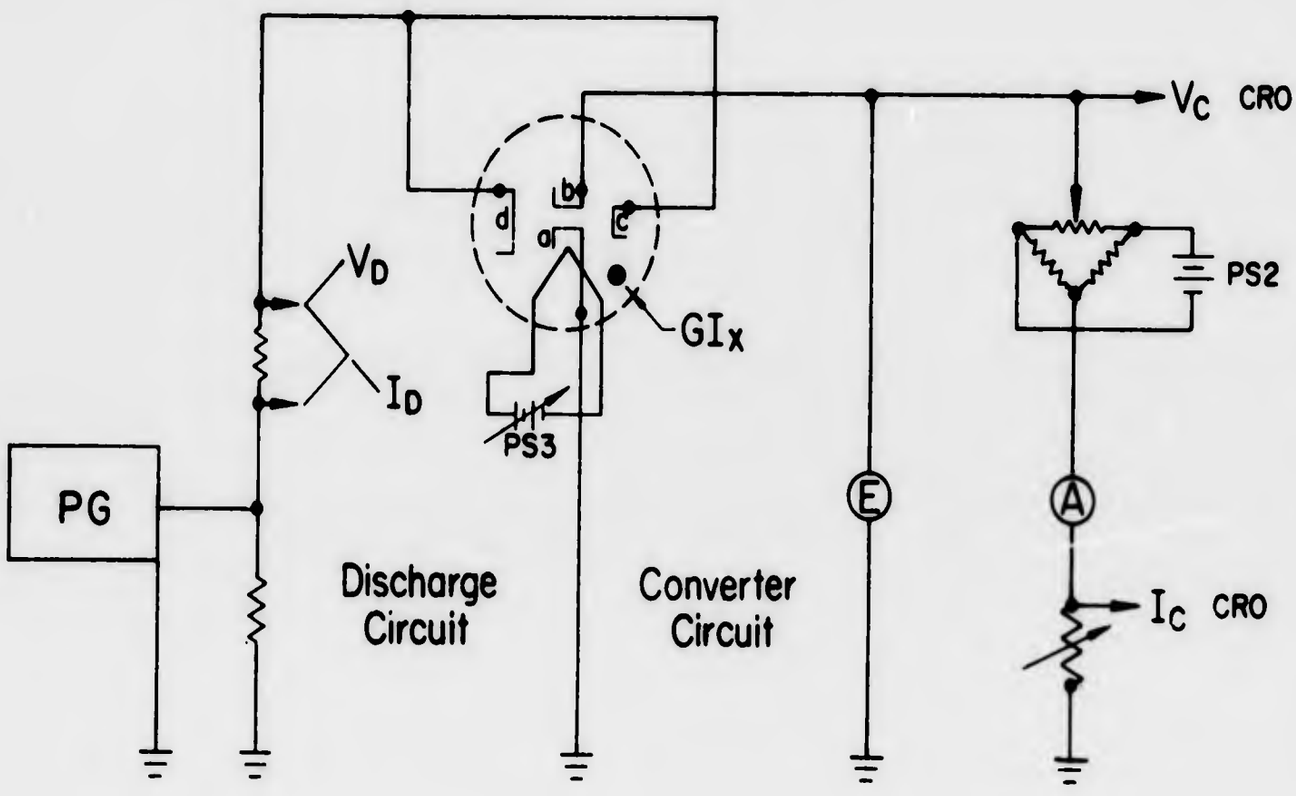

Figure 13 - Circuit for pulsing an auxiliary electrode.

2. Circuit for Pulsing the Collector Directly to Obtain Time Decay Curves

In order to obtain the time rate of decay of the diode voltage and current the circuit shown in Figure 14 was used. The bias voltage was used to maintain tube operation at the saturated current level.

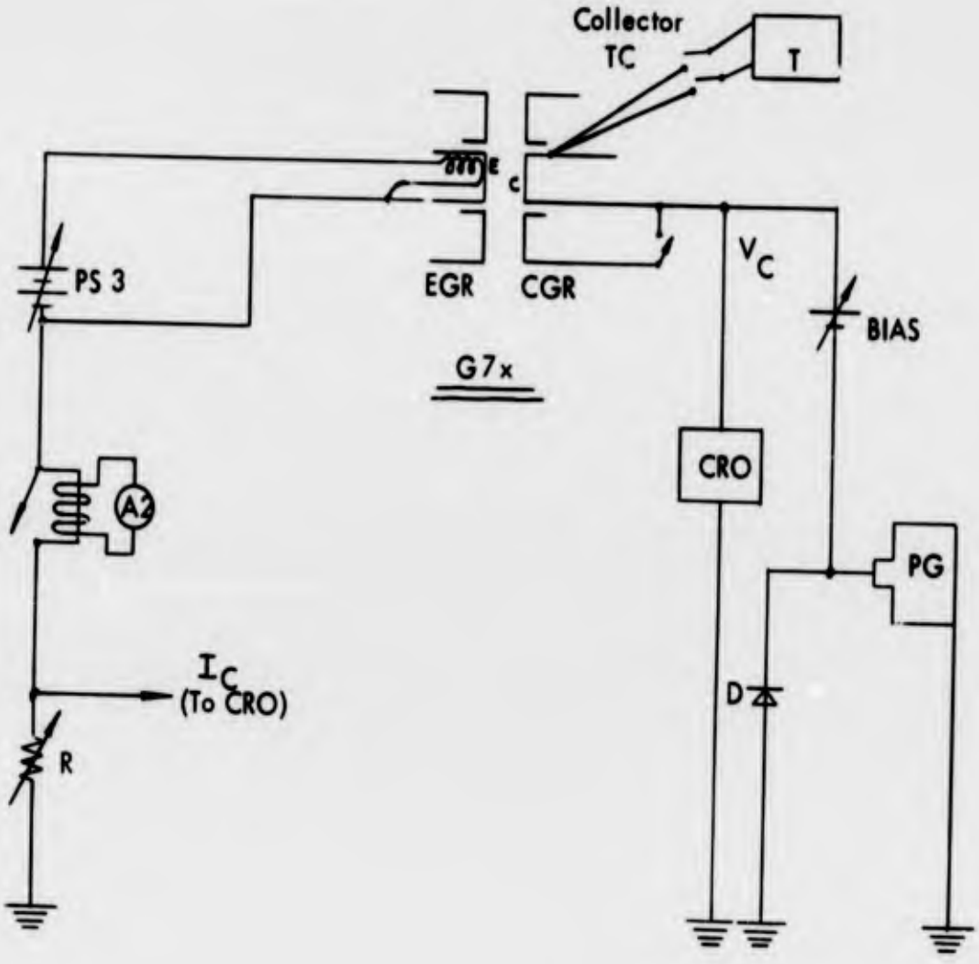

Figure 14 - Circuit for pulsing collector to obtain time decay curves.

3. Circuit for Pulsing the Collector Directly to Obtain Voltage-Current Characteristics

Two pulse generators are used in the circuit shown in Figure 15 to obtain the voltage current characteristics. The first pulse generator is used to create the plasma and the second to create a voltage pulse at a predetermined time delay after the first pulse. Details of the delay circuit will be presented in a later section.

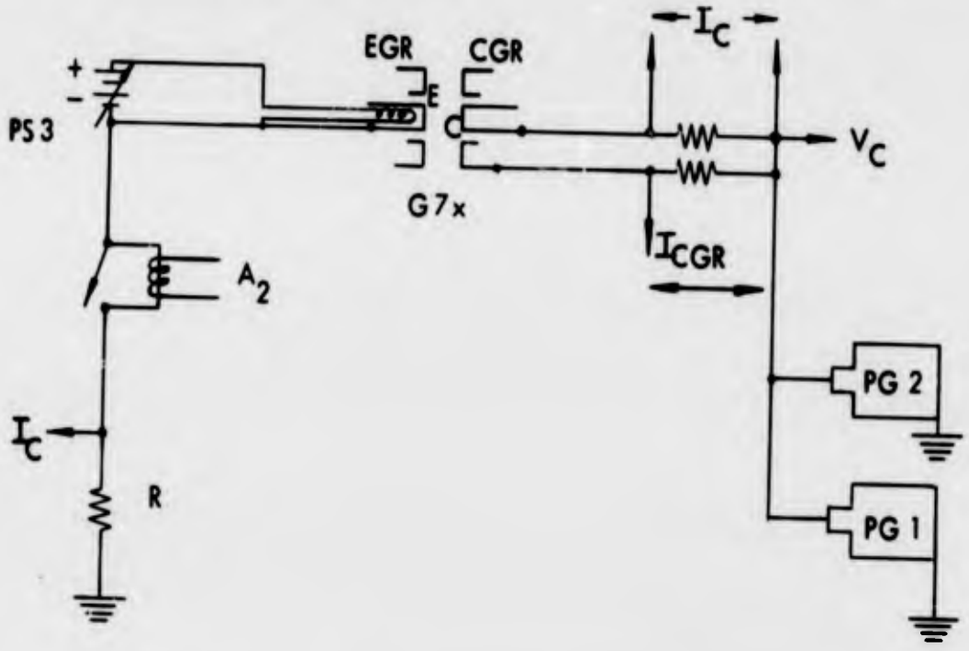

Figure 15 - Circuit for pulsing collector to obtain V-I data.

4. Circuit for D.C. Measurements

In order to obtain the voltage-current characteristics without ionization the circuit in Figure 16 has been developed. Data obtained from this circuit can be used in mobility limited space charge theory studies.

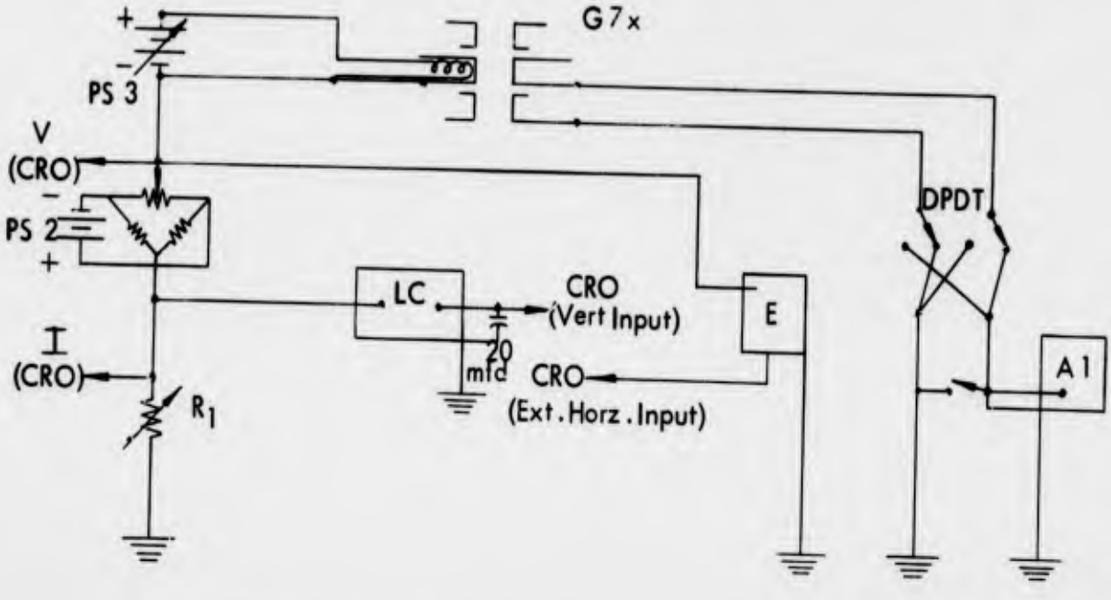

Figure 16 - Circuit for D.C. measurements.

C. Double Pulsing Circuit

The signal from circuits under conditions of rapid change are sometimes distorted because of undesirable circuit inductances and interelectrode capacitances. For the pulsed discharge studies a number of plasma parameters are to be deduced from the theory and the shape of the current and voltage signals. Serious errors would be introduced if the shape of the current and voltage decay curves were significantly affected by such circuit inductances. In order to check for this possibility a double pulsing technique[3] was applied to the circuit (see Figure 17). Pulse generator No. 1 was used to ionize the gas and pulse generator No. 2 was used to appiy a small non-ionizing pulse at a predetermined delay time after the first pulse. The absence of significant circuit inductances is shown by the fast rise and fall time of the diode current in phase with the second voltage pulse as is shown for the circuit in Figure 18A.

This double pulsing technique has been modified to give the voltage-current characteristic at a fixed delay time after the ionizing pulse. In the circuit shown in Figure 14 the ionizing pulse adds to the bias voltage and complicates the V-I curve by varying the degree of ionization with varying bias voltage. With this modified technique the V-I curves are obtained from the second pulse without affecting the degree of ionization. By taking full advantage of the delay circuits in the 555 Tektronix oscilloscope and in both pulse generators and by modifying the intensifier circuit in the 555 oscilloscope it is now possible to photograph the V-I curve at a fixed delay after the ionizing pulse directly on the oscilloscope. The trigger circuit is shown in Figure 17. The diode current signal was fed to the vertical deflection system on the CRO (see Figure 18A) and the diode voltage signal was fed to the CRO external horizontal input. Of course during one cycle between one ionization pulse and the next, the instantaneous "voltage-current dot" would sweep the entire range covering both pulses and the decay period. Using the intensifier pulse feature of the scope, however, the beam intensity was decreased until only that instantaneous (.1 μ sec) V-I point at the peak of the second pulse was preserved. The pulse amplitude on PG2 was then manually operated to sweep out the V-I curve at the predetermined delay after the ionizing pulse as shown in Figure 18B.

VI REFERENCES

1. C. B. Leffert, "A Plasma Sheath Theory with Voltage Independent Ion Source", 1961 ONR Annual Report, ASTIA AD No. 273 067.

2. C. B. Leffert, "A Plasma Sheath Theory for Noble Gas Thermionic Converters", GMR-368, (May 14, 1962).

3. T. E. Firle, "Observations of Current Decay in an Isothermal Cesium Cell", 21st Annual Conference on Physical Electronics at MIT, (March 29-31, 1961).

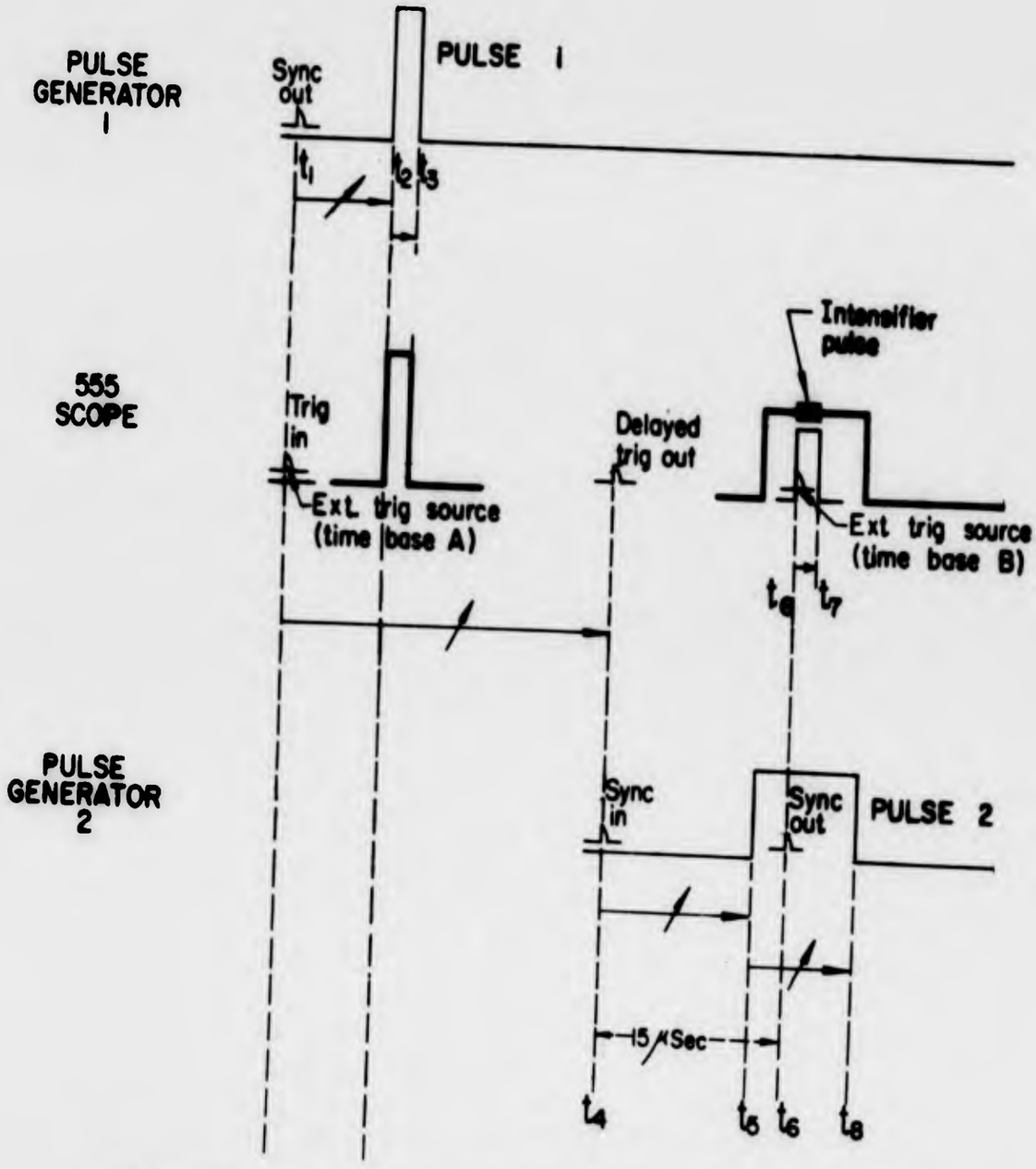

Note: Trigger mode on CRO: "Trig. once for each A Del. Trig."

Figure 17 - Double pulsing trigger circuit used to obtain a delayed V-I trace on oscilloscope.

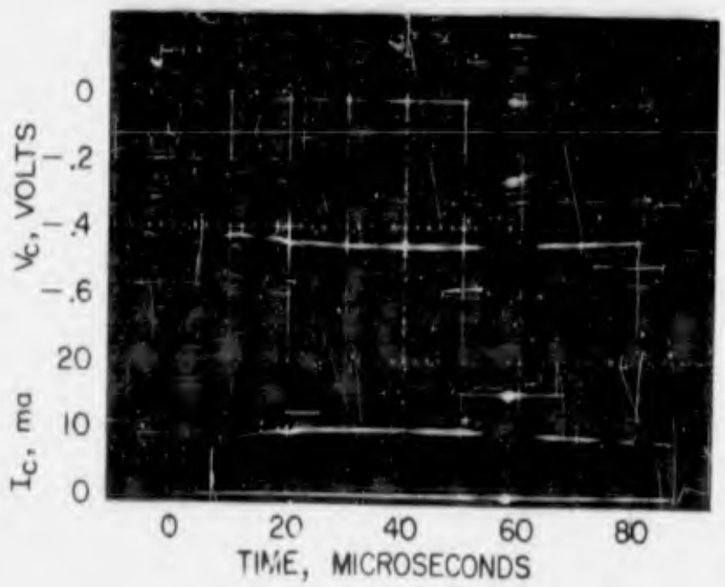

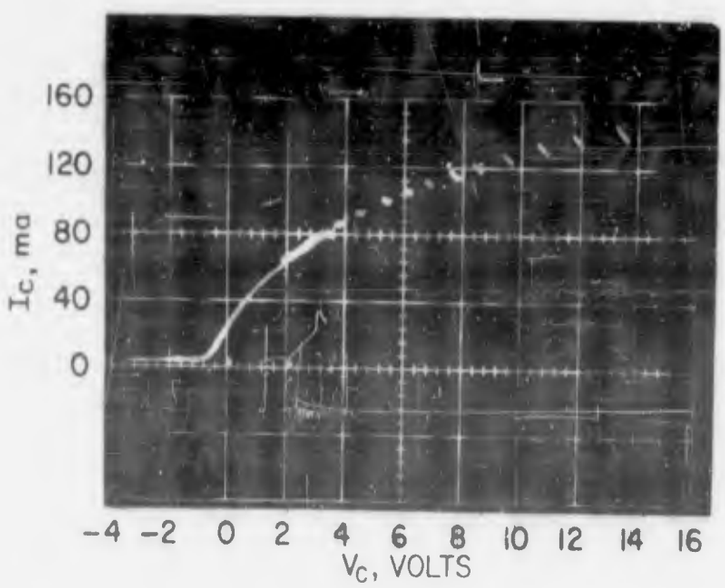

Figure 18 - Double pulsing technique to obtain delayed V-I trace. The upper photograph shows the second pulse during the time decay of the diode voltage and current. The ionizing pulse is at the extreme left end of the trace and is off the photograph. The bright dot is the intensifier pulse. The lower photograph shows the V-I trace obtained by feeding the current signals to the CRO vertical input, the voltage signal to the CRO horizontal input and varying the PG2 pulse amplitude.

SECTION B (2)

ION DECAY RATE IN THE PULSED DISCHARGE IONIZATION OF XENON

C. B. Leffert and J. F. Walkup

ABSTRACT

A series of measurements of the ion decay rate following the pulsed discharge ionization of xenon were made as a function of the gas pressure. Data were taken on two tubes with a hot emitter: one with parallel plate geometry and guard rings and one with a cylindrical geometry. The objective for this study was to provide information to guide the optimization of type of gas, gas pressure, and diode spacing for the current fission fragment ionization studies at the University of Michigan reactor. It was found that the ion lifetime in xenon reached a maximum between 20 and 100 Torr pressure but additional data are needed to fix the optimum pressure. The data indicate that ion losses by both diffusion and volume recombination are significant and a fair correlation of the data was obtained with the reported value for the dissociative recombination coefficient for xenon of 2×10^{-6} cm^3 sec^{-1}.

TABLE OF CONTENTS

		Page No.
I	INTRODUCTION	2
II	THEORY	2
	A. Determination of Ion Number Density from Measured Currents	2
	B. Ion Loss by Volume Recombination	4
	C. Ion Loss by Ambipolar Diffusion	5
	D. Combined Diffusion and Recombination Loss	6
III	DESCRIPTION OF APPARATUS AND PROCEDURE	6
	A. Basic Parameters Studied	6
	B. Circuit for Pulsed Discharge Measurements	7
	C. Outline of Experimental Procedure	8
IV	RESULTS AND DISCUSSION	8
	A. Number Densities	9
	B. Volume Recombination Coefficient, α	9
	C. Current Decay Constant, τ	9
	D. Transition Region	10
V	CONCLUSIONS	10
VI	REFERENCES	11

I INTRODUCTION

One of the objectives for the pulsed discharge project is to guide and complement the current inpile noble gas fission fragment studies.[1] In partial fulfillment of this objective a series of measurements of the ion decay rate following the pulsed discharge ionization of xenon were made as a function of the gas pressure. Details of the design, construction and electrical circuits have been reported previously.[2]

In these studies a low density plasma (10^9-10^{13} ions/cm^3) is created in a xenon filled diode by applying a short (several μ sec) voltage pulse between the collector and a hot electron emitter. The plasma is established in a few microseconds by inelastic collisions between the electrons and the gas atoms. At the end of the ionizing pulse the ion density decays (several millisec) at a rate dependent upon the predominant ion loss mechanisms which in turn depend upon the applied fields, the tube geometry and the type and pressure of the gas. These controlling parameters are common to both the laboratory and nuclear reactor environments and provide the basis for using laboratory tests to guide inpile experiments. The tubes employed were the G7x and G11x diodes.[2] The G7x diode has parallel plate geometry with each electrode consisting of a Philips cathode surrounded by a molybdenum guard ring, and a fixed interelectrode spacing. The G11x is a cylindrical geometry tube with the same interelectrode spacing. By pulsing the collectors of these two xenon filled tubes, and studying the current decay curves, it was possible to calculate the ion number density, the ion decay constants, and the volume recombination coefficient. Although the main variable in the runs was pressure, the effects of varying the emitter temperature, pulse amplitude and width, pulse rate and collector bias were also noted and recorded.

II THEORY

For the plasmas created in these studies (10^9 - 10^{13} ions/cm^3) the previously developed plasma-sheath theory[3] is considered applicable. In this theory the interelectrode plasma between the emitter and collector sheaths is assumed neutral. The number densities of ions and electrons are assumed spatially uniform throughout the plasma but may vary with voltage and time. For these transient studies it is further assumed that the plasma is in a quasi-steady state, that is, both the electrons and ions will have reached a Boltzmann distribution of velocities even though the electrons may not be at the same temperature as the ions or the neutral gas atoms.

A. Determination of Ion Number Density from Measured Currents

The subsequent analysis of the experimental data to determine the controlling ion loss mechanism depends upon the determination of the ion number density, n, from the value of the measured diode current, I, at any given time, t. From the plasma-sheath theory[3] it was shown that in general the ion number density is also a function of the diode voltage as well as the diode current, i.e., $n = n\ (I, V, T, t)$.

For the pulsed discharge studies reported here the pulse amplitude is of the order of or less than the ionization potential of the gas and the discharge is in the ball of fire or Langmuir mode.[4] The current during the discharge is of the order of or less than the Richardson current of the emitter so that a plasma limited current can also be expected after the discharge.

In the plasma limited mode of operation it was shown[4] that the diode current saturated to

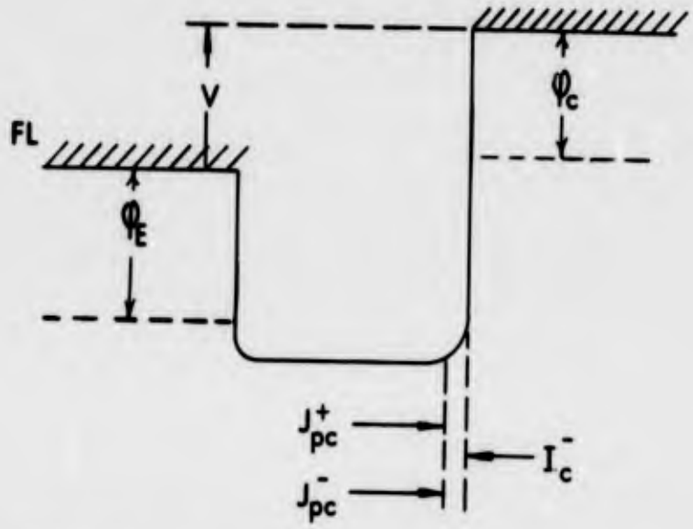

Motive diagram for plasma limited operation.

a value, I_s, at increased collector voltage and the ion number density became independent

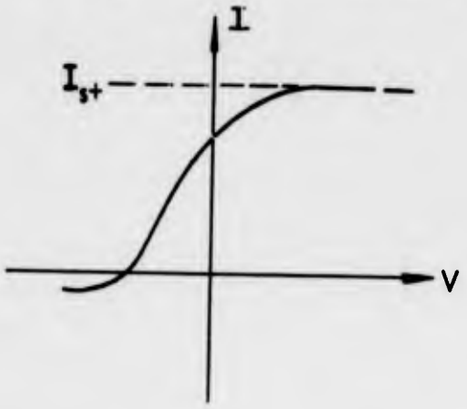

V-I characteristic for plasma limited operation.

of the diode voltage. For $J^+_{pc} << J^-_{pc}$ and $I^-_c = 0$ ("cold" collector)

$$J^-_{pc}(\text{amp cm}^{-2}) = \frac{I}{A_c} = \frac{\epsilon n^- \langle v \rangle_{avg}}{4}$$

or

$$J^-_{pc} = 100\, \epsilon n^- \left(\frac{\epsilon T^-_{pc}}{2\pi m} \right)^{1/2} .$$

where,

A_c = Collector area, cm^2

I_c^- = Richardson emission from collector, amps

J_{pc}^z = Random current density of particle z in the plasma at the collector sheath, amps cm^{-2}, (z = -= electrons, z = += ions)

m = Mass of electron, 9.1084×10^{-31} kg

T_{pc}^z = Temperature of particle z in the plasma at the collector, volts

$\langle v^z \rangle$ = Average velocity of particle z, cm sec^{-1}

ϵ = Electronic charge, 1.6021×10^{-19} coulombs.

Therefore $n^-(t)(cm^{-3}) = K \times I(t)$ amps and evaluating K,

$$K = 4.03 \times 10^{13} \frac{1}{\left[T_{pc}^-(°K)\right]^{1/2} A_c(cm^2)} . \qquad (1)$$

If we assume that $T_{pc}^- = T_e$ (emitter temperature in °K) and that $n^- = n^+ = n$ (i.e. neutral plasma) then n (ion number density) can be calculated from:

$$n(t)(cm^{-3}) = \frac{4.03 \times 10^{13} I(t)}{\left[T_e(°K)\right]^{1/2} A_c(cm^2)} \qquad (2)$$

B. Ion Loss by Volume Recombination

Two types of volume ion recombination loss in a plasma are given by the reaction equations as follows:[5]

1) Radiative Recombination Loss

$$X_e^+ + e^- \longrightarrow X_e + h\nu$$

where $h\nu$ is the radiant energy loss and

2) Dissociative Recombination Loss

$$X_e^+ + 2X_e \longrightarrow X_e + X_{e_2}^+$$

$$X_{e_2}^+ + e^- \longrightarrow X_e + X_e^*$$

The second of these processes, or dissociative recombination, is expected to be the dominant method of recombination loss in the xenon plasma. Therefore, for losses by volume

recombination only

$$\frac{\partial n}{\partial t} = -\alpha n^2 \tag{3}$$

or

$$\frac{1}{n} = \frac{1}{n_o} + \alpha t. \tag{4}$$

The slope of a 1/n versus t plot gives the recombination coefficient, α

$$\frac{\partial(1/n)}{\partial t} = \alpha. \tag{5}$$

Combining equations (2) and (5) for the case of volume recombination loss only:

$$\boxed{\alpha = \frac{1}{K} \quad \frac{d(1/I)}{dt}} \tag{6}$$

Using equation (6) one can obtain the volume recombination coefficient, α, from the slope of a $1/I$ vs time curve for the tube.

C. Ion Loss by Ambipolar Diffusion

Ions can also be lost by diffusion to the walls enclosing the plasma and by ambipolar diffusion out the interelectrode gap. After the end of the ionizing pulse, ions are no longer created and the loss rate of ions by diffusion in the absence of applied electric fields is

$$\frac{\partial n}{\partial t} = D_a \nabla^2 n \tag{7}$$

where D_a is the ambipolar diffusion coefficient.

Assuming an exponential decay of the ions

$$n(x,y,z,t) = n_o(x,y,z,t) \exp\left[-t/\tau\right] \tag{8}$$

where τ is the decay constant.

Using equation (2)

$$I = I_o e^{-t/\tau} \tag{9}$$

or

$$\boxed{\tau = -\frac{d(\ln I)}{dt}} \tag{10}$$

for the case of ion loss by diffusion only.

D. Combined Diffusion and Recombination Loss

At low pressures and at low ion densities the diffusion loss rate and the volume recombination loss rate can be of the same order of magnitude. For this case

$$\frac{\partial n}{\partial t} = -\frac{n}{\tau} - \alpha n^2 \tag{11}$$

where τ is the mean decay time due to diffusion.[6] The solution of equation (11) is

$$\frac{n}{1+\alpha \tau n} = \left[\frac{n_o}{1+\alpha \tau n_o}\right] \exp -t/\tau \tag{12}$$

where $n_o = n(t = o)$. If α is known, equation (12) can be used to correct the data to obtain τ.

III DESCRIPTION OF APPARATUS AND PROCEDURE

A. Basic Parameters Studied

The range of the basic parameters studied were as follows:

Type of Gas	Xenon
Pressure	1/4 mm Hg*
	2.0 mm Hg*
	20 mm Hg*
	100 mm Hg**
Emitter Temperature***	900°C(Br)(1186°K)
	1000°C(Br)(1296°K)
	1160°C(Br)(1471°K)
G7x Geometry	Collector guard ring floating or tied to collector.

Other parameters were sometimes changed during the course of the runs in order to produce the proper mode of operation. These were: (1) pulse amplitude; (2) pulse width; and (3) collector bias. It was necessary to vary these parameters to ensure that operation at saturated current was being achieved without entering the continuous ball-of-fire mode of operation.

The method of varying the pressure is described in detail in reference (2).

---

* Measured with Hastings DV-16 M gauge.

** Calculated after expansion of 1L flask to system.

*** Measured with optical pyrometer; conversion to °K from calibration of brightness temperature versus thermocouple reading.

B. Circuit for Pulsed Discharge Measurements

The circuit used for these studies was described in reference (2) and is reproduced below:

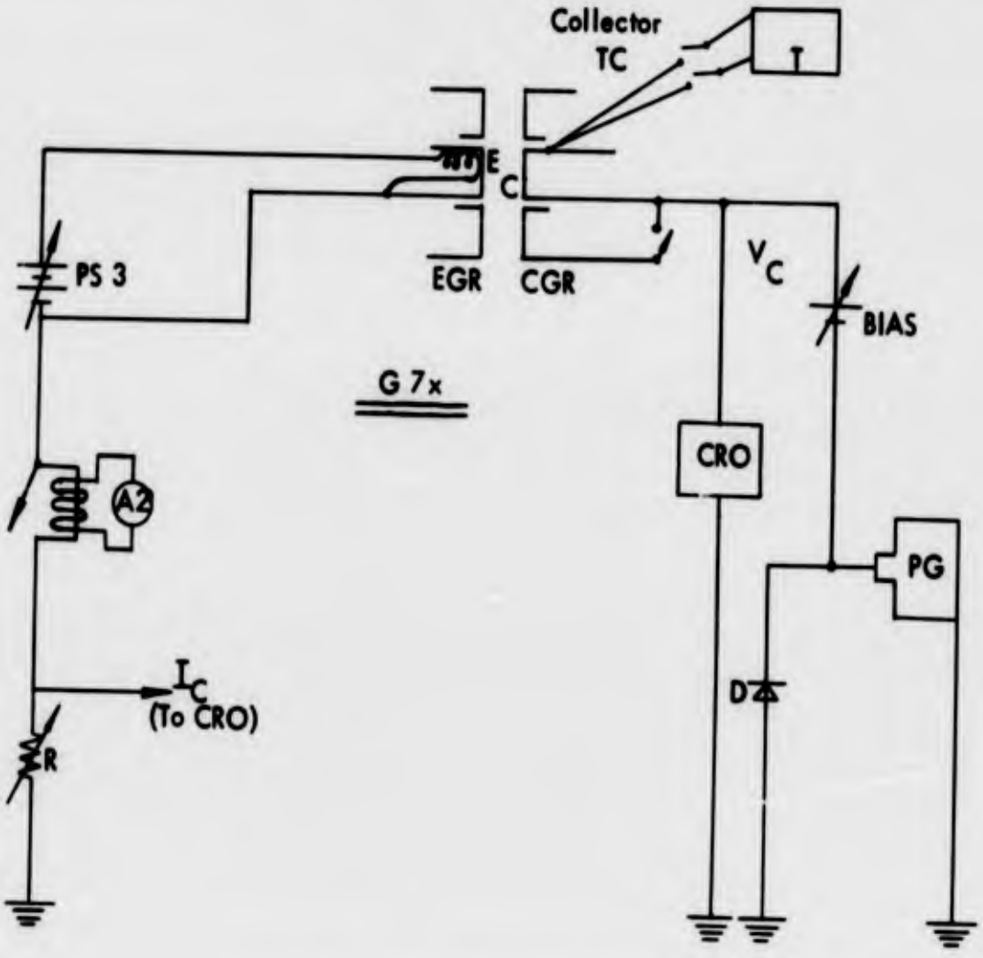

Circuit for pulsing collector to obtain time decay curves.

The symbols in the circuit diagram are

PG	=	Hewlett-Packard 212A pulse generator
A_2	=	Hewlett-Packard 428A clip-on milliammeter
R	=	Variable shunt resistance
D	=	4 Sarkes-Tarzian 40-LF silicon rectifiers in parallel (to eliminate drop across the internal impedance of 50 Ω of PG after pulse)
Bias	=	either Burgess dry cells or NJE solid state dc power supply
T	=	Technique Associates 9B potentiometer
CRO	=	Tektronix 555 oscilloscope
PS3	=	Batteries, filament power supply

A positive bias voltage was applied to the collector to ensure saturated current operation. It should be noted from the above circuit diagram, in the case of the G7x, that although the emitter guard ring was always floating with respect to the filament heated emitter, the collector guard ring could be made floating with respect to the collector, or it could be connected directly to the collector in order to obtain data regarding its effect on the ion number density and decay rate. In the case of G11x a cylindrical anode was used without a guard ring. For both tubes the emitter temperature was obtained using an optical pyrometer and the collector temperature was obtained from Ni-Mo thermocouple measurements.

C. Outline of Experimental Procedure

The basic ion decay data were obtained photographically with the Tektronix 555 dual beam oscilloscope and a Hewlett-Packard scope camera. For each of the four pressures and three temperatures studied, data were obtained according to the schedule below:

	G7x	G7x	G11x
Circuit:	G. R. floating	G. R. tied to collector	
Traces:			
During pulse	V_c vs t V_{gr} vs t I_s vs t	V_c vs t I_s vs t	V_c vs t I_s vs t
After pulse	V_c vs t V_{gr} vs t I_s vs t	V_c vs t I_s vs t	V_c vs t I_s vs t

Schedule for Data Recording

Utilizing the schedule outlined above, data were taken consecutively on the G7x and G11x at the pressures and temperatures mentioned above. These data were plotted in the form of current decay curves from which the data shown in Tables 1 and 2 and the appended figures were obtained.

IV RESULTS AND DISCUSSION

A summary of the results is presented in Tables 1 and 2. The values selected for the variable parameters for the runs made on the two tubes are listed. Also included are the calculated ion number densities at t = 50 μ sec (after start of pulse) and the values of the recombination coefficients (α) calculated from the plots of $1/I$ vs t. An example of a plot of $1/I$ vs t is shown in Figure 1. In no case was there an extended linear section of the curve immediately following the pulse as would be expected for a recombination controlled plasma. An example of a plot of $\ln I$ vs t to determine, τ, is shown in Figure 2.

A. Number Densities

G7x - As shown in Table 1, the ion number density, n, at a fixed time delay after the pulse tends to increase as the pressure is increased, with a range of 7.6×10^8 to 1.7×10^{12} cm^{-3} where the guard ring is floating, and 9×10^7 to 1×10^{11} cm^{-3} where the guard ring is tied to the collector. The lower ion density at the end of the pulse when the collector guard ring is tied to the collector may be due to the production of a more diffuse plasma during the pulse (notice that in general the initial current is greater when the guard ring is tied to the collector).

G11x - The range of n for the G11x was 2.5×10^{10} to 1.4×10^{11} cm^{-3}, as shown in Table 2. Thus the range in n is not nearly as large as that for the G7x. In general n increased with increasing pressure and increasing collector bias but showed no definite trend with increasing emitter temperature, T_e. The pulse voltage adds to the bias voltage so that more ions are generated during the pulse for a greater bias voltage. The effect of increasing the pulse width, amplitude, or repetition rate is again to increase n for any fixed time after the pulse.

B. Volume Recombination Coefficient, α

At selected points on the curves of $1/I$ vs t values of α were calculated from Equation (6) and recorded in Tables 1 and 2. The reported experimental value of α for xenon is 2×10^{-6} cm^3 sec^{-1}.[7] However, as shown in Tables 1 and 2, in no cases were values of α as large as this obtained. Where two values of α are given in the Tables, they were calculated by measuring the slope at two different places (such as shown in Fig. 1). From the tables one immediately notices that the calculated values of α are from two to ten times smaller than the reported value. Both volume recombination and diffusion are probably taking place simultaneously but this should produce a calculated value greater than α.

C. Current Decay Constant, τ

G7x - Plots of log I vs t were made to determine τ according to Equation (10). One of these plots is presented in Figure 2. Figures 3 and 4 illustrate the variation of the decay constant, τ, (towards end of decay) with pressure over the range of pressure studied (0.25 to 100 Torr). In general, for each of the three temperatures studied, τ increases with increasing pressure, up to a point which appears to be between 20 mm Hg and 100 mm Hg. This would indicate that future studies should concentrate on obtaining data in this region to establish the maximum for the curves. Comparing Figures 3 and 4 it is seen that tying the collector guard ring to the collector increases the lifetime of the plasma. This effect can be explained from the difference in the ion loss rate to the collector guard ring during the current decay for the two cases. When the collector guard ring is floating it collects ions but it floats at a negative potential due to the greater random electron current in the plasma. When it is tied to the collector it is biased positively and repels ions back into the plasma.

G11x - The current decay constant, τ, versus the xenon pressure is shown graphically in Figure 5 for G11x. These curves were shown dotted without maxima but the data from G7x would indicate that maxima could very well occur in the pressure range not studied. Future studies could readily establish the presence of such maxima. The collector bias was not the same for all runs presented in Figure 5 (or in Figure 4) and since $\tau = f(B+)$ these curves show only the gross effect. It was found necessary to lower the bias in many of these runs to prevent a continuous dc discharge. For future studies it will be necessary to study the effect of the bias voltage in order to finally obtain curves of τ vs p at constant B_+.

D. Transition Region

Neither the plot of $1/I$ vs t nor the plot of log I vs t fits the data over a very large range, however, the $1/I$ plot for volume recombination loss fits the data best immediately following the pulses as it should for the highest number densities. Similarly the log I plot for diffusion loss fits the data best towards the end of the decay curve where the ion number density is less. In the transition region ion loss by volume recombination and diffusion are both significant.

If the recombination coefficient, α, is known Equation (12) suggests a method for plotting the related variables τ, n, and α which is valid even where diffusion and volume recombination are taking place at the same time. This involves plotting $n/(1+\alpha n\tau)$ vs time. This was done in Figure 6, for Run 8-16.2 on G11x, using the value of τ found experimentally and the reported value $\alpha = 2 \times 10^{-6}$ cm^3 sec^{-1} for xenon.[7] As expected, after a period for allowing the electrons to come to thermal equilibrium, the plot is linear, indicating that both diffusion and volume recombination are taking place and that the reported value of $\alpha = 2 \times 10^{-6}$ cm^{3}sec^{-1} for dissociative recombination fits this xenon data. Figure 7 shows a similar plot for G7x and again the relationship is linear with time. Similar plots should be made on the remaining data to confirm these conclusions.

V CONCLUSIONS

The data reported here for the effect of gas pressure on the ion decay constant for a xenon plasma in a thermionic converter geometry indicate a maximum ion lifetime in the pressure range between 20 and 100 Torr. Sufficient data were not taken during this study to define the optimum pressure but additional data are being obtained. The analysis of the data presented here show that the ion loss mechanism is neither predominantly diffusion nor volume recombination but rather a combination of both. A reasonable correlation of the data was obtained with the reported dissociative recombination coefficient for xenon of 2×10^{-6} cm^3 sec^{-1}.

The volume of the system used in calculating the upper limit of the system pressure was estimated very roughly and a more accurate volume measurement should be made after completion of the runs on xenon. It is important to find a bias level which can be held constant over a series of runs because of the sensitivity of n and τ to the bias level.

Several interesting phenomena were observed during the course of the experimental runs which may warrant further study. Regions of oscillations were observed which were quite sensitive to the bias level. Also one run (8-17.2) on G7x with the guard ring connected to the collector showed oscillations which suggest that the tube might be made to pulse itself similar to the self-pulsing operation reported by Schuder.[8]

VI REFERENCES

1. See previous Section A.

2. See previous Section B (1).

3. C. B. Leffert, "A Plasma Sheath Theory for Noble Gas Thermionic Converters", GMR-368, (May, 1962).

4. L. Malter, E. O. Johnson and W. M. Webster, "Studies of Externally Heated Hot Cathode Arcs", RCA Review, (Sept. 1951).

5. S. C. Brown, "Basic Data of Plasma Physics", John Wiley and Sons, Inc. (1959).

6. M. A. Biondi and S. C. Brown, Phys. Rev. 75, 1700 (1949).

7. S. C. Brown, loc. cit., p. 195.

8. J. C. Schuder, "The Transient Conduction of Current in a Hot-Cathode Gas Diode", Proc. Nat. Electronics Conf., 9, pp. 626-634 (1953).

Table 1

SUMMARY OF DATA FOR PULSED OPERATION OF G7x

Run No.	State of Guard Ring	Pressure (mm Hg)	Filament amps/volts	Emitter Temp. °C(Br)	Emitter Temp. °K	Collector Temp. °K	B+(Collector Bias) volts	Pulse Amplitude Setting	Pulse Width (μsec)	R_s (shunt) Ω	I_s 50μ sec after pulse (amps)	n (t^e density) at 50 μ sec	$\alpha_1 \frac{1}{K}\frac{d(I_s/I)}{dt}$	α_2
7-26.3	Tied to circuit thru' 50Ω Res.	0.25		---	1200 (TC)	---	0	Max. on 10 DB Atten.	5	50	Not available			
8-6.1	Floating			900	1186	368	6 v		5	50	6×10^{-5}	7.602×10^{8}		
"	Tied			900	1186	368					1.3×10^{-4}	9.546×10^{7}		
8-3.2	Floating			1000	1296	393					1.0×10^{-4}	1.212×10^{8}		
"	Tied			1000	1296	393					1.05×10^{-3}	7.376×10^{8}		
8-6.2	Floating			1160	1471	451					3.6×10^{-2}	4.097×10^{11}		
"	Tied	0.25		1160	1471	451					5.6×10^{-2}	3.693×10^{10}		
8-8.1	Floating	2.0	0.81/7.9	900	1186	390					2.2×10^{-4}	2.787×10^{9}		
"	Tied		0.81/7.9	900	1186	390					2.6×10^{-4}	1.909×10^{8}		
8-8.2	Floating		0.87/9.5	1000	1296	419					5.3×10^{-2}	6.424×10^{11}		
"	Tied		0.87/9.5	1000	1296	419					5.5×10^{-2}	3.869×10^{10}		
8-8.3a	Floating		1.1/12.8	1163	1472	468				50	5.6×10^{-2}	6.373×10^{11}		
"	Floating		1.1/12.8	1163	1472	468				10	9.3×10^{-2}	1.058×10^{12}		
"	Tied	2.0	1.1/12.8	1163	1472	468	6				9.4×10^{-2}	6.198×10^{10}		
*8-14.1	Floating	20	0.86/8.8	900	1186	423	2.5				6.3×10^{-2}	7.982×10^{11}		
"	Tied		0.86/8.8	900	1186	423	2.4				7×10^{-2}	5.140×10^{10}		
8-14.2	Floating		0.94/10.5	1000	1296	447	2.7				1.38×10^{-1}	1.672×10^{12}		
"	Tied		0.94/10.5	1000	1296	447	2.45				1.36×10^{-1}	9.554×10^{10}		
8-14.3	Floating		1.07/14	1157	1470	491	2.60				1.57×10^{-1}	1.787×10^{12}		
"	Tied	20	1.07/14	1157	1470	491	2.0	Max. on 10DB Atten.	5		1.23×10^{-1}	8.111×10^{10}		
8-17.2	Floating	100	0.88/9.0	900	1186	427	4.0	Max. on 0 DB Atten.	6.5		7.5×10^{-2}	9.502×10^{11}	1.168×10^{-7}	2.028×10^{-7}
"	Tied		0.88/9.0	900	1186	427	4.0		6.5		9.5×10^{-2}	6.976×10^{10}	6.81×10^{-7}	1.437×10^{-6}
8-20.1	Floating		0.96/10.8	1000	1296	447	4.0		6.0		1.25×10^{-1}	1.515×10^{12}	0.886×10^{-7}	2.54×10^{-7}
"	Tied		0.96/10.8	1000	1296	447	3.8		6.0		1.5×10^{-1}	10.538×10^{10}	7.12×10^{-7}	0.953×10^{-6}
8-20.2	Floating		1.1/14.7	1160	1471	495	3.0		6.0		1.5×10^{-1}	1.707×10^{12}	2.54×10^{-7}	
"	Tied	100	1.1/14.7	1160	1471	495	3.0	Max. on 0 DB Atten.	6.0	10	1.55×10^{-1}	1.022×10^{11}	0.59×10^{-6}	

* Diodes present in circuit for all following runs.

NOTE: Pulse Rate = 200 pulses/sec in all runs on G7x.

Table 2

SUMMARY OF DATA FOR PULSED OPERATION OF G11x

Run No.	Pressure (mm Hg)	Filament amps/volts	Emitter Temp. °C(Br)	Emitter Temp. °K	Collector Temp. °K	B+ Volts (Collector Bias)	Pulse Amplitude Setting	Pulse Width μ sec	R_s, ohms (shunt resistance)	I_s, amps at t_D = 50 μ sec	n, cm^{-3} at t_D = 50 μ sec	Recombination Coefficient from 1/I vs t plots α_1	α_2
8-6.4	0.25	1.69/5.6	900	1186	568	6v	Max. on 10 DB Atten.	5	50	5.7×10^{-2}	2.527×10^{10}		
8-6.3	0.25	1.85/6.5	1000	1296	617	6			50	5.9×10^{-2}	2.503×10^{10}		
8-6.5	0.25	2.14/8.5	1153	1468	733	6			50	6.0×10^{-2}	2.389×10^{10}		
8-8.5	2.0	1.71/5.7	900	1186	593	6			10	9.8×10^{-2}	4.345×10^{10}		
8-8.4	2.0	1.86/6.7	1000	1296	651	6				9.4×10^{-2}	3.987×10^{10}		
8-8.6	2.0	2.2/9.0	1160	1471	803	6				9.5×10^{-2}	3.783×10^{10}		
*8-10.5	20.0	1.74/5.6	900	1186	594	3				1.8×10^{-1}	7.981×10^{10}	4.8×10^{-7}	1.0×10^{-6}
8-13.1	20.0	1.9/6.6	1000	1296	671	2.70				1.75×10^{-1}	7.424×10^{10}	5.52×10^{-7}	
8-13.2	20.0	2.2/8.8	1160	1471	841	4.06	Max. on 10 DB Atten.			3.3×10^{-1}	13.141×10^{10}	1.23×10^{-7}	
8-16.1	100	1.76/5.5	900	1186	607	2.40	Max. on 0 DB Atten.			1.4×10^{-1}	6.208×10^{10}	9.89×10^{-7}	
8-16.2	100	1.94/6.6	1000	1296	671	2.2				1.2×10^{-1}	5.090×10^{10}	1.625×10^{-7}	4.82×10^{-7}
8-17.1a	100	2.22/8.8	1160	1471	768	1.5				1.15×10^{-1}	4.579×10^{10}	0.912×10^{-7}	
8-17.1b	100	2.22/8.8	1160	1471	768	2.5				2.2×10^{-1}	8.760×10^{10}	7.66×10^{-8}	1.93×10^{-7}
8-17.1c	100	2.22/8.8	1160	1471	768	3.0	Max. on 0 DB Atten.	5	10	2.7×10^{-1}	10.751×10^{10}	8.47×10^{-8}	2.445×10^{-7}

* Diodes present in circuit for all following runs.

NOTE: Pulse Rate = 200 pulses/sec in all runs on G11x.

FIGURE 1: 1/I vs t for Run 8-16.2 (G11x at 1000°C (Br) and 100 mm Hg)

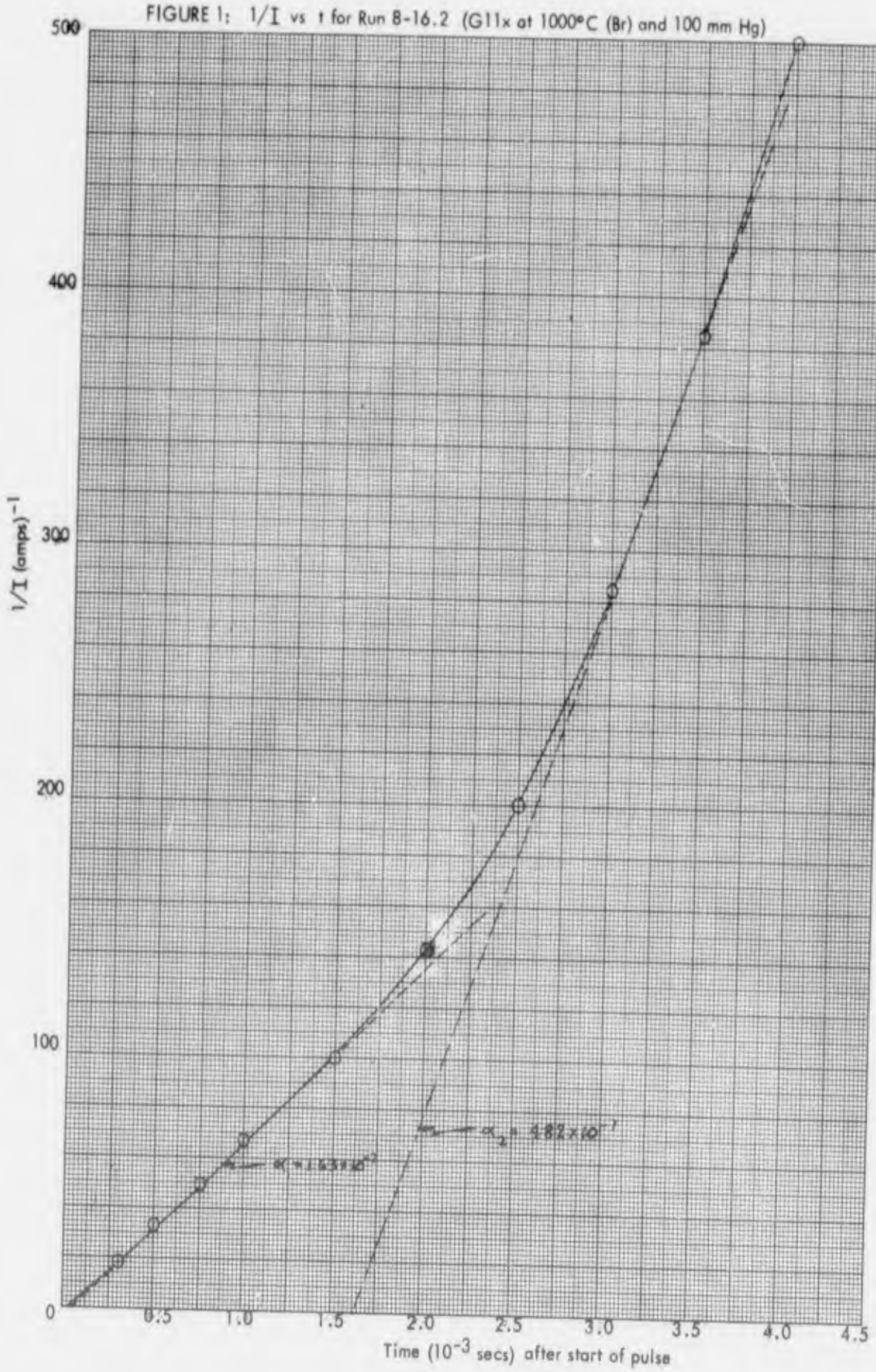

FIGURE 2: Log I vs t for Run 8-16.2 (G11x at 1000°C (Br) and 100 mm Hg)

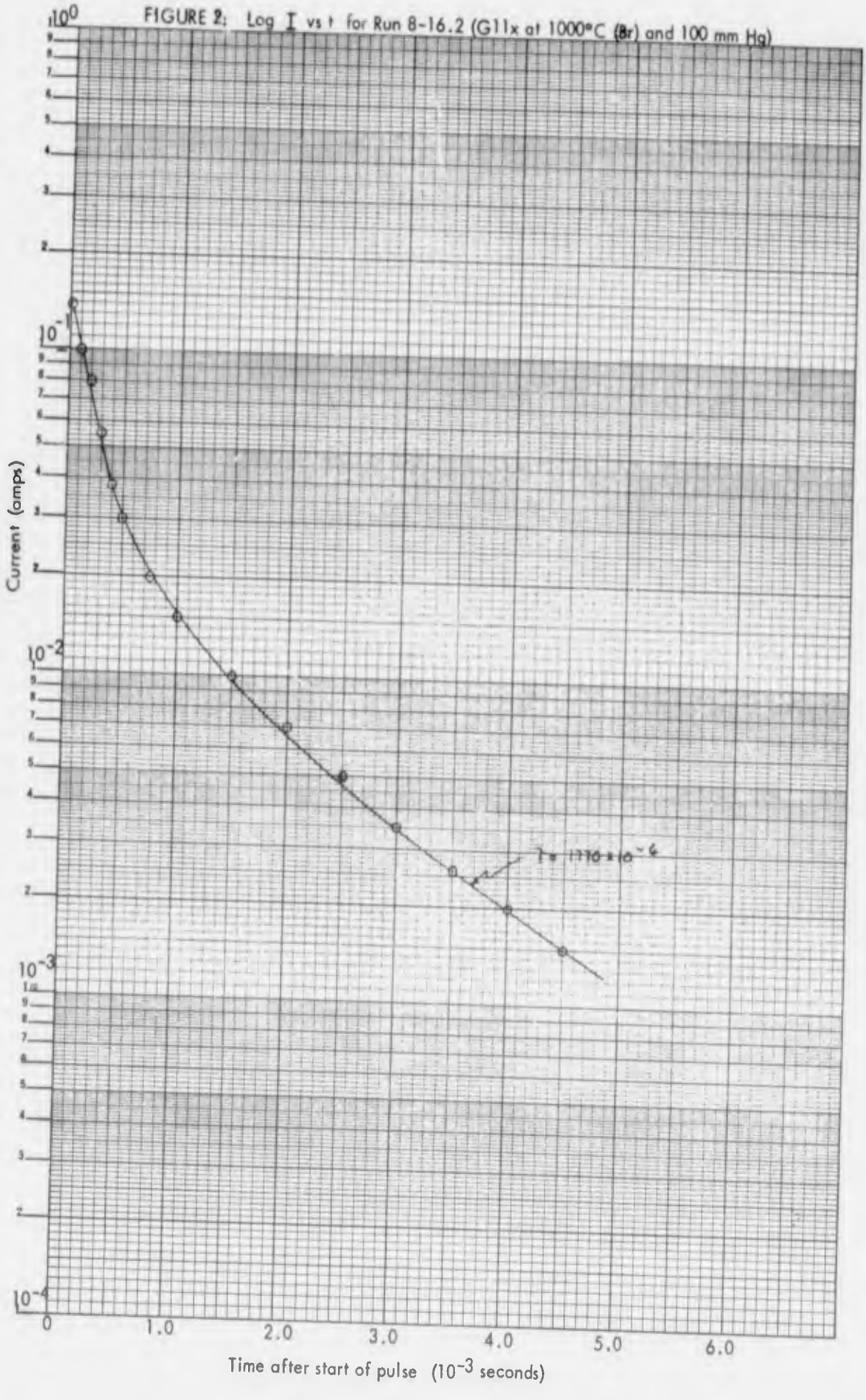

FIGURE 3: τ vs Pressure for G7x - Guard Ring Floating

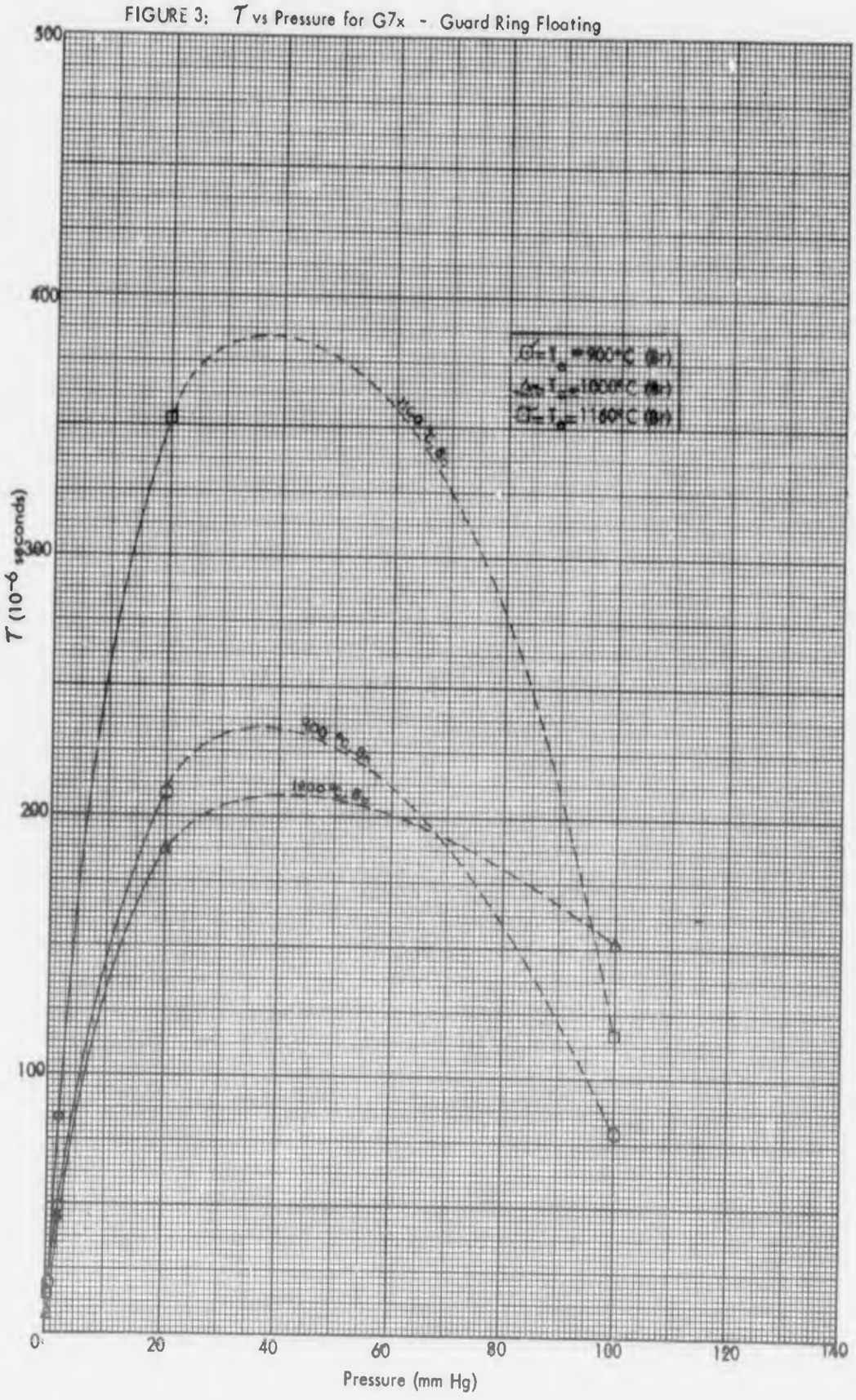

FIGURE 4: τ vs Pressure for G7x - Guard Ring Tied to Collector

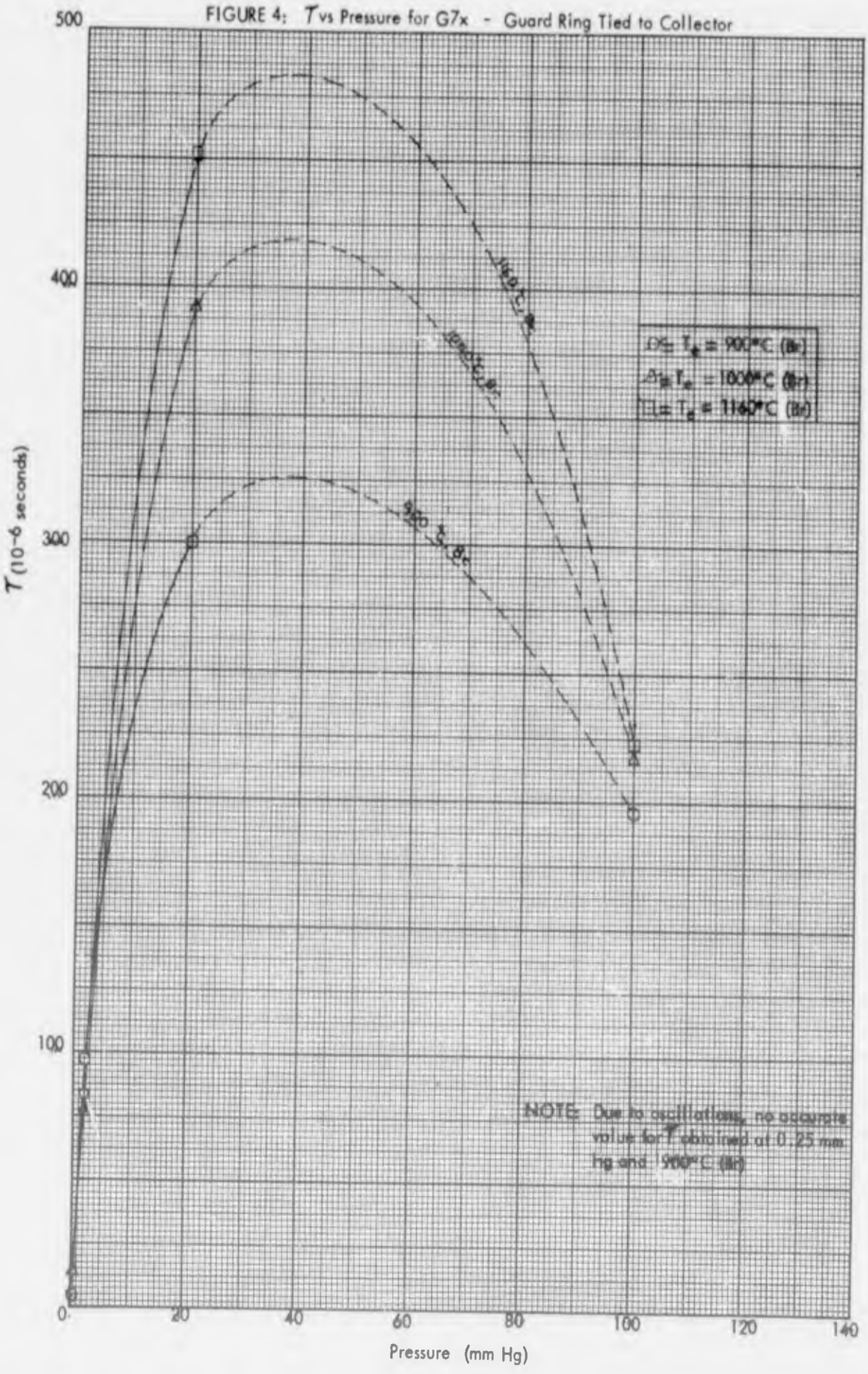

FIGURE 5: τ vs Pressure for G11x

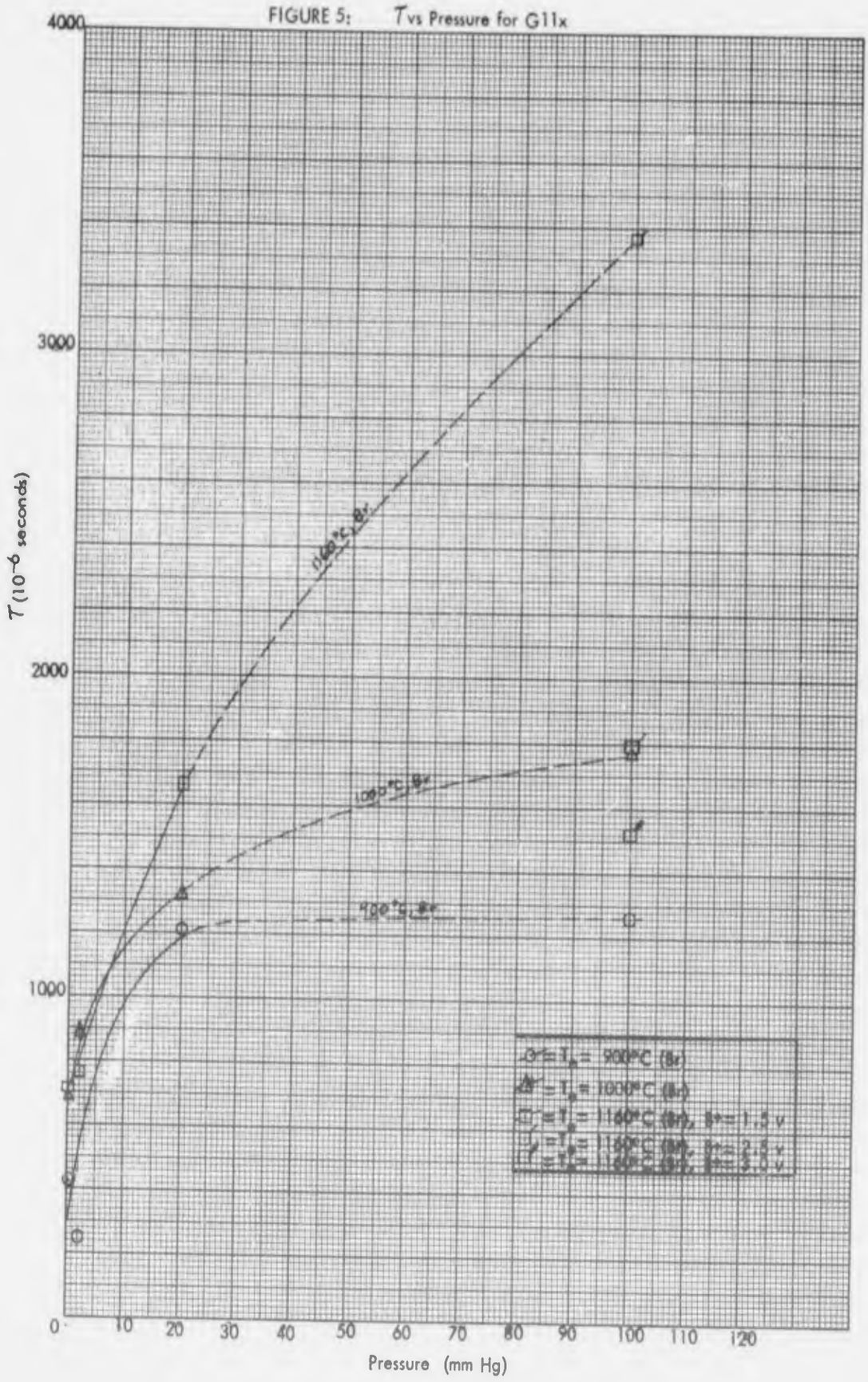

FIGURE 6: Run 8-16.2 (G11x at 1000°C (Br) and 100 mm Hg)

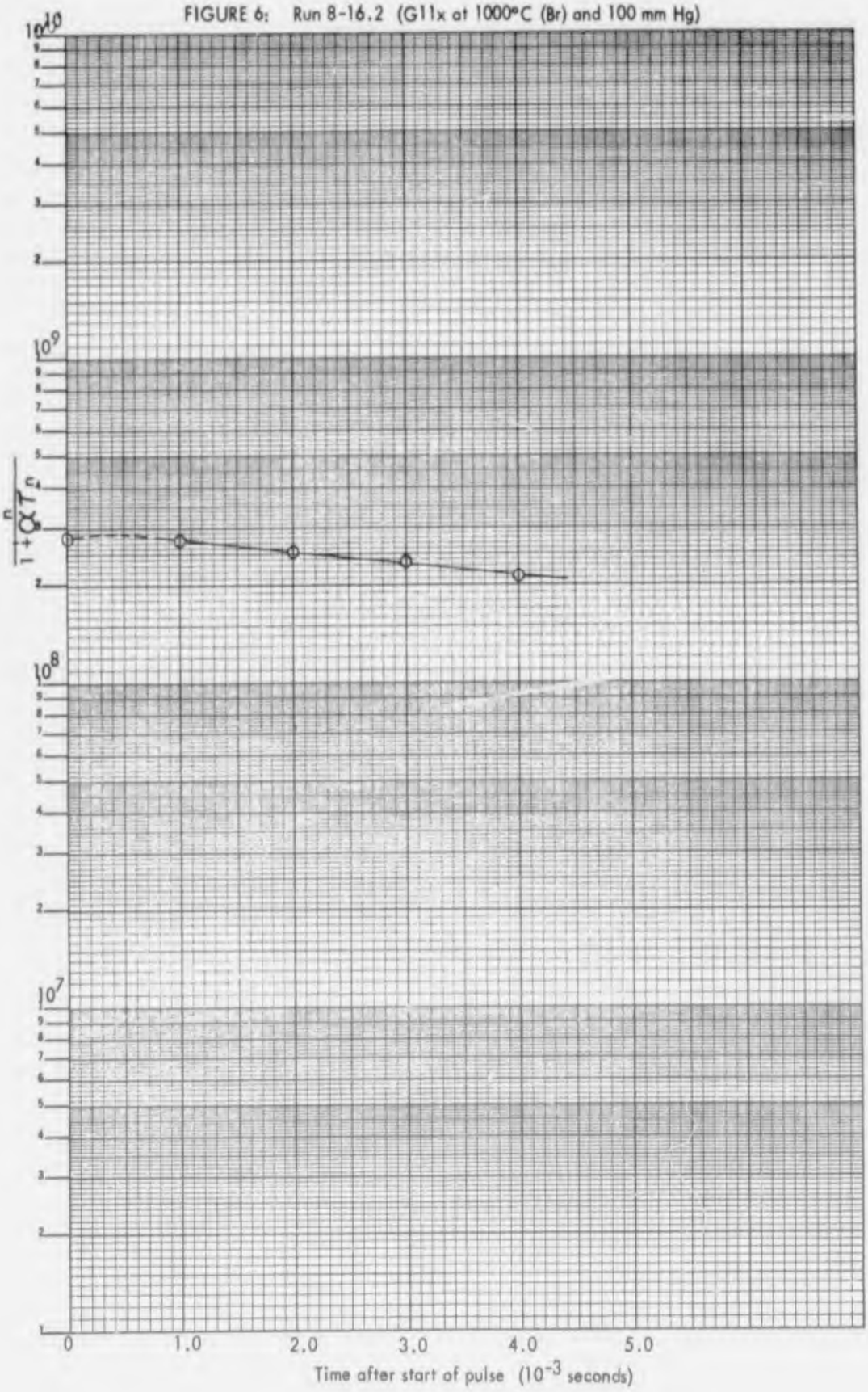

FIGURE 7: Run 8-20.1 (G7x at 1000°C (Br) and 100 mm Hg) Guard Ring Tied to Collector

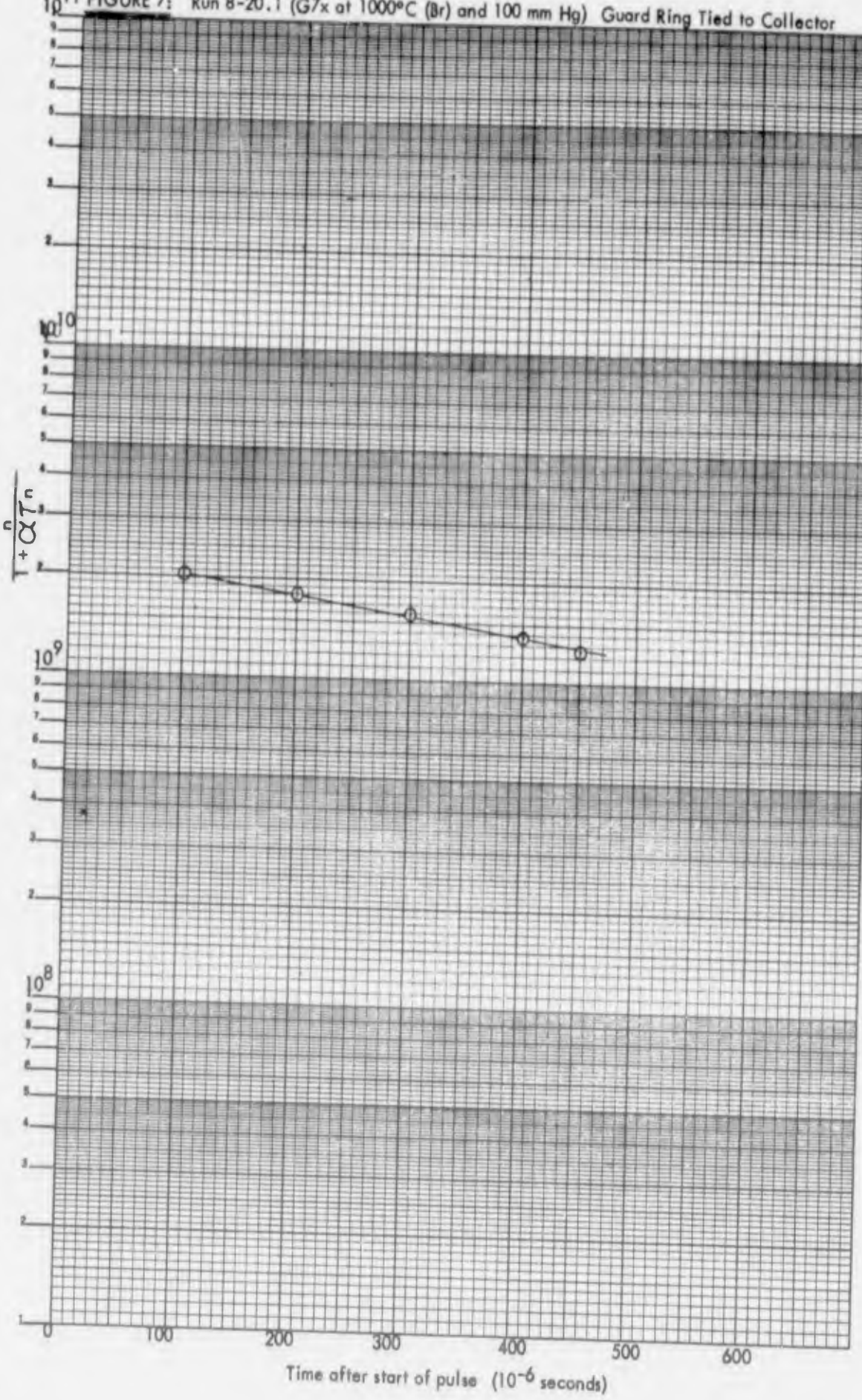

SECTION C

ELECTRON MOBILITY IN GASES

W.P.Allis* and F. E. Jamerson
General Motors Research Laboratories, Warren, Michigan

Abstract

Electron mobility in gases is an important quantity in determining plasma resistivity in a weakly ionized gas. Unfortunately the literature does not contain all values of interest and it is sometimes necessary to convert collision probability data into mobility or drift velocity data. This report summarizes the relevant definitions and theory and gives a compilation of mobilities for helium, neon, argon, krypton and xenon.

Definition

The reduced pressure p_o of a gas for this report is defined by+:

$$p_o = 300\, p/T_K \tag{1}$$

where p is the observed gas pressure, T_K the gas temperature in degrees Kelvin, T_g the gas temperature in electron-volts

$$T_K = 11600\, T_g \tag{2}$$

The reduced pressure is really a measure of the molecular concentration

$$n_g = 3.22 \times 10^{16}\, p_o \text{ molecules cm}^{-3} \tag{3}$$

when p_o is in Torr.

The misnamed "probability of collision" P_c is the total collision cross section of all the molecules in a cubic centimeter of gas at one Torr reduced pressure, so

$$p_o P_c = n_g\, q \tag{4}$$

or

$$P_c = 3.22 \times 10^{16}\, q \text{ cm}^{-1} \tag{5}$$

where q is the cross section for elastic scattering (cm^2).

---

* Professor W. P. Allis of MIT was consultant to General Motors Research Laboratories.

+ Brown[1] defines $p_o = 273\, p/T_K$ however in this report use is made of drift velocity data plotted in terms of the reduced pressure of equation (1).

The collision probability is directly related to the mean free path

$$l = 1/p_o P_c \text{ cm} \tag{6}$$

An electron beam of intensity I is reduced by dI in traveling a path dx (or a time $dt = dx/v$) due to collisions

$$dI/I = - p_o P_c dx = - \nu_c dt \tag{7}$$

which defines the collision frequency

$$\nu_c = p_o P_c v = p_o P_c \sqrt{2 e V_b/m} \text{ sec}^{-1} \tag{8}$$

in terms of the voltage V_b used to accelerate the beam.

Electron Mobility Theory

The theory of mobility makes use of a "collision frequency for momentum transfer"

$$\nu_m = \nu_c \overline{(1 - \cos \phi)} \tag{9}$$

which takes no account of small angle deflections ($\phi \approx 0$) but counts large angle deflections ($\phi \approx \pi/2$) twice. The relations between ν_m, ν_c, and the experimental P_c are somewhat ambiguous as the measurements do not count small angle deflections either due to the finite size of the beam catcher. It is customary to neglect the difference between ν_m and ν_c and use equation (8) for either one.

The collision frequency ν_m acts as a friction force on an electron swarm so that its equation of motion in an ac field $Ee^{i\omega t}$ may be written

$$m \, dv_d/dt + \nu_m v_d = -e E \exp i\omega t \tag{10}$$

This gives for the drift velocity of the swarm

$$v_d = - \frac{e/m}{\nu_m + i\omega} E = - \mu E \tag{11}$$

and hence for the dc mobility

$$\mu = \frac{e}{m \nu_m} = \frac{\sqrt{e/2m V_b}}{p_o P_c} \text{ cm}^2 \text{ volt}^{-1} \text{ sec}^{-1} \tag{12}$$

and

$$v_d = \sqrt{\frac{e}{2m V_b}} \frac{E}{p_o p_c} \quad \text{cm sec}^{-1} \tag{13}$$

The collision frequency ν_m is a function of the electron's speed v, that is of V_b, and equation (12) should be averaged over a distribution function f(v).

The current average is derived from Boltzmann theory[2] and is

$$\mu = -\frac{e}{m} \frac{4\pi}{3} \int_0^\infty \frac{v^3}{\nu_m(v)} \frac{\partial f}{\partial v} \, dv \tag{14}$$

If the distribution is Maxwellian

$$f = \left(\frac{m}{2\pi k T_K} \right)^{3/2} \exp - V_b/T_g \tag{15}$$

This yields

$$\mu = \frac{4\pi e}{3 k T_K} \int_0^\infty \frac{v^4}{\nu_m(v)} f \, dv \tag{16}$$

This formula leads to Eq. (12) when ν_m is independent of v. On the other hand if the mean-free-path $l = v/\nu_m$ is constant one finds[3]

$$\mu = \frac{8\pi}{3} \frac{el}{m} \sqrt{\frac{m}{2\pi k T_K}} \tag{17}$$

The diffusion coefficient D ($\text{cm}^{-2}\ \text{sec}^{-1}$) is obtained from the mobility μ by the Einstein relation[2]

$$\frac{D}{\mu} = \frac{m \bar{v}^2}{3e} = T_g \tag{18}$$

Mobility from Collision Probability

The distribution function f is frequently not Maxwellian and in order to use the simpler formula (12) and the experimental plots of P_c vs. $\sqrt{V_b}$ it is necessary to be able to select the proper electron speed $\sqrt{V_b}$ corresponding to a given value of applied field E/p_o. This can be done in terms of the equipartition theorem.

Consider a frame of reference moving with the average electron velocity v_d. In this frame the gas has a wind velocity $- v_d$ and therefore the gas particles of mass M have a mean kinetic energy

$$\frac{1}{2} M v_d^2 + \frac{3}{2} e T_g$$

Due to collisions the electrons acquire a random kinetic energy

$$\frac{1}{2} m v^2 = e V_b$$

equal to the mean kinetic energy of the particles with which they are colliding

$$e V_b = \frac{1}{2} M v_d^2 + \frac{3}{2} e T_g \tag{19}$$

Equations (13) and (19) give the proper coordinate transformations to go from a plot of P_c vs. $\sqrt{V_b}$ to v_d vs. E/p_o. They may be rewritten

$$v_d = \sqrt{\frac{2 e V_b}{M}} \sqrt{1 - \frac{3 T_g}{2 V_b}} \tag{20}$$

$$\frac{E}{P_o} = \sqrt{\frac{4m}{M}} V_b P_c \sqrt{1 - \frac{3 T_g}{2 V_b}} \tag{21}$$

Equations (20) and (21) can be used to determine μp_o from P_c and V_b.

Equation (19) relates to electrons which have come to dynamic equilibrium with the gas through which they are diffusing. This is not always the case, particularly when the electrons come from a hot cathode. Whenever the temperature T_- of the electrons has a constant known value one should use $V_b = 3T_-/2$ in equations (12) and (13) along with a collision probability corresponding to this value of V_b. The mobility as computed from (12) will be a constant up to a value of E/p_o where electron heating due to the field takes place. This is satisfied for a μ from (12) with $V_b = 3/2\, T_-$.

$$\mu = \frac{\sqrt{e/3\, m T_-}}{P_o P_c} \tag{22}$$

Computations

The collision probability data of Ramsauer and Kollath[4] are used to compute the electron drift velocity as a function of E/p_o using equations (20) and (21). Comparison is made to the data of Park and Phelps[5] (P.P.) and Bowe[6].

The electron mobility is calculated in reduced pressure units from:

$$\mu' = v_d (E/p_o)^{-1} \text{ cm}^2 \text{ Torr sec}^{-1} \text{ volt}^{-1} \quad (23)$$

Thus the mobility is given by

$$\mu = \mu'(p_o)^{-1} \text{ cm}^2 \text{ sec}^{-1} \text{ volt}^{-1} \quad (24)$$

A compilation of all the calculations is given in Table 1. Values of μ' are given for all the computed points and μ' is computed from experimental data only in the range of E/p_o where theory and experiment do not agree.

Helium

The P.P. data for electron drift velocity in helium are shown in Fig. 1 with the calculated values of drift velocity. Ramsauer's data for P_c are given in Figs. 2 and 3. The points for $3 < E/p_o < 0.2$ are computed from P_c of Fig. 2 and show good agreement with data around an E/p_o of 1.0. In order to extend the analysis to values of $E/p_o < 0.2$, assumed values of P_c are used. Ramsauer's data are given only to 0.25 volts whereas calculations require P_c for $V_b < 0.25$. Consequently values of P_c and V_b were computed to fit the analysis and experiment for $E/p_o < 0.2$ with T = 300°K. The P_c values used are shown in Fig. 3 with the resulting drift velocity plotted in Fig. 1. The value for P_c at 0.2 volt is above Ramsauer's data if it were extrapolated, however the values at $V_b < 0.1$ volt indicate a constant magnitude of 20 cm^{-1} for P_c which gives good agreement for v_d with P.P. data. This is a reasonable value of P_c on the basis of the relative flatness of P_c for $V_b < 1$ volt.

Using these same values of P_c but taking T = 77°K gives good agreement between the computed values of v_d and experiment as shown in Fig. 1. This agreement is consistent with the conclusion of P.P. who analyzed their data for a momentum transfer cross section and found it to be constant for electron energies from 0.003 to 0.05 volts. This is the

range of voltage values over which a constant P_c was assumed as seen in Table 1.

From (5) the collision cross section for a $P_c = 20$ as assumed in Fig. 3 is 6.2×10^{-16} cm^2 which is in reasonable agreement with the value of 5.3×10^{-16} cm^2 computed by P.P. from their data.

Neon

Drift velocity versus E/p_o is given in Fig. 4 with Ramsauer's data in Figs. 5 and 6. Values of v_d computed for $0.05 < E/p_o < 0.6$ are in reasonable agreement with P.P. data. Computations for $E/p_o < 0.05$ were made using assumed P_c values for low V_b to fit computations to P.P. data. These assumed points are shown in Fig. 6 where a P_c decreasing with V produces the best fit made for a T = 300°K. This dependence of P_c on V_b is consistent with the trend of Ramsauer's data at low V_b, however the assumed point at 0.2 volt is 50% higher than Ramsauer's data. Applying these assumed values of P_c to the theory with T = 77°K gives v_d values in Fig. 4 which show good agreement between computations and P.P. data.

Argon

The drift velocity data for argon (Fig. 7) indicate a reversal in temperature dependence from that of helium and neon in that at a fixed E/p_o the drift velocity increases with gas temperature. Ramsauer's data of Figs. 8 and 10 are used to compute values for $0.01 < E/p_o < 1.0$ which exhibit a poor fit to the data of P.P. as seen in Fig.7. To obtain a fit to data for $E/p_o < 2 \times 10^{-3}$ in the temperature dependent part of the data, two different values of P_c need to be used as seen in Figs.7 and 8. All of these values, but one, lie at voltage values below Ramsauer's data. Only the trend of P_c, which is increasing for very low V_b, is consistent with Ramsauer's data but the magnitudes are smaller than if his data were extrapolated. It is noted that the drift velocity calculation is quite sensitive to

P_c as the assumed values for these two temperatures are not far apart over a portion of this voltage range. Two points were computed to indicate the change in P_c necessary to arrive at a v_d consistent with P.P. data for $E/p_o > 10^{-2}$. These are shown at $V_b = 0.4$ and 0.8 in Fig. 8 to be a factor of 3 and 2 respectively higher than Ramsauer's data.

Krypton

Ramsauer's data for krypton are given in Figs. 9 and 10 and drift velocity in Fig. 11. The data for v_d are from Bowe where a log-log plot has been made of his linear presentation so that some error may exist in the first part of the curve at low E/p_o. The calculated drift velocity using Ramsauer's data for P_c does not agree with Bowe's data except at one cross point for $E/p_o = 1.7$ and both curves are parallel over the lower range of E/p_o. Using values of P_c below the Ramsauer minimum at $V_b = 0.5$ volt results in a v_d which decreases while E/p_o increases. Additional v_d data are required before estimating what the magnitude of P_c is at low V_b.

Xenon

Xenon data for P_c are given in Figs. 9 and 10 and drift velocity in Fig. 12. Data for v_d are due to Bowe and computations and results are similar to those for krypton. Again agreement between theory and experiment is exhibited at only one cross point and computed drift velocity is 50% higher than Bowe's data over most of the curve.

Summary

A method has been developed for converting electron collision probability data to drift velocity which subsequently allows a mobility to be computed. Computations for $E/p_o > 10^{-2}$ show good agreement with recent data of drift velocity for helium and neon whereas poor agreement is exhibited for argon, krypton and xenon. At $E/p_o < 10^{-2}$ insufficient collision probability data preclude making accurate computations. However fitting

drift velocity data with the appropriate P_c indicate agreement with the extrapolated trend of the collision probability data for helium, neon and argon.

References

1. S. C. Brown, Basic Data of Plasma Physics, Technology Press (1959).
2. W. P. Allis, Motion of Ions and Electrons, MIT Report 299 (1956).
3. W. Verweij, Probe Measurements and Determination of Electron Mobility in the Positive Column of Low-Pressure Hg-A Discharges, Philips Res. Rpts., Supplement #2, 1961.
4. C. Ramsauer and R. Kollath, Ann.d Physik, 3, 536 (1929).
5. J. L. Pack and A. V. Phelps, Drift Velocities of Slow Electrons in A, Ne, He, H_2 and N, Phys. Rev. 121, 802 (1961).
6. J. C. Bowe, Drift Velocity of Electrons in He, Ne, A, Kr and Xe. Phys. Rev. 117, 1411 (1960).

TABLE 1

Gas	V (volts)	P_c (cm^{-1})	T (°K)	Computed: v_d ($cm\ sec^{-1}$)	Computed: E/p_o (volts $cm^{-1}Torr^{-1}$)	Computed: μ' ($cm^2 Torr\ volt^{-1}sec^{-1}$)	Experiment: v_d (at computed E/p_o) ($cm\ sec^{-1}$)	Experiment: μ' ($cm^2 Torr\ volt^{-1}\ sec^{-1}$)
Helium	9	15	-	2.1×10^6	3.1 -	6.8×10^5		
	6.25	16.5	-	1.7	2.4 -	7.1		
	4	17.5	-	1.4	1.6 -	8.7		
	2.25	20	-	1.0	1.1	9.1	1.0×10^6	1×10^6
	1.0	19	-	6.8×10^5	4.4×10^{-1}	1.5×10^6	6×10^5	1.3
	0.5	20	-	4.7	2.2	2.1	3.9	1.8
	0.2	29	300	3.0	1.3	2.3		
	0.1	23		1.7	4.2×10^{-2}	4.0		
	0.06	20		1.0	1.7	5.9		
	0.05	20		5.7×10^4	8.6×10^{-3}	6.6		
	0.04	20		2.4	3.2	7.5		
	0.2	29	77	3×10^5	1.3×10^{-1}	2.3		
	0.1	23		2.1	5.1×10^{-2}	4.1		
	0.06	20		1.5	2.6	5.8		
	0.04	20		1.2	1.6	7.5		
	0.02	20		6.9×10^4	6.6×10^{-3}	1.0×10^7		
	0.015	20		4.9	4	1.2		
	0.011	20		2.2	1.5	1.5		
Neon	6.25	9	-	7.8×10^5	5.8×10^{-1}	1.3×10^6	9×10^5	1.6×10^6
	4	8	-	6.2	3.4	1.8	6.2	1.8
	2.25	7	-	4.7	1.7	2.8	4.1	2.4
	1	5.9	-	3.1	6.2×10^{-2}	5	2.7	4.4
	0.2	5.5	300	1.3	1.1	1.2×10^7		
	0.1	3.4		7.6×10^4	2.8×10^{-3}	2.7		
	0.06	2.5		4.5	9.4×10^{-4}	4.8		
	0.05	1.9		2.6	3.7	7×10^8		
	0.2	5.5	77	1.4×10^5	1.1×10^{-2}	1.3×10^7		
	0.1	3.4		9.3×10^4	3.4×10^{-3}	2.7		
	0.06	2.5		6.9	1.4	4.9		
	0.05	1.9		6.2	8.8×10^{-4}	7.1×10^8		
Argon	4	29	-	4.4×10^5	8.5×10^{-1}	5.2×10^5	3.9×10^5	
	2.25	13	-	3.3	2.2	1.5×10^6	2.6	
	1.5	7.5	-	2.7	1	2.7	2.1	
	1.0	4.5	-	2.2	3.3×10^{-2}	6.7	1.7	
	0.7	2.6	-	1.8	1.4	1.3×10^7	1.4	
	0.8	10	-	2	5.9×10^{-2}	3.4×10^6		
	0.4	4	-	1.4	1.2	1.2×10^7		
	0.2	1.1	300	8.8×10^4	1.5×10^{-3}	5.9		
	0.1	1.5		5.4	8.7×10^{-4}	6.2		
	0.06	2.5		3.2	6.5	4.9		
	0.04	4		7.6×10^3	2	3.8		
	0.08	2.7	77	5.9×10^4	1.5×10^{-3}	4.9		
	0.04	5.2		3.8	1.3	2.9		
	0.02	10		2.2	1	2.2		
	0.012	15		9.8×10^3	5.3×10^{-4}	1.8		

TABLE I (Continued)

Gas	V (volts)	P_c (cm^{-1})	T (°K)	Computed v_d ($cm\ sec^{-1}$)	Computed E/p_o (volts cm^{-1} $Torr^{-1}$)	Computed μ' (cm^2 Torr $volt^{-1}$ sec^{-1})	Experiment v_d (at computed E/p_o) ($cm\ sec^{-1}$)	Experiment μ' (cm^2 Torr $volt^{-1}$ sec^{-1})
Krypton	10.6	95	-	4.9×10^5	5.3 -	9.2×10^4		
	9	94	-	4.5	4.4 -	1×10^5		
	6.25	88	-	3.8	2.5 -	1.5	5×10^5	2×10^5
	4	45	-	3	9.6×10^{-1}	3.1	2.2	2.3
	2.25	20	-	2.3	2.3	1×10^6	1.6	7
	1.56	10	-	1.9	7.9×10^{-2}	2.4	1.3	1.6×10^6
	1	4	-	1.5	2.1	7.1		
Xenon	6.25	140	-	3×10^5	3.6 -	8.3×10^4	5×10^5	1.4×10^5
	4	110	-	2.4	1.8 -	1.3×10^5	2.6	1.4
	2.25	50	-	2	5.6×10^{-1}	3.6	1.5	2.7×10^6
	1.56	23	-	1.5	1.4	1.1×10^6	1.1	7.8×10^5
	1.0	8	-	1.2	3.2×10^{-2}	3.7		

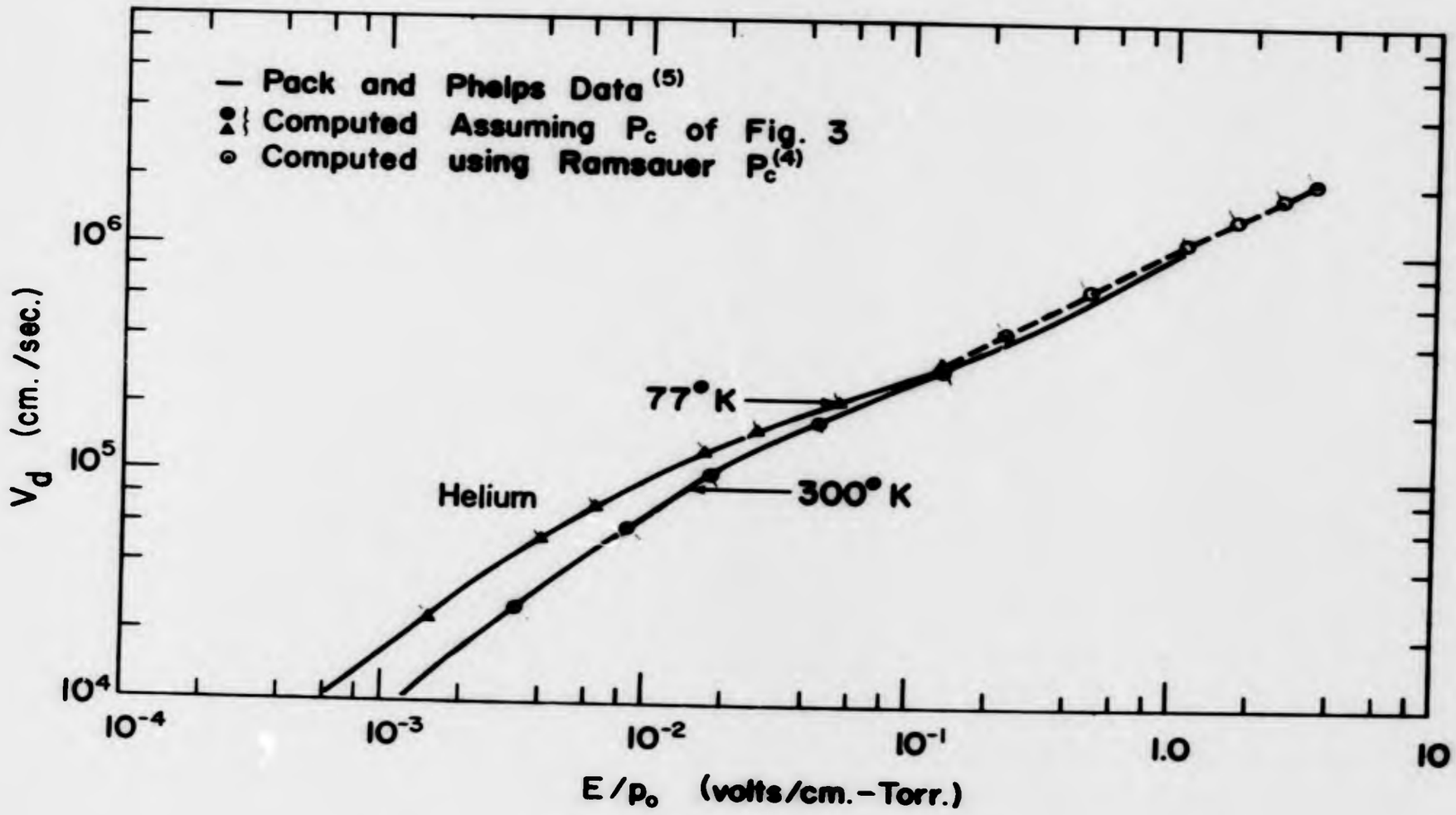

Figure 1 - Electron drift velocity in helium.

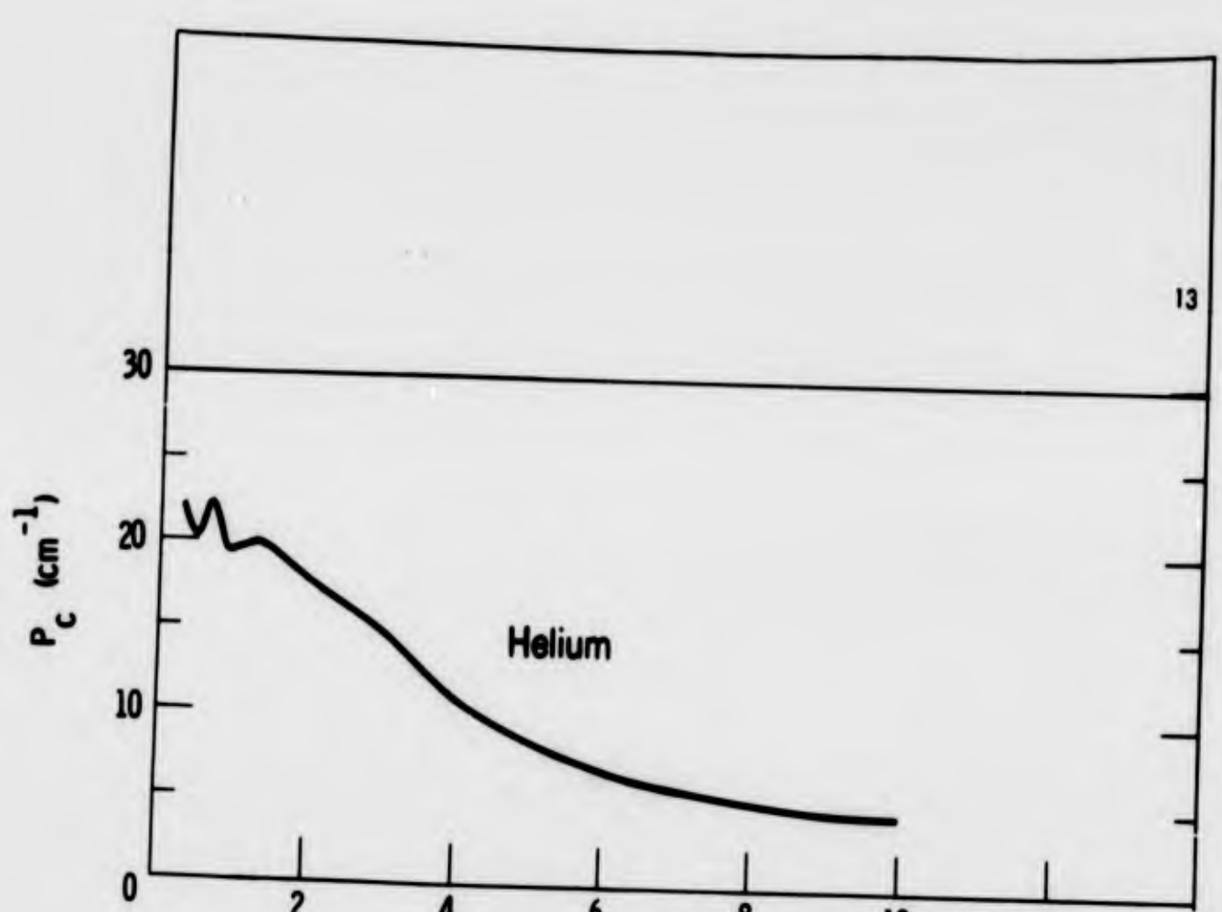

Figure 2 - Collision probability in helium.

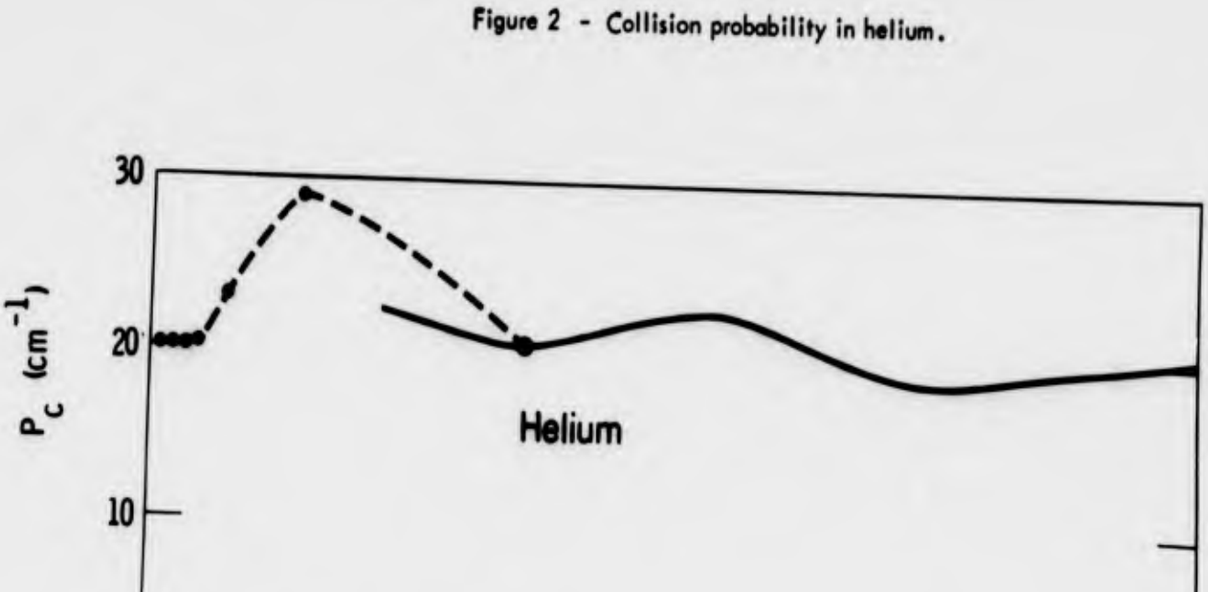

Figure 3 - Collision probability in helium.

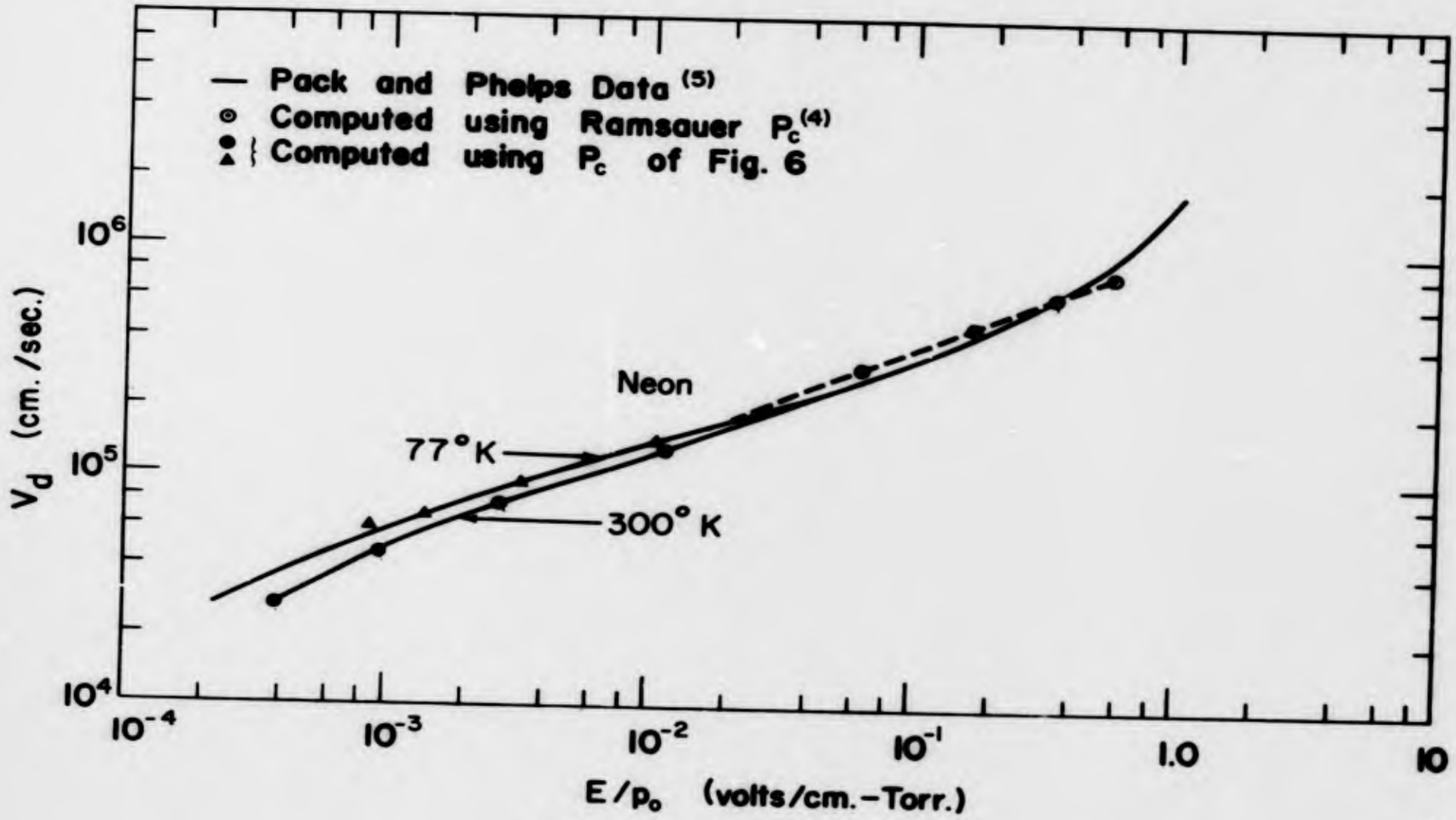

Figure 4 - Electron drift velocity in neon.

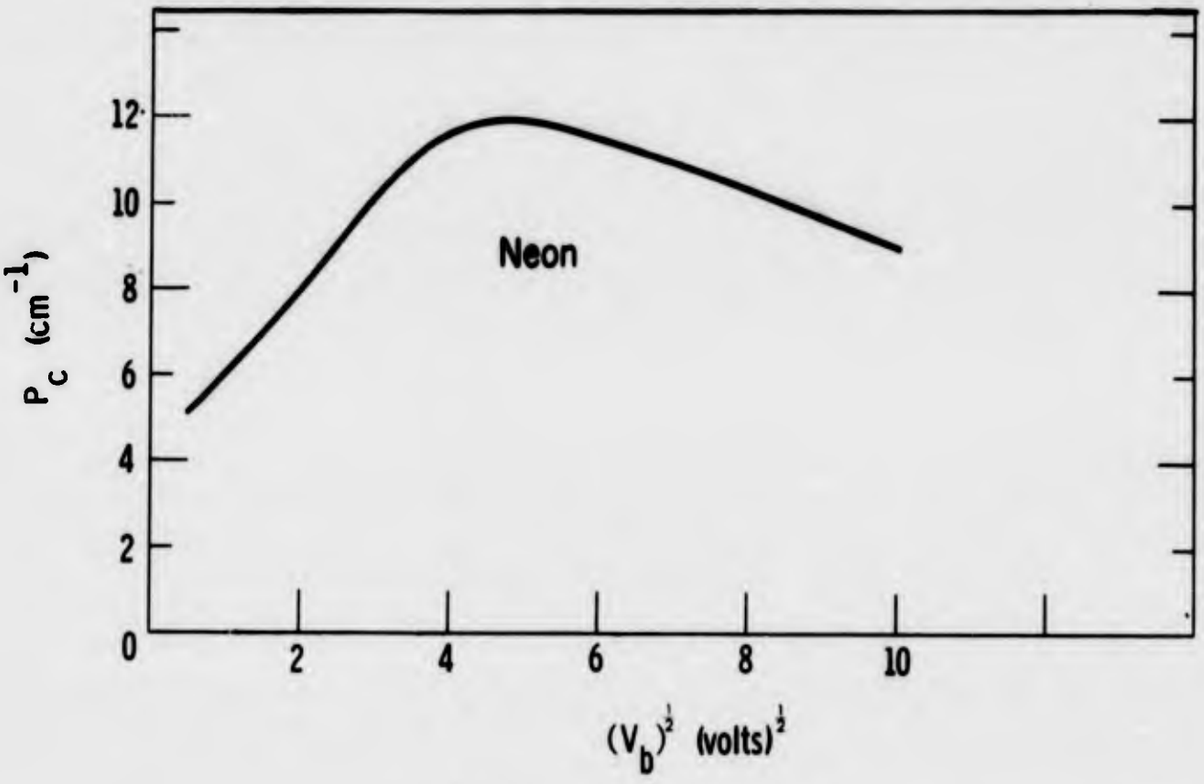

Figure 5 - Collision probability in neon.

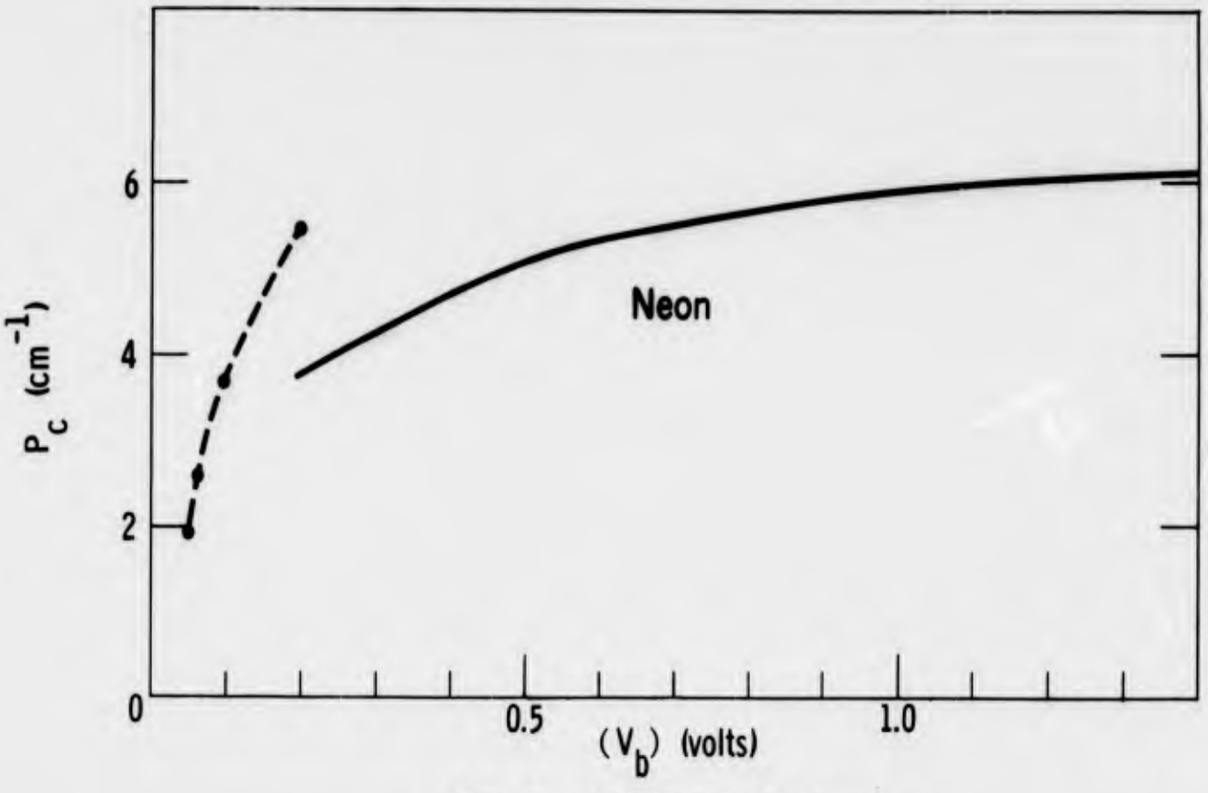

Figure 6 - Collision probability in neon.

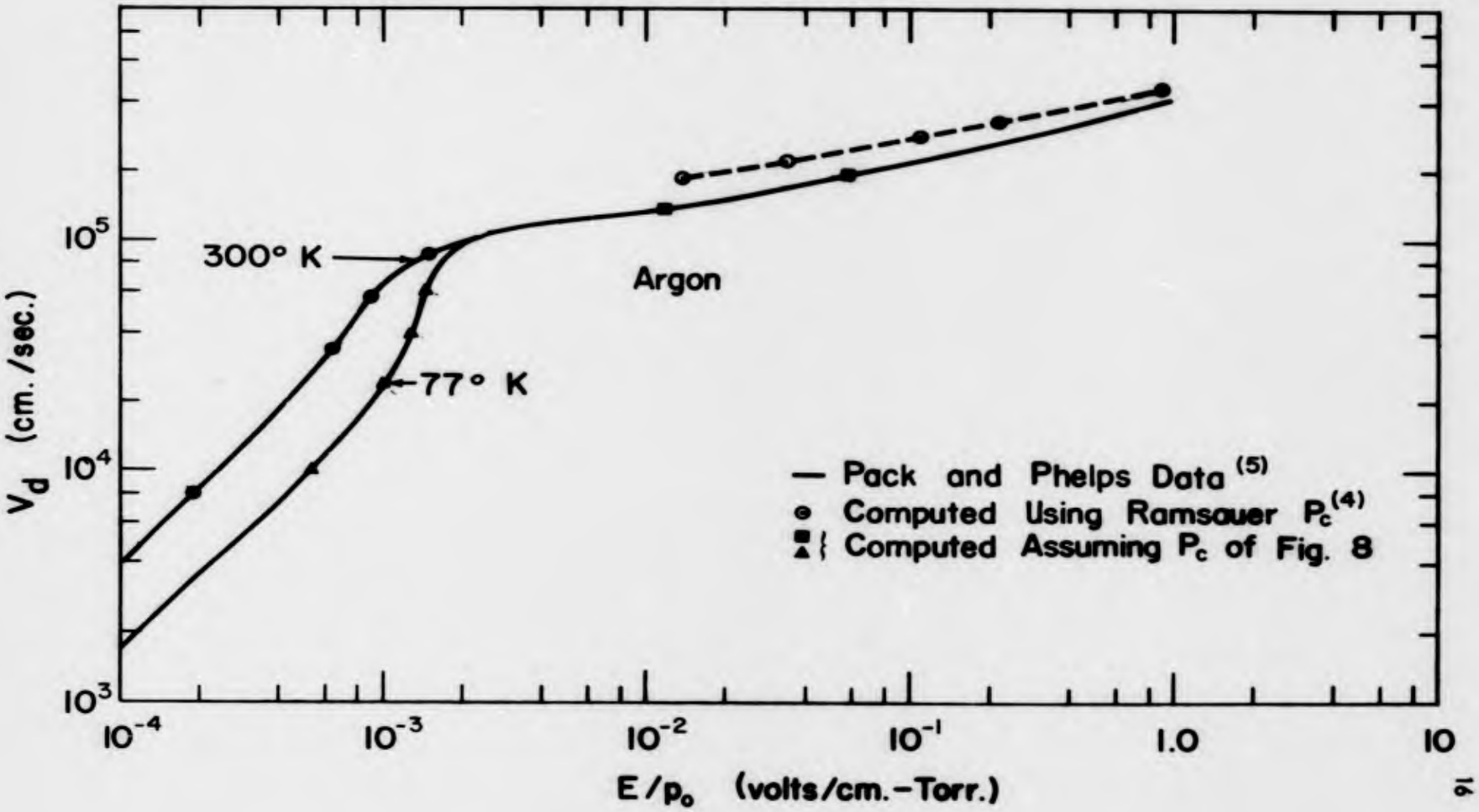

Figure 7 - Electron drift velocity in argon.

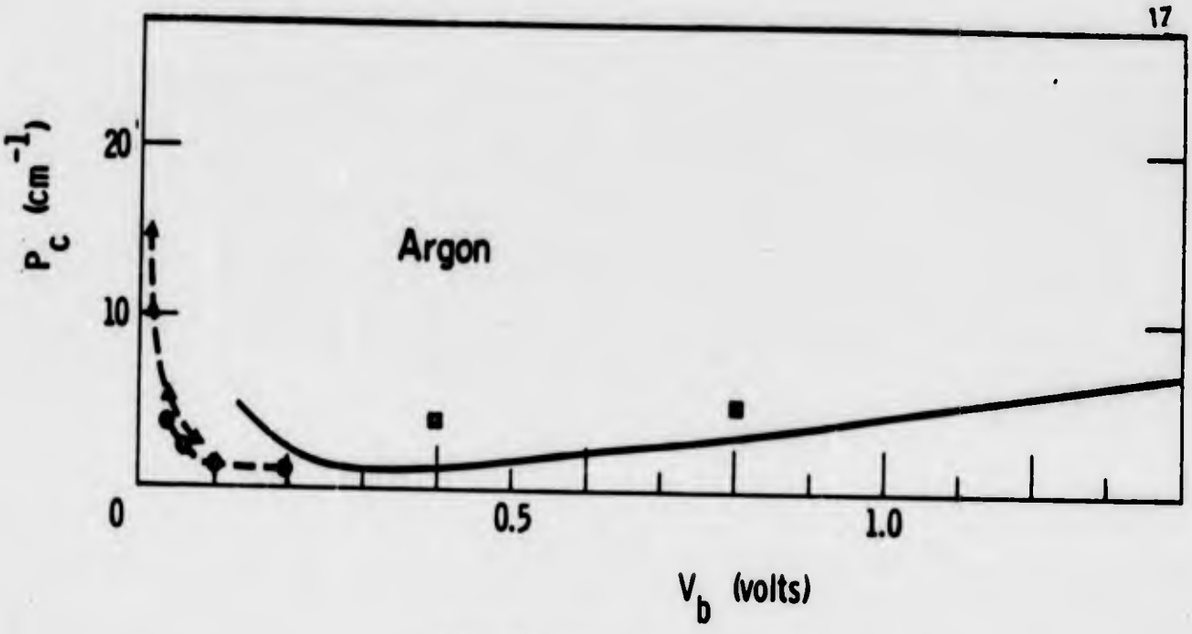

Figure 8 - Collision probability in argon.

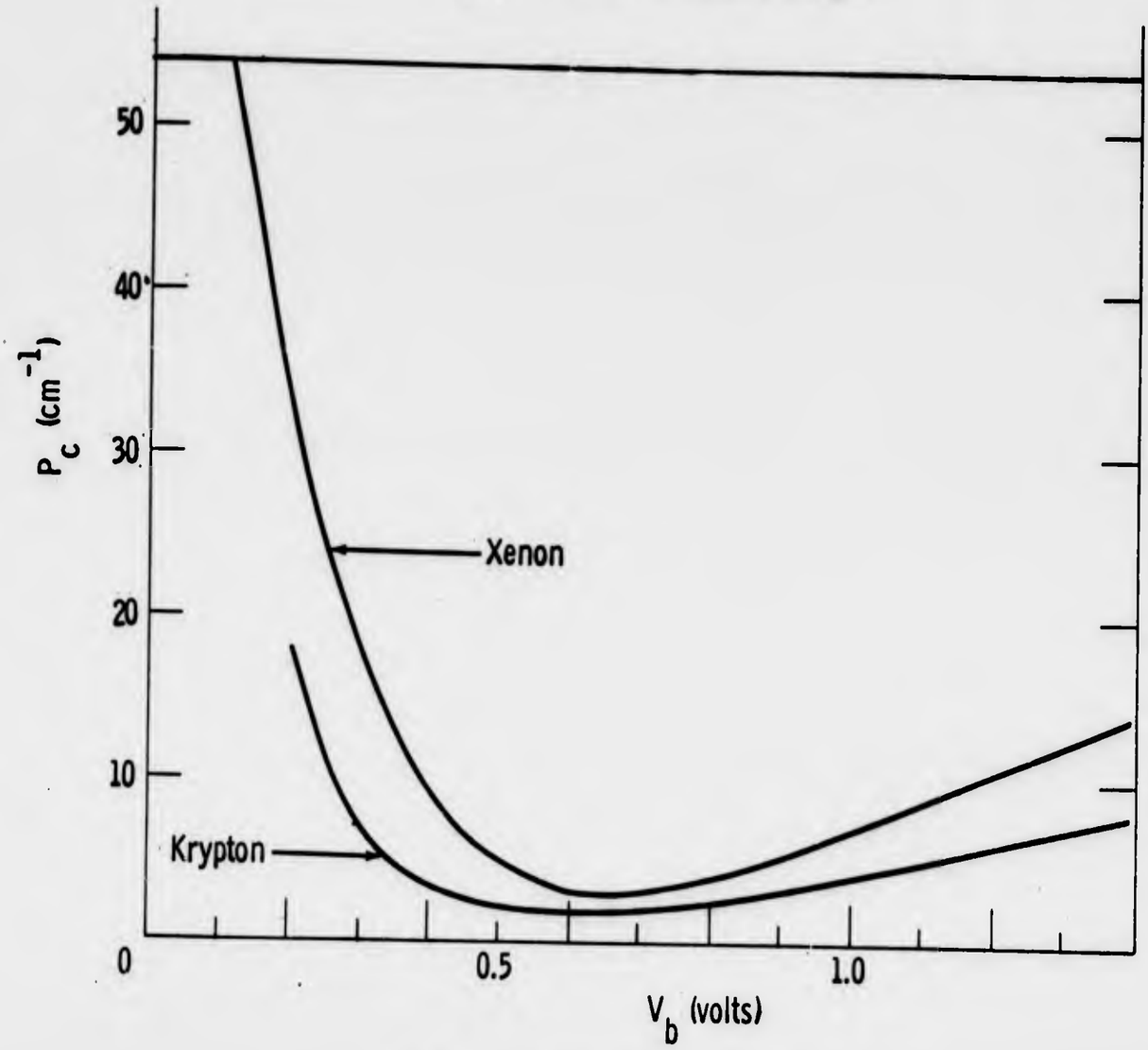

Figure 9 - Collision probability in xenon and krypton.

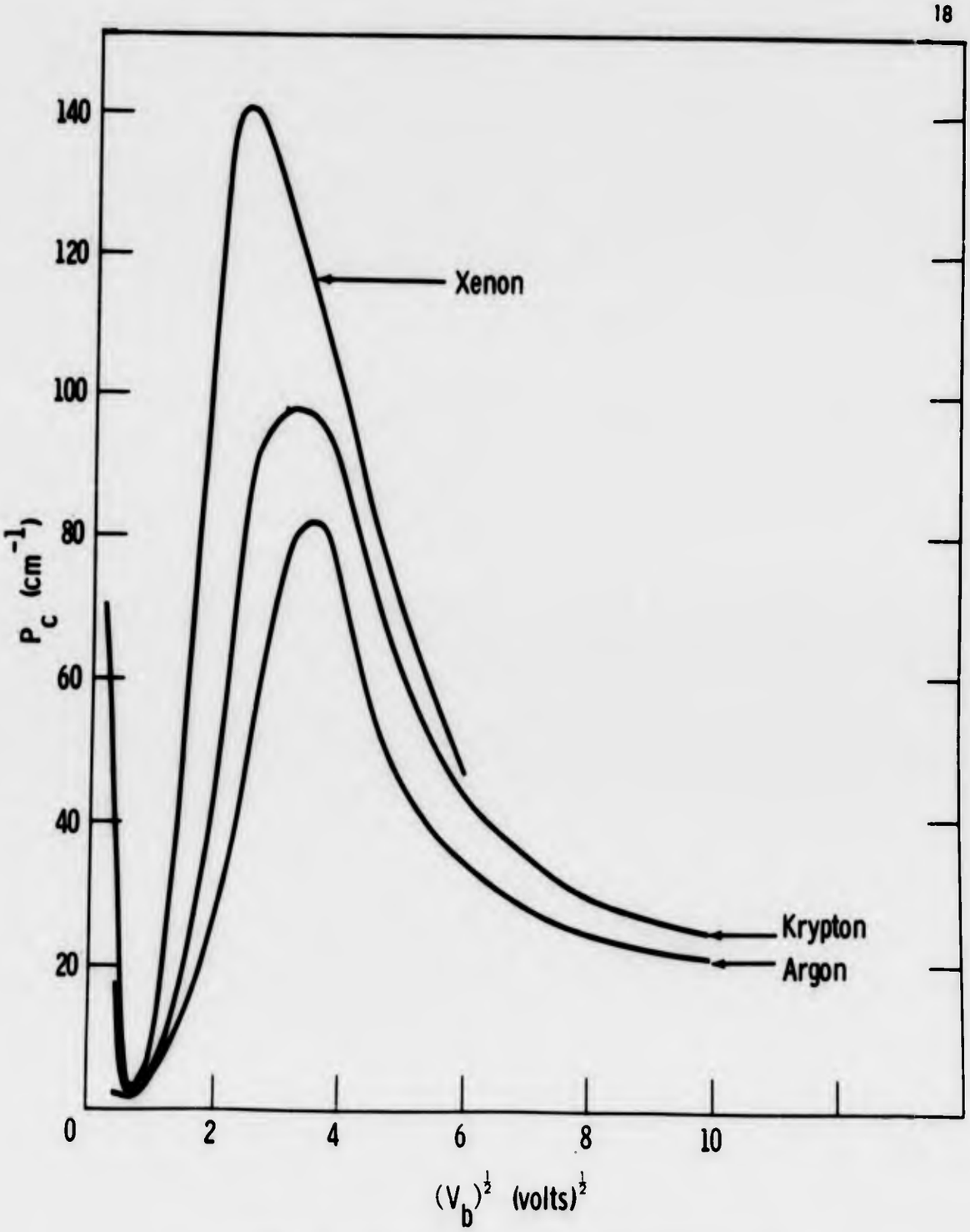

Figure 10 - Collision probability in xenon, krypton and argon.

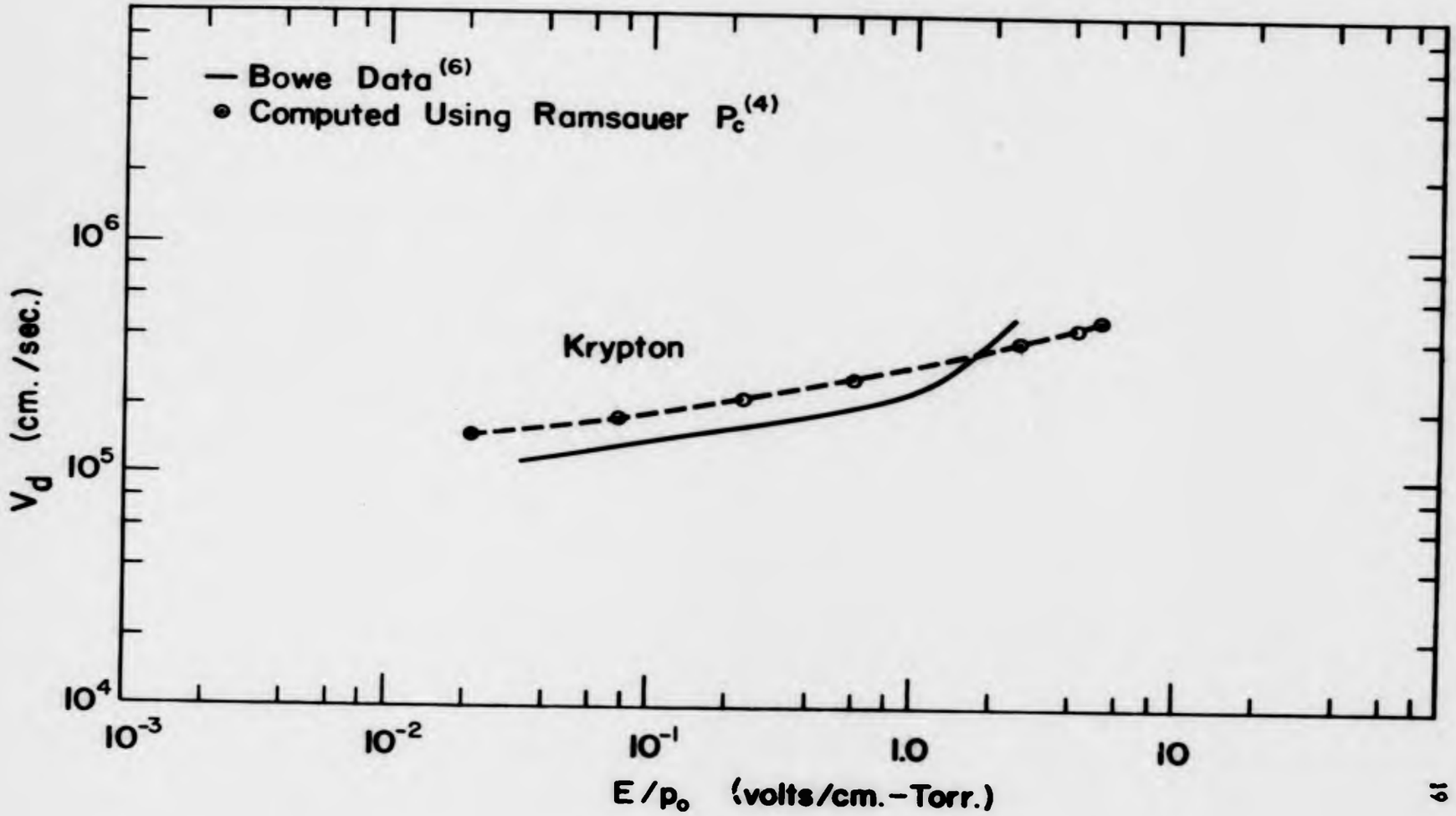

Figure 11 - Electron drift velocity in krypton.

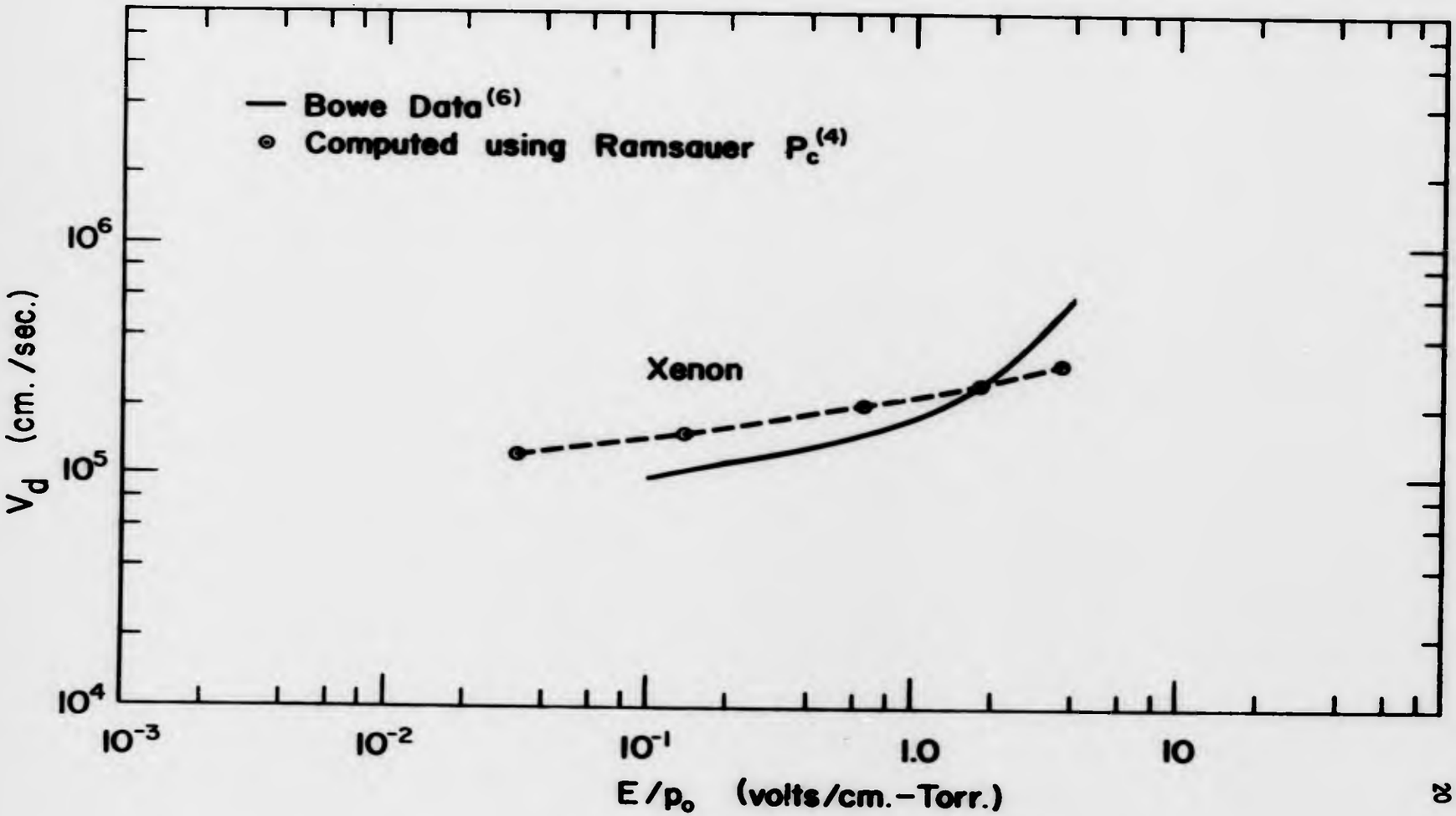

Figure 12 - Electron drift velocity in xenon.

SECTION D

SPECTROSCOPIC MEASUREMENTS IN A CESIUM LOW VOLTAGE ARC CONVERTER

R. J. Donohue and R. F. Majkowski

ABSTRACT

The knowledge of the plasma parameters of a cesium low voltage arc thermionic converter is essential for the development of a detailed analysis of this mode of thermionic converter operation. A converter employing a Philips cathode as emitter and a nickel collector spaced 2 mm apart has been operated in the low voltage arc mode in the retarding field (power producing region) and accelerating field regions. The optical spectra of the plasma generated in the arc was measured and analyzed to determine electron number density and electron temperature.

INTRODUCTION

The operation of a cesium diode in the low voltage arc mode has been discussed in the literature.[1] The low voltage arc allows operation at low emitter temperature (down to 1100°C) and low vapor pressure (0.1 mm of Hg). Operation of the diode at these low pressures allows the emitter-collector gap to be 2 mm without appreciable transport loss in the cesium vapor.

Pressure and emitter temperature values such as the above preclude cesium ionization by surface contact ionization.[2] It has been proposed[3] that in a low voltage arc the sheath at the emitter is accelerating for emitted electrons so that ionization occurs in the bulk of the plasma as a result of electron impact. The potential diagram for this is shown in Figure 1 along with a typical voltage-current characteristic for the low voltage arc. In the figure the arc fires at a positive collector potential, however, under certain conditions (namely higher emitter temperature) the arc can fire in the retarding region.

The use of spectroscopic techniques to study the cesium plasma has been developed[4] and is applied to a low voltage arc thermionic converter described below. The principal objective is to investigate the magnitudes for electron temperature and number density for a characteristic similar to 1a.

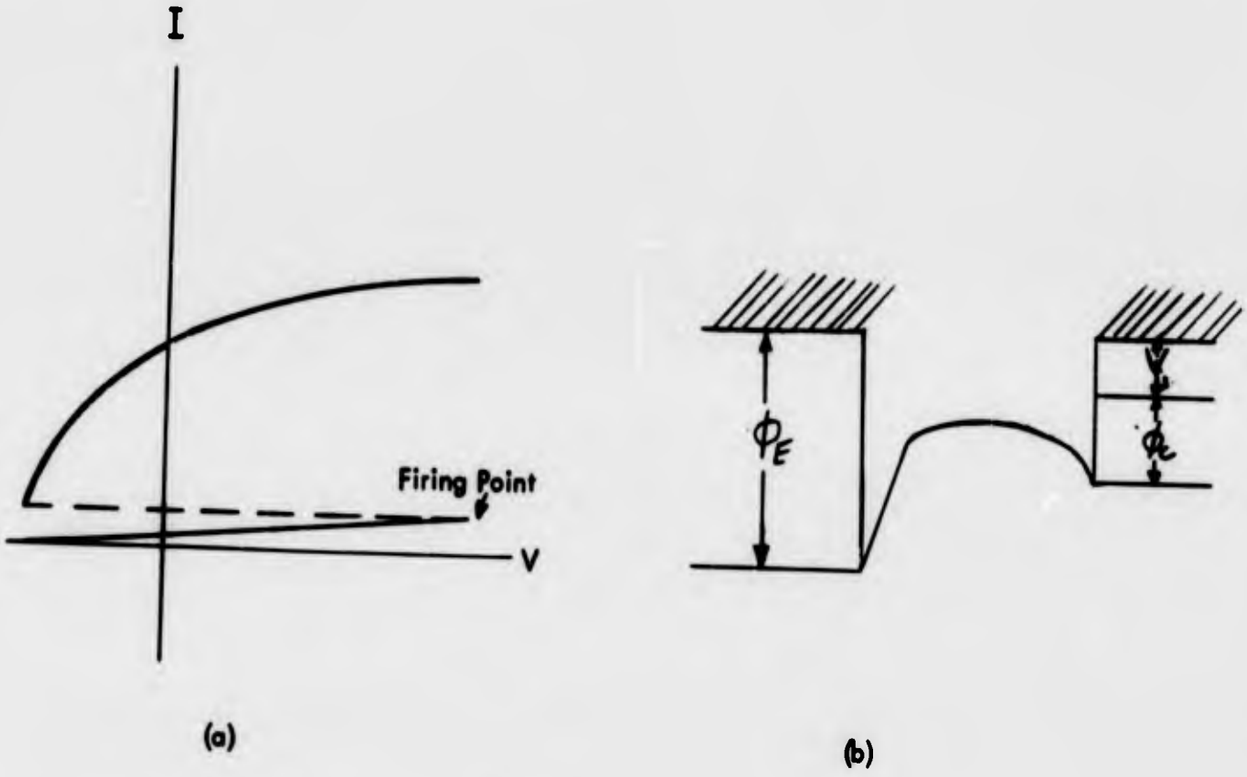

Figure 1

Apparatus

The measurements reported here were compiled on one of several diodes being investigated for low voltage arc mode operation.[5] Although optical measurements were made on several tubes diode C16x provided the most complete set of data. These tubes failed after some 10 to 20 hours of operation due to the cesium vapor attack on the nonex presses.[6] These presses were used in lieu of cesium resistant seals presently under development.

The C16x diode consists of a 3 mm o.d. Philips cathode emitter and 13 mm diameter nickel collector spaced 2 mm apart. Cesium was generated after processing the tube as a vacuum tube by firing cesium chromate pellets which are situated in an arm attached to the side of the tube. The diode was operated in an oven where cesium bath temperature was controlled by a Capacitrol thermocouple controller. Bath temperature was adjusted to allow the diode to operate in the power producing region.

Figure 2 illustrates the circuit employed for recording the V-I characteristic on an oscilloscope. The filament was heated with half wave a.c. and the V-I trace recorded during the off time of the heating pulse by using a blanking circuit on the intensifier in the oscilloscope.

The optical measurements were carried out in the Physical Electronics Laboratory using the Perkin-Elmer spectrometer. The plasma was viewed through a small hole in the oven and the plasma in the entire interelectrode gap was focused on the slit of the spectrometer. A plasma also exists at the base of the tube between the incoming filament leads. This is because six volts or more are required to heat the cathode, and this is enough voltage to create a cesium discharge at the base of the tube. Observations were made to determine whether the radiation from this plasma was detected by the spectrometer when the interelectrode gap was focused

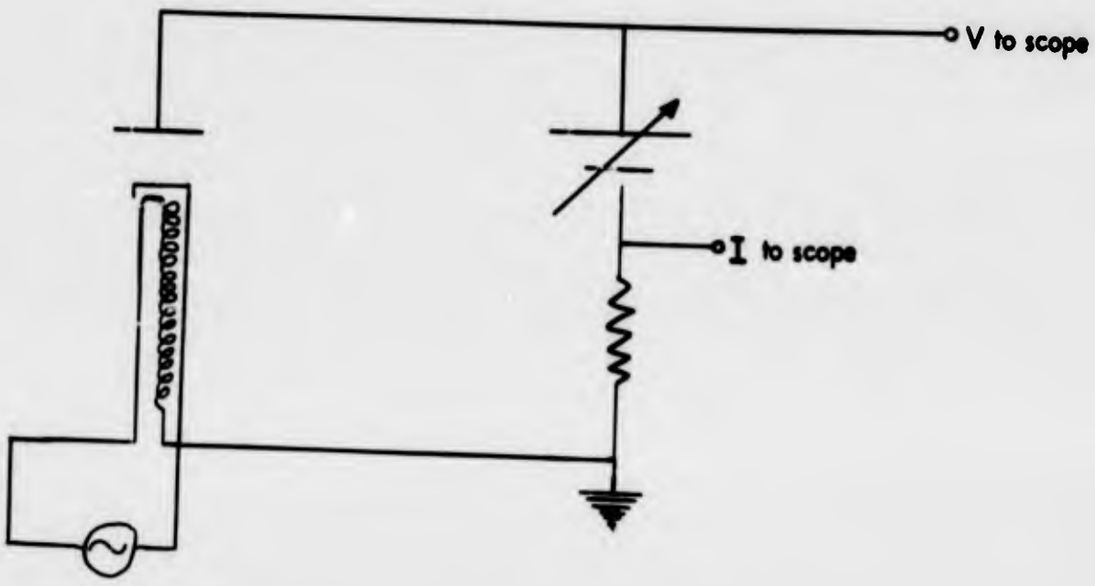

Figure 2

on the spectrometer slit. These observations indicated that this unwanted radiation was not detected. Also, the intensity of the Cs 4555Å line was observed as a function of time by means of an oscilloscope tracing of the output of the photomultiplier detector. This was done to see whether the intensity and hence the plasma temperature changed during the period of the cathode heating cycle. No change in this intensity was observed during this cycle so that it is assumed that the plasma parameters are independent of the heating cycle and can be considered to be constant with time.

Spectroscopic Theory

Recent theoretical calculations of the oscillator strengths of many spectral lines of cesium have been made by P. Stone of Los Alamos.[7] The last reported spectral measurements made at our laboratories used the principal series of cesium[4] since these lines were the only ones for which the oscillator strengths were known. However, the principal series lines ($nP-6S_{1/2}$ transitions) are self reversed because the lower state is the ground state of the atom and the intensity of these lines must be corrected for this effect. The evaluation of the oscillator strengths for lines from other series allows a choice of non principal series lines for absolute and relative intensity measurements.

Figure 3 is a display of some of the electronic states of cesium with the arrows indicating the transitions for some of the more prominent lines. Lines from $S \rightarrow P$ or $D \rightarrow P$ transitions will not be reversed in the cold cesium layer between the plasma and viewing port. Also, in low temperature plasmas these lines will not be significantly reversed in the plasma itself. A strong line should be used for absolute intensity measurements and a pair of lines with a large energy difference between their upper states should be chosen for the relative intensity measurements (a large energy gap leads to an accurate evaluation of the electron temperature). The

$7\,^2S_{1/2} \rightarrow 6\,^2P_{1/2}$ transition (13,589Å) was used for the absolute intensity measurements and this line was combined with the $8\,^2D_{3/2} \rightarrow 6\,^2P_{1/2}$ transition (6010Å) for the relative intensity measurements.

The intensity ratio of any two optically thin lines is:[4]

$$\frac{I_{ul}}{I_{u'l'}} = \frac{f_{lu}}{f_{l'u'}} \frac{(\nu_{ul})^3}{(\nu_{u'l'})^3} \frac{g_l}{g_{l'}} e^{-(E_u - E_{u'})/kT} \qquad (1)$$

where T is the electron temperature in a collision dominated plasma and the subscripts u and l refer to the upper and lower states of the transition.

The oscillator strengths[7] for the pair of lines chosen are:

$$f_{ul}(13,589) = 0.171$$

and $$f_{u'l'}(6010) = 0.0419$$

Therefore, equation (1) becomes: $(g_l = g_{l'})$

$$\frac{I_{ul}}{I_{u'l'}} = \left(\frac{0.171}{.0419}\right) (.0875)\, e^{\frac{1.34 \times 10^4}{T}}$$

and

$$\frac{I_{ul}}{I_{u'l'}} = 0.357\, e^{\frac{1.34 \times 10^4}{T(^\circ K)}} \qquad (2)$$

Figure 2 is a plot of Eq. 2 as a function of T. If the electrons are Maxwellian and the electron states are populated according to Boltzmann statistics, the Saha equation can be used to yield the electron number densities.

The Saha equation is:

$$\frac{N_e^2}{N_o} = \frac{2g_{io}}{g_o}\, 2.41 \times 10^{15}\, T^{3/2}\, e^{-\frac{(V_i - \Delta X)}{T}} \qquad (3)$$

where N_o = number density of atoms in the ground state

g_{io} = statistical weight of the ground state of the ion = 1

g_o = statistical weight of the ground state of atom = 2

V_i = ionization potential of cesium

$$\text{and } \Delta X = \frac{e^2}{P_D} = \frac{e^2}{\sqrt{\frac{kT}{8\pi N_e e^2}}} = 2.94 \times 10^{-8} \sqrt{\frac{N_e}{T(°K)}} \qquad (4)$$

ΔX is a factor which reduces the effective ionization potential because of the presence of ions.(8)

For $N_e = 10^{14}$ and $T = 3000°K$, $\Delta X = 5.3 \times 10^{-3}$ ev. This value is negligible compared to V_i and will be neglected since the plasmas generated in the low voltage arc have values of $N_e \sim 10^{14}$ and $T \sim 2700°K$.

The Saha equation is rewritten:

$$N_e^2 = N_o \; 2.41 \times 10^{15} \; S\,A\,(T) \qquad (5)$$

where $S\,A\,(T) = T^{3/2} \; e^{-V_i/kT}$ and is plotted as a function of T in Fig. 3.

Through the use of Eqs. 2 and 5, the task of measuring the temperatures and densities of the electrons reduces to the measurement of the ratio of the Cs 13,589 Å line to the Cs 6010Å line and the measurement of the absolute intensity of the 13,589 Å line. (N_o is related to the absolute intensity through Eq. 10.)

Relative Intensity Calibration

A tungsten ribbon filament lamp calibrated for brightness by The National Bureau of Standards was used to calibrate the spectrometer detecting equipment. The intensity of radiation is given by Planck's black body formula with a suitable emissivity value for tungsten.(9) The brightness temperature listed is the value for T used in the formula.

The Standard lamp was operated at a brightness temperature of 1500°C and the radiation was detected with a RCA 1P28 photomultiplier at 6010Å and a lead sulfide cell at 13,589Å. The ratio of the readings, R, on the recording unit for continuous radiation is:(10)

$$\frac{R}{R'} = \alpha \; \frac{G \left| \frac{\Delta\lambda}{\Delta s} \right|}{G' \left| \frac{\Delta\lambda}{\Delta s} \right|'} \; \frac{I\lambda}{I\lambda'} \qquad (6)$$

G is the amplification factor; the primes refer to radiation at 6010Å, and α is the relative response of the two detectors at these wavelengths. Figure 4 shows the dispersion of radiation at the exit slit of the monochromator as a function of wavelength.

From these data:

$$\left|\frac{\Delta\lambda}{\Delta s}\right| = 65\ \text{Å/div. of recording paper}$$

$$\left|\frac{\Delta\lambda}{\Delta s}\right|' = 22.5\ \text{Å/div. of recording paper}$$

Table I lists the data taken for this calibration:

TABLE I

Line	R	Gain	I_λ
13,589 Å	64	13	2.1×10^{11} ergs/cm^3-sec-ster
6,010 Å	53	8	9.6×10^{9} ergs/cm^2-sec-ster

Substitution of this data into Eq. 6 yields: $\alpha = 0.00191$

Temperature Measurement

The intensity ratios of the 13,589 Å line to the 6010 Å line were measured for the diode characteristics listed in Table II. Radiation from the entire length of the interelectrode gap was detected for those measurements, and the filament temperature was 1100°C. Here G 12 and G' 16, and the slit widths were equal (25 μ's).

TABLE II

Diode Characteristics V(Volts)	I(Amps)	$R_{13,589} = R$	$R_{6,010} = R'$	R/R'	I/I'	T (°K)
-0.2	0.4	17	29.5	0.576	48	2760
0.0	0.525	22	39.3	0.56	46.5	2770
0.2	0.6	26	45.0	0.577	48	2760
0.4	0.655	28.9	50.0	0.577	48	2760
0.6	0.70	31.7	53.8	0.59	49	2740
0.8	0.755	34.5	56.5	0.611	50.8	2720
1.0	.80	37.3	59.5	0.626	52	2720

The equation which relates the ratio of the line intensities is:

$$\frac{I}{I'} = \frac{\int_{line} I_\lambda \, d\lambda}{\int_{line} I'_\lambda \, d\lambda'} = \alpha^{-1} \frac{R}{R'} \frac{G}{G'}$$

$$\therefore \frac{I}{I'} = 82.7 \frac{R}{R'} \qquad (7)$$

Using Eq. 7 and Fig. 2, the temperatures were computed and listed in Table II.

Absolute Intensity Calibration

The absolute intensity of a line is determined by comparing its intensity with the intensity of the standard lamp at the same wavelength over a suitable wavelength interval. If the external geometries of the line source (plasma) and the continuous source (standard lamp) are the same, the relation between the line intensity and standard lamp intensities for a spectrometer whose exit slit width is wide enough to include the entire line (the spectrometer used satisfies these conditions) is:

$$I_{line} = \int I_\lambda \, d\lambda = \left(\frac{R_l}{R_{sl}}\right)\left(\frac{G_l}{G_{sl}}\right) \frac{h_{sl}}{h_l} \frac{(SW)_{sl}}{(SW)_l} (I_\lambda \Delta\lambda)_{sl} \qquad (8)$$

where h and SW are the height and width of the slit respectively, l refers to the line and sl to the standard lamp.

The data for the calibration are the following:

$h_{sl} = 1$ mm
$h_l = 2$ mm
$(SW)_{sl} = 50\mu$'s
$(SW)_l = 25\mu$'s
$G_{sl} = 13$
$G_l = 12$
$\Delta\lambda = 37$ Å
$I_\lambda = 2.1 \times 10^{11}$ ergs/cm^3-sec-ster
$R_{sl} = 64$

$\Delta\lambda$ is calculated in the following manner:

$\Delta\lambda$ at 6000 Å is 51.2 Å for 100μ exit slit width.

$$\Delta\lambda\,(13{,}589\text{ Å}) = \Delta\lambda\,(6000\text{ Å}) \frac{(\Delta\lambda/\Delta S)}{(\Delta\lambda/\Delta S)'} \frac{25\mu}{100}$$

or, $\Delta\lambda\,(13{,}589\text{ Å}) = 37$ Å for an exit slit width of 25μ's.

Therefore: $$\int I_\lambda d\lambda = 480\, R_l \text{ ergs/cm}^2\text{-sec-ster}. \qquad (9)$$

Electron Number Density Calculation

The number density of atoms in the ground state must be calculated to utilize the Saha equation for electron density evaluations. The intensity of radiation for an optically thin line is:[3]

$$\int I_\lambda d\lambda = I_{ul} = \frac{2\pi e^2 h \nu^3}{mc^3} \frac{g_l}{g_o} f_{lu} e^{-E_u/kT} N_{ol}$$

An evaluation of the constants and parameters for the 13,589 line yields:

$$\int I_\lambda d\lambda = N_o \frac{1.06 \times 10^{-5}}{\lambda^3} \frac{g_l}{g_o} f_{lu} e^{-\frac{E_u}{kT}} \text{ l ergs/cm}^2\text{-sec-ster}. \qquad (10)$$

and, where λ is in microns and l in cm.

$$\int_{13,589\,\text{Å}} I_\lambda \, d\lambda = N_o \, 7.18 \times 10^{-7} \, e^{\frac{-26,700}{T}} \, l \text{ ergs/cm}^2\text{-sec-ster} \tag{11}$$

The diameter of the cathode was 3 mm. Therefore, if the plasma is assumed to be uniform over this width, l equals 3 mm, so that:

$$\int_{13,589\,\text{Å}} I_\lambda \, d\lambda = N_o \, 2.15 \times 10^{-7} \, e^{\frac{-26,700}{T}} \text{ ergs/cm}^2\text{-sec-ster} \tag{12}$$

Substituting Eq. (12) into Eq. (9) yields:

$$N_o = \frac{480 \times 10^7}{2.15} \, e^{\frac{26,700}{T}} \, R_l \text{ atoms/cm}^3 = 2.23 \times 10^9 \, e^{\frac{26,700}{T}} \, R_l \text{ atoms/cm}^3 \tag{13}$$

Table III is a listing of the diode characteristics and temperature along with N_o and the values of $SA(T)$ and N_e calculated using these data and Eq. (5). Since these values were determined from measurements of the radiation emanating from the entire interelectrode gap they must be considered average values for the plasma. (Filament temperature was 1100°C.)

TABLE III

Diode Characteristics V (volts)	I (amps)	T (°K)	N_o (atoms/cm^3)	$SA(T)$ (°K)$^{3/2}$	N_e^2 (cm^{-6})	N_e (cm^{-3})	P (mm of Hg)
-0.2	0.40	2760	6.2×10^{14}	1.15×10^{-2}	1.72×10^{28}	1.31×10^{14}	0.075
0.0	0.525	2770	7.1×10^{14}	1.25×10^{-2}	2.14	1.46	0.085
0.2	0.60	2760	9.45×10^{14}	1.15×10^{-2}	2.62	1.62	0.101
0.4	0.655	2760	10.5×10^{14}	1.15×10^{-2}	2.91	1.71	0.11
0.6	0.70	2740	12.4×10^{14}	1.0×10^{-2}	3.0	1.73	0.12
0.8	0.755	2720	14.3×10^{14}	$.84 \times 10^{-2}$	2.9	1.71	0.13
1.0	0.80	2720	15.4×10^{14}	$.84 \times 10^{-2}$	3.12	1.77	0.135

Figure 5 is a plot of T_l N_e, and I as a function of voltage.

N_e was also determined roughly by counting the number of lines which appear in the sharp series (S-P series). This Inglis-Teller[4] method of determining the electron number yielded a value of N_e of $1.75 \pm 0.25 \times 10^{14}$ cm^{-3}. This number agrees with the electron number density calculated from the Saha equation.

Pressure Calculation

The cold spot temperature of the cesium bath was 195°C. This corresponds to a cesium vapor pressure of 6×10^{-2} mm of Hg. The pressure in the plasma should be:

$$P = 1.036 \times 10^{-19} \sum_i N_i \, T_i$$

where the i's are summed over the ions, electrons and neutral atoms. The ion and atom temperatures are assumed to be that of the bath (468°K) and the electron temperature to be the value of T measured.

Now, the total number of atoms, N_a is:

$$N_a = N_o\left[1 + \sum_{1}^{n'} \frac{g_n}{g_o}\, e^{-E_n/kT}\right]$$

$$\simeq N_o \quad , \text{ for } T = 2750°K$$

Therefore, $$P = (N_o + N_e)\, T_b + N_e\, T_e$$

With T_b = bath temperature and $T_e = T$

i.e. for the 0.4 volt - 0.655 amp data:

$$P = 1.036 \times 10^{19} \left[1.7\,(2750) + 12\,(468)\right] \times 10^{14}$$

$$= 1.036 \times 10^{-5} \left[4.67 \times 10^{3} + 5.7 \times 10^{3}\right]$$

$$= 0.11 \text{ mm of Hg.}$$

Table III lists the pressure as a function of the diode characteristics.

Conclusions

The electron number density measured from the Saha equation agrees with the value determined from the Inglis-Teller measurement. This agreement appears to substantiate the value. However, the increase in the atom number density with increasing voltage does not agree with a constant total pressure for the cesium atoms. However, a change in the bath temperature of only + 17°C would be enough to yield the higher values for atom number density and pressure. It is difficult to predict which values are incorrect: cold spot temperature or number density measurement. Certainly within the limits of accuracy of all of the data, the results agree satisfactorily.

References

1. M. Silverberg, Appendix H, PIC - CLE - TI 3/2 March 20, 1961
2. I. Langmuir and K. H. Kingdon, Science, 57, 58 (1923)
3. W. B. Nottingham, "General Theory of the Plasma Diode Energy Converter", TEECO 7002-5
4. R. J. Donohue and R. F. Majkowski, "Spectroscopic Measurements of Temperatures and Densities in a Cesium Plasma", J. Appl. Phys. 33, 1, (1962)
5. Studies being made by F. E. Jamerson.
6. R. J. Donohue, internal report
7. P. M. Stone, "Cesium Oscillator Strengths", (to be published)
8. Personal communication with Professor H. Griem
9. J. C. DeVos, Physica 20, 690 (1954); G. A. Rutgers and J. C. DeVos, Physica 20, 715 (1954)
10. R. J. Donohue, internal report

FIGURE 3

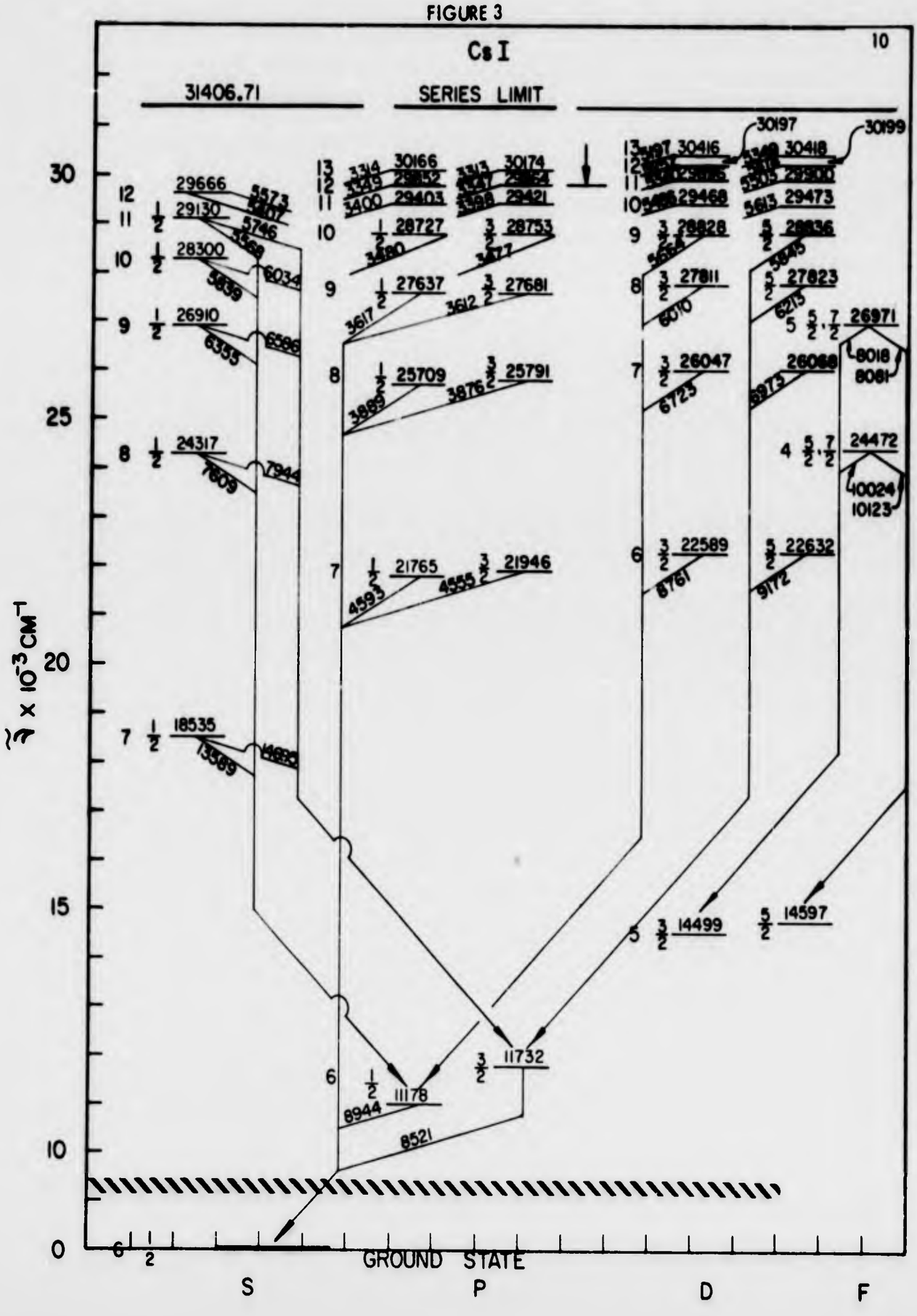
Cs I
10
31406.71
SERIES LIMIT
$\tilde{\nu} \times 10^{-3}$ CM^{-1}
30
25
20
15
10
0
GROUND STATE
S
P
D
F
30197
30199
30166
30174
29666
29130
28300
26910
24317
18535
28727
28753
27637
27681
25709
25791
21765
21946
11732
11178
8944
8521
30416
30418
29468
29473
28828
28836
27811
27823
26971
26047
26068
8018
8081
24472
40024
10123
22589
22632
14499
14597

FIGURE 4

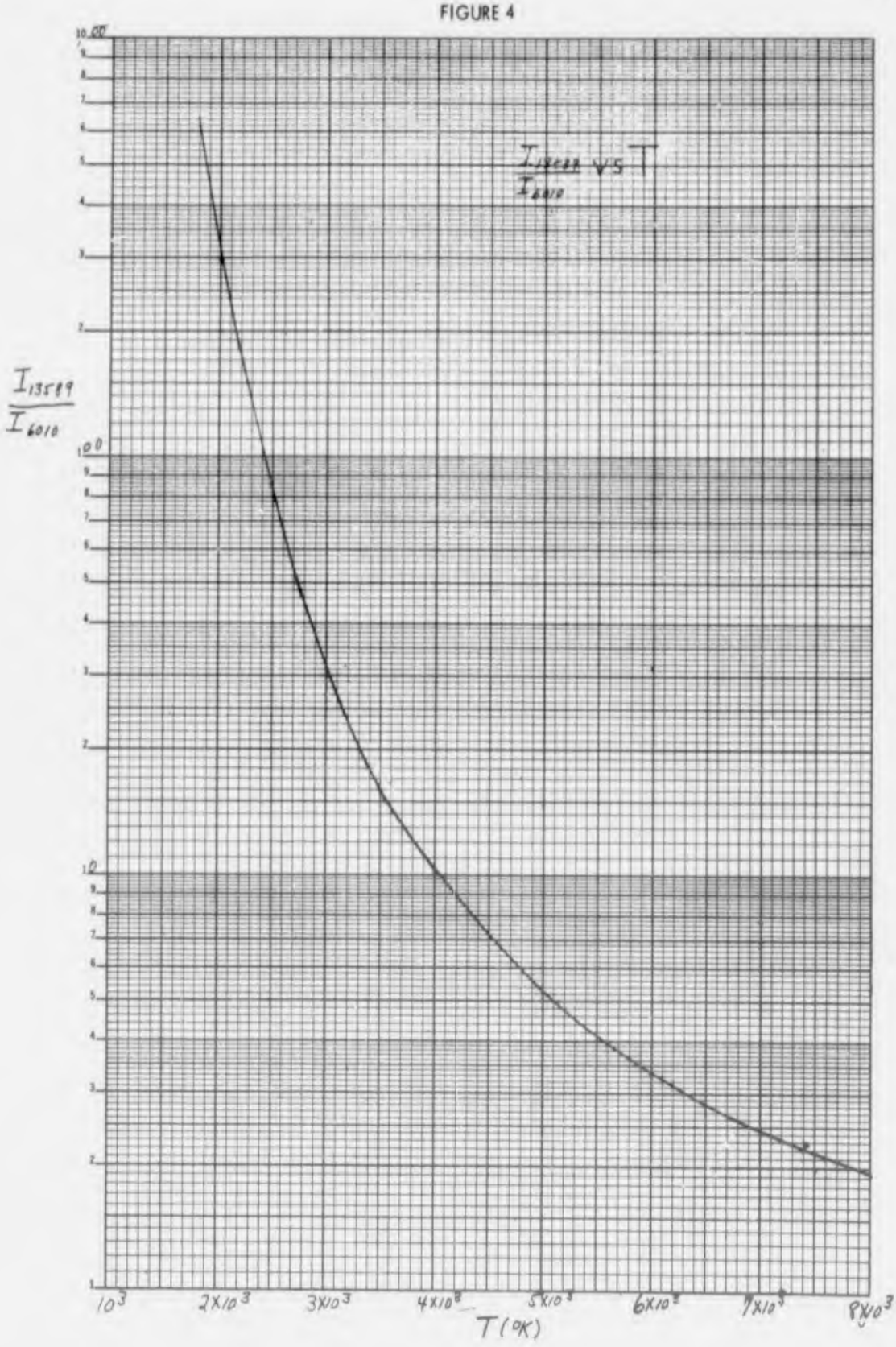
I_{13589} VS T
I_{6010}
$\frac{I_{13589}}{I_{6010}}$
10.00
1.00
10
1
10^3
2×10^3
3×10^3
4×10^3
5×10^3
6×10^3
7×10^3
8×10^3
T (°K)

FIGURE 5

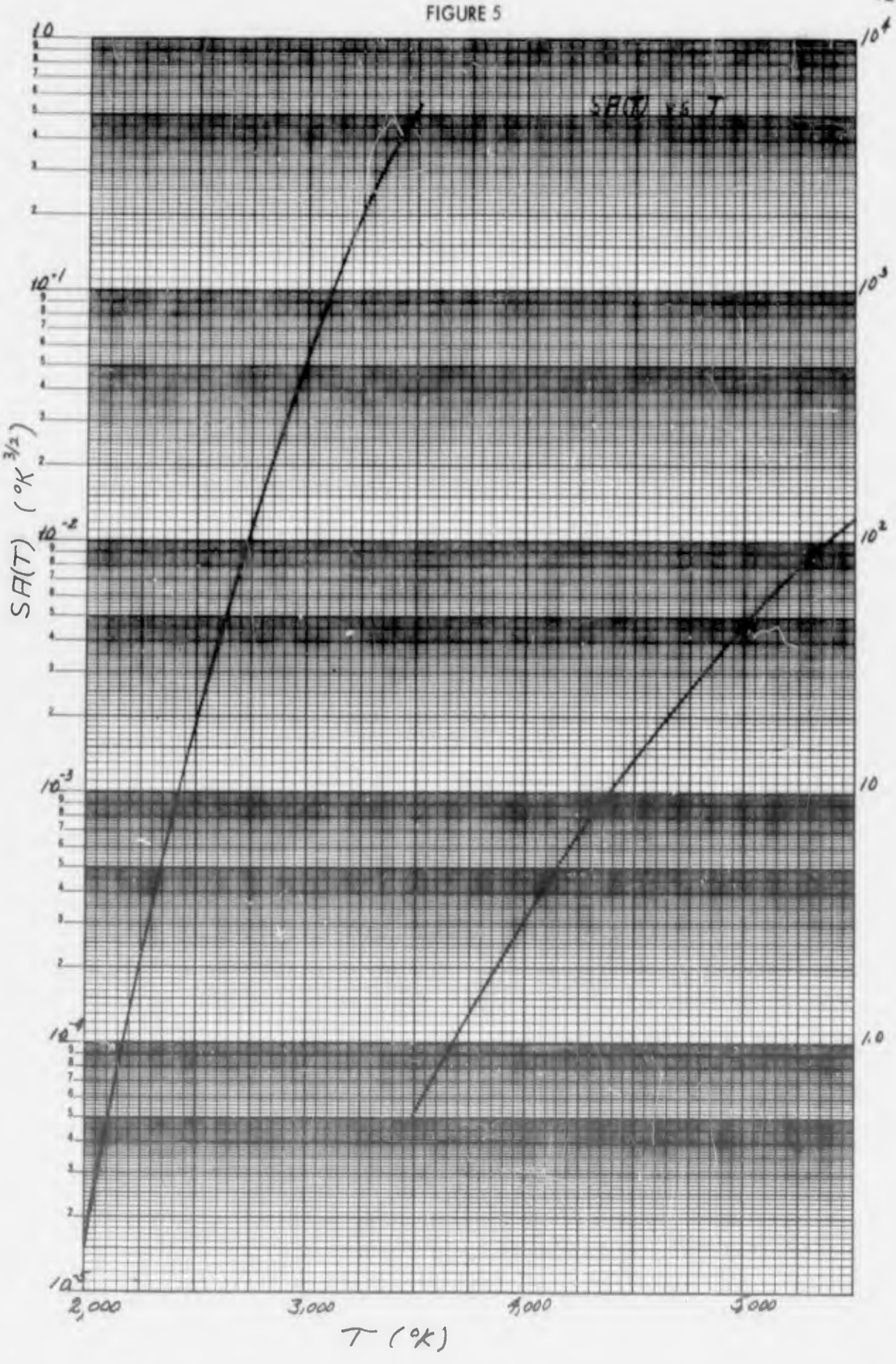
SA(T) vs T
SA(T) (°K^3/2)
T (°K)
2,000
3,000
4,000
5,000
10
10^-1
10^-2
10^-3
10^-4
10^4
10^3
10^2
10
1.0

FIGURE 6

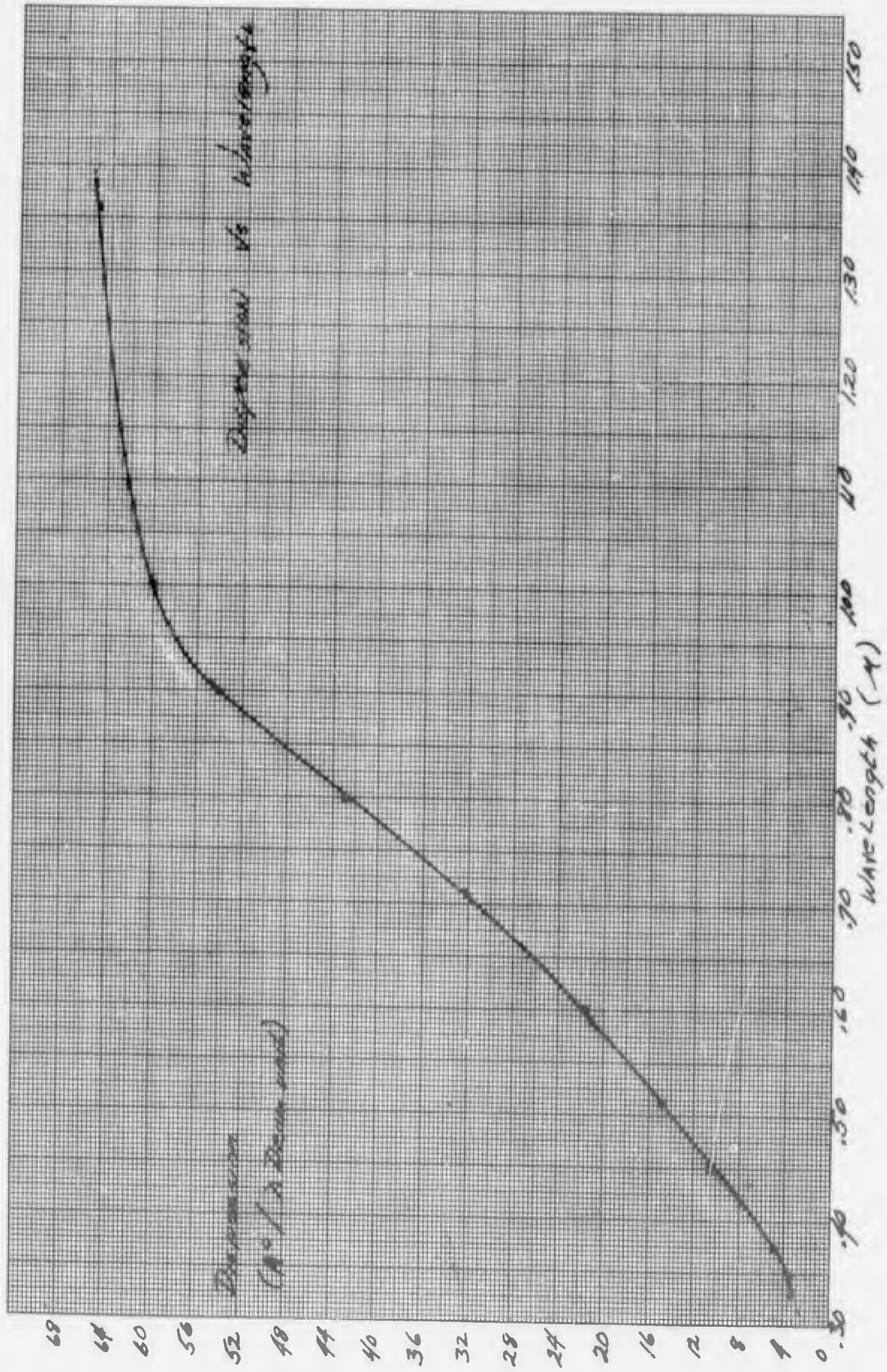

FIGURE 7

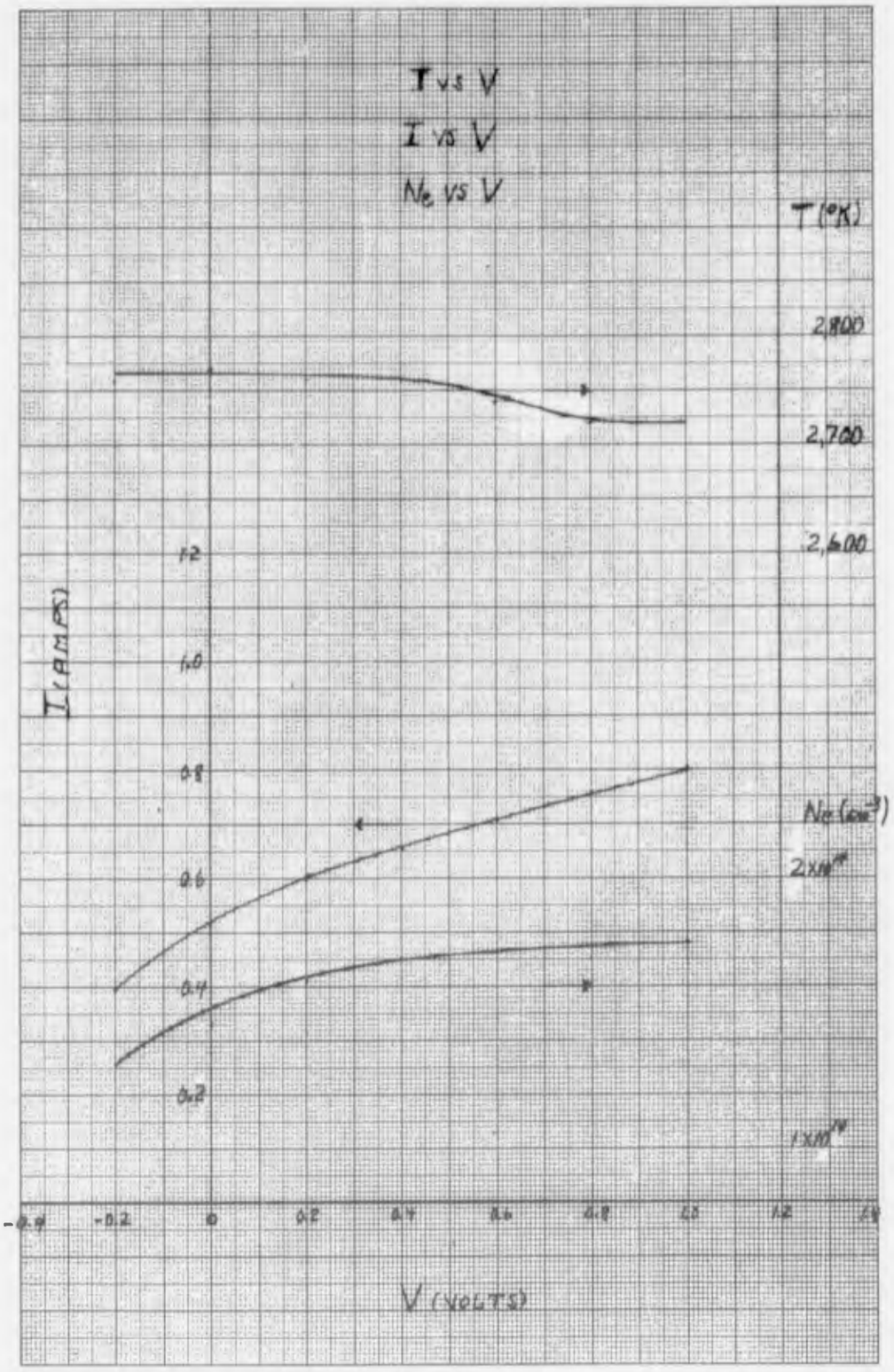
I vs V
I vs V
Ne vs V
T (°K)
2,800
2,700
2,600
I (AMPS)
1.2
1.0
0.8
0.6
0.4
0.2
Ne (cm⁻³)
2x10¹⁴
1x10¹⁴
-0.4
-0.2
0
0.2
0.4
0.6
0.8
1.0
1.2
V (VOLTS)

SECTION D

SPECTROSCOPIC MEASUREMENTS IN A CESIUM LOW VOLTAGE ARC CONVERTER

R. J. Donohue and R. F. Majkowski

ABSTRACT

The knowledge of the plasma parameters of a cesium low voltage arc thermionic converter is essential for the development of a detailed analysis of this mode of thermionic converter operation. A converter employing a Philips cathode as emitter and a nickel collector spaced 2 mm apart has been operated in the low voltage arc mode in the retarding field (power producing region) and accelerating field regions. The optical spectra of the plasma generated in the arc was measured and analyzed to determine electron number density and electron temperature.

INTRODUCTION

The operation of a cesium diode in the low voltage arc mode has been discussed in the literature.[1] The low voltage arc allows operation at low emitter temperature (down to 1100°C) and low vapor pressure (0.1 mm of Hg). Operation of the diode at these low pressures allows the emitter-collector gap to be 2 mm without appreciable transport loss in the cesium vapor.

Pressure and emitter temperature values such as the above preclude cesium ionization by surface contact ionization.[2] It has been proposed[3] that in a low voltage arc the sheath at the emitter is accelerating for emitted electrons so that ionization occurs in the bulk of the plasma as a result of electron impact. The potential diagram for this is shown in Figure 1 along with a typical voltage-current characteristic for the low voltage arc. In the figure the arc fires at a positive collector potential, however, under certain conditions (namely higher emitter temperature) the arc can fire in the retarding region.

The use of spectroscopic techniques to study the cesium plasma has been developed[4] and is applied to a low voltage arc thermionic converter described below. The principal objective is to investigate the magnitudes for electron temperature and number density for a characteristic similar to 1a.

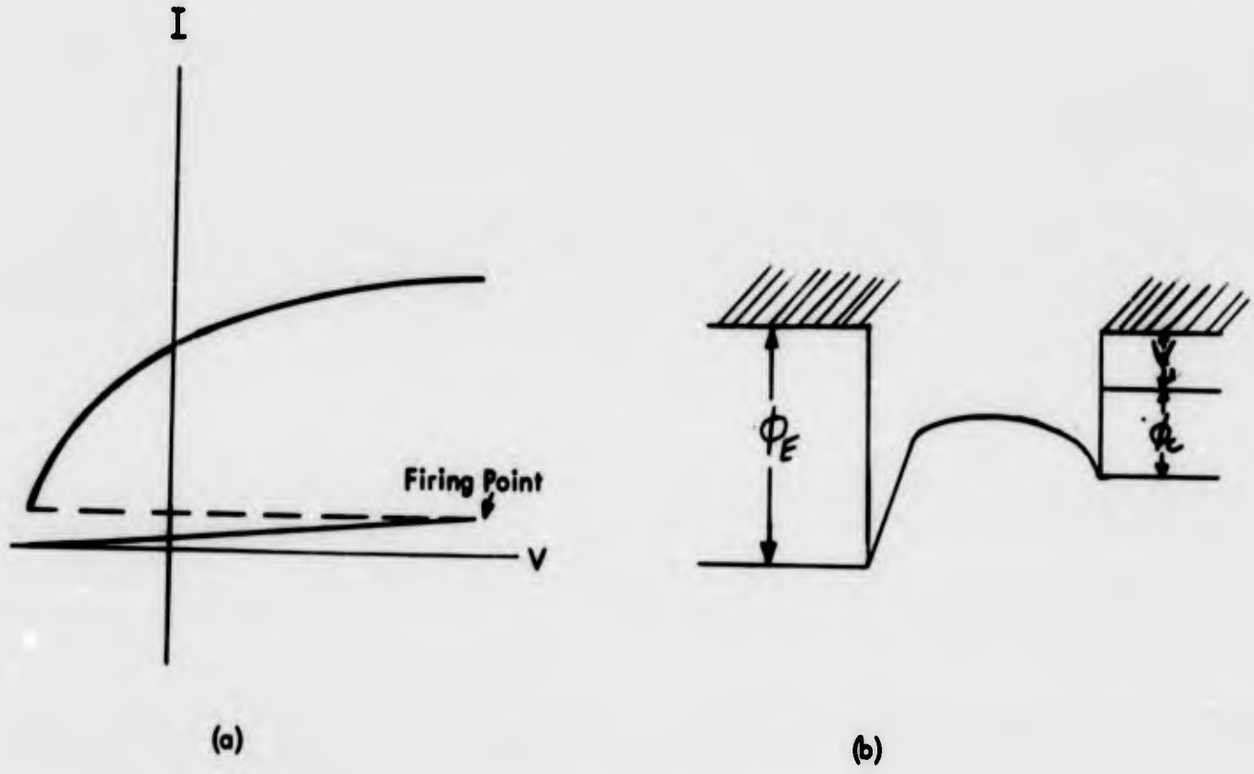

Figure 1

Apparatus

The measurements reported here were compiled on one of several diodes being investigated for low voltage arc mode operation.[5] Although optical measurements were made on several tubes diode C16x provided the most complete set of data. These tubes failed after some 10 to 20 hours of operation due to the cesium vapor attack on the nonex presses.[6] These presses were used in lieu of cesium resistant seals presently under development.

The C16x diode consists of a 3 mm o.d. Philips cathode emitter and 13 mm diameter nickel collector spaced 2 mm apart. Cesium was generated after processing the tube as a vacuum tube by firing cesium chromate pellets which are situated in an arm attached to the side of the tube. The diode was operated in an oven where cesium bath temperature was controlled by a Capacitrol thermocouple controller. Bath temperature was adjusted to allow the diode to operate in the power producing region.

Figure 2 illustrates the circuit employed for recording the V-I charcteristic on an oscilloscope. The filament was heated with half wave a.c. and the V-I trace recorded during the off time of the heating pulse by using a blanking circuit on the intensifier in the oscilloscope.

The optical measurements were carried out in the Physical Electronics Laboratory using the Perkin-Elmer spectrometer. The plasma was viewed through a small hole in the oven and the plasma in the entire interelectrode gap was focused on the slit of the spectrometer. A plasma also exists at the base of the tube between the incoming filament leads. This is because six volts or more are required to heat the cathode, and this is enough voltage to create a cesium discharge at the base of the tube. Observations were made to determine whether the radiation from this plasma was detected by the spectrometer when the interelectrode gap was focused

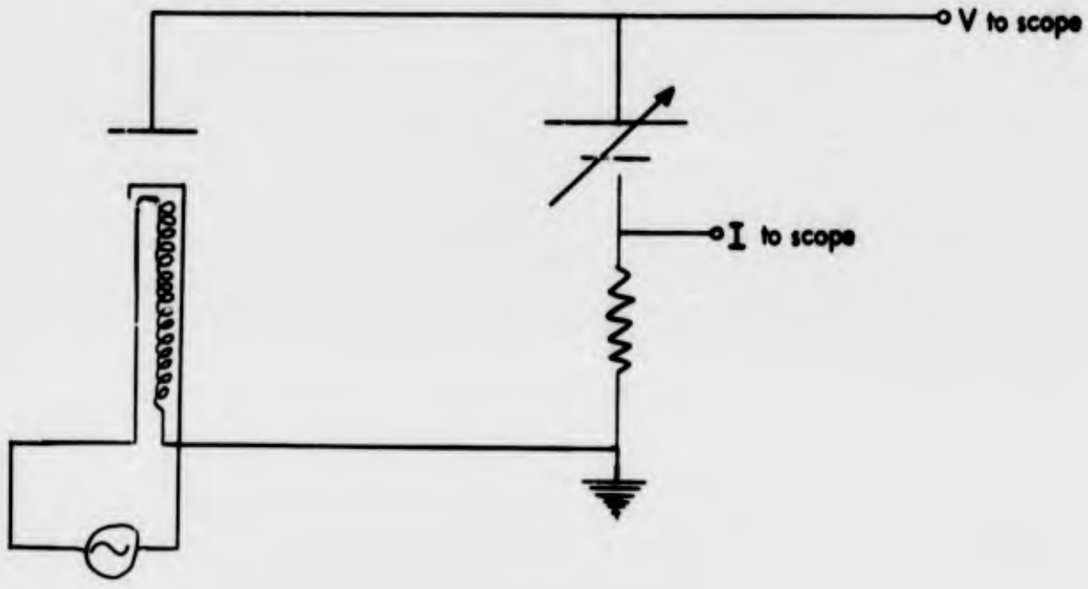

Figure 2

on the spectrometer slit. These observations indicated that this unwanted radiation was not detected. Also, the intensity of the Cs 4555Å line was observed as a function of time by means of an oscilloscope tracing of the output of the photomultiplier detector. This was done to see whether the intensity and hence the plasma temperature changed during the period of the cathode heating cycle. No change in this intensity was observed during this cycle so that it is assumed that the plasma parameters are independent of the heating cycle and can be considered to be constant with time.

Spectroscopic Theory

Recent theoretical calculations of the oscillator strengths of many spectral lines of cesium have been made by P. Stone of Los Alamos.[7] The last reported spectral measurements made at our laboratories used the principal series of cesium[4] since these lines were the only ones for which the oscillator strengths were known. However, the principal series lines (nP-$6S_{1/2}$ transitions) are self reversed because the lower state is the ground state of the atom and the intensity of these lines must be corrected for this effect. The evaluation of the oscillator strengths for lines from other series allows a choice of non principal series lines for absolute and relative intensity measurements.

Figure 3 is a display of some of the electronic states of cesium with the arrows indicating the transitions for some of the more prominent lines. Lines from $S \rightarrow P$ or $D \rightarrow P$ transitions will not be reversed in the cold cesium layer between the plasma and viewing port. Also, in low temperature plasmas these lines will not be significantly reversed in the plasma itself. A strong line should be used for absolute intensity measurements and a pair of lines with a large energy difference between their upper states should be chosen for the relative intensity measurements (a large energy gap leads to an accurate evaluation of the electron temperature). The

$7\,^2S_{1/2} \rightarrow 6\,^2P_{1/2}$ transition (13,589Å) was used for the absolute intensity measurements and this line was combined with the $8\,^2D_{3/2} \rightarrow 6\,^2P_{1/2}$ transition (6010Å) for the relative intensity measurements.

The intensity ratio of any two optically thin lines is:[4]

$$\frac{I_{ul}}{I_{u'l'}} = \frac{f_{lu}}{f_{l'u'}} \frac{(\nu_{ul})^3}{(\nu_{u'l'})^3} \frac{g_l}{g_{l'}} e^{-(E_u - E_{u'})/kT} \quad . \tag{1}$$

where T is the electron temperature in a collision dominated plasma and the subscripts u and l refer to the upper and lower states of the transition.

The oscillator strengths[7] for the pair of lines chosen are:

$$f_{ul}\,(13,589) = 0.171$$

and $$f_{u'l'}\,(6010) = 0.0419$$

Therefore, equation (1) becomes: $(g_l = g_{l'})$

$$\frac{I_{ul}}{I_{u'l'}} = \left(\frac{0.171}{.0419}\right) (.0875)\, e^{\frac{1.34 \times 10^4}{T}}$$

and

$$\frac{I_{ul}}{I_{u'l'}} = 0.357\, e^{\frac{1.34 \times 10^4}{T(^\circ K)}} \tag{2}$$

Figure 2 is a plot of Eq. 2 as a function of T. If the electrons are Maxwellian and the electron states are populated according to Boltzmann statistics, the Saha equation can be used to yield the electron number densities.

The Saha equation is:

$$\frac{N_e^2}{N_o} = \frac{2g_{io}}{g_o}\, 2.41 \times 10^{15}\, T^{3/2}\, e^{-\frac{(V_i - \Delta X)}{T}} \tag{3}$$

where N_o = number density of atoms in the ground state

g_{io} = statistical weight of the ground state of the ion = 1

g_o = statistical weight of the ground state of atom = 2

V_i = ionization potential of cesium

$$\text{and } \Delta X = \frac{e^2}{\rho_D} = \frac{e^2}{\sqrt{\frac{kT}{8\pi N_e e^2}}} = 2.94 \times 10^{-8} \sqrt{\frac{N_e}{T(^\circ K)}} \qquad (4)$$

ΔX is a factor which reduces the effective ionization potential because of the presence of ions. (8)

For $N_e = 10^{14}$ and $T = 3000^\circ K$, $\Delta X = 5.3 \times 10^{-3}$ ev. This value is negligible compared to V_i and will be neglected since the plasmas generated in the low voltage arc have values of $N_e \sim 10^{14}$ and $T \sim 2700^\circ K$.

The Saha equation is rewritten:

$$N_e^2 = N_o \; 2.41 \times 10^{15} \; S\,A\,(T) \qquad (5)$$

where $S\,A\,(T) = T^{3/2} \; e^{-V_i/kT}$ and is plotted as a function of T in Fig. 3.

Through the use of Eqs. 2 and 5, the task of measuring the temperatures and densities of the electrons reduces to the measurement of the ratio of the Cs 13,589 Å line to the Cs 6010Å line and the measurement of the absolute intensity of the 13,589 Å line. (N_o is related to the absolute intensity through Eq. 10.)

Relative Intensity Calibration

A tungsten ribbon filament lamp calibrated for brightness by The National Bureau of Standards was used to calibrate the spectrometer detecting equipment. The intensity of radiation is given by Planck's black body formula with a suitable emissivity value for tungsten. (9) The brightness temperature listed is the value for T used in the formula.

The Standard lamp was operated at a brightness temperature of 1500°C and the radiation was detected with a RCA 1P28 photomultiplier at 6010Å and a lead sulfide cell at 13,589Å. The ratio of the readings, R, on the recording unit for continuous radiation is: (10)

$$\frac{R}{R'} = \alpha \; \frac{G \left| \frac{\Delta\lambda}{\Delta s} \right|}{G' \left| \frac{\Delta\lambda}{\Delta s} \right|'} \; \frac{I_\lambda}{I_\lambda'} \qquad (6)$$

G is the amplification factor; the primes refer to radiation at 6010Å, and α is the relative response of the two detectors at these wavelengths. Figure 4 shows the dispersion of radiation at the exit slit of the monochromator as a function of wavelength.

From these data:

$$\left|\frac{\Delta\lambda}{\Delta s}\right| = 65\ \text{Å/div. of recording paper}$$

$$\left|\frac{\Delta\lambda}{\Delta s}\right|' = 22.5\ \text{Å/div. of recording paper}$$

Table I lists the data taken for this calibration:

TABLE I

Line	R	Gain	I_λ
13,589 Å	64	13	2.1×10^{11} ergs/cm^3-sec-ster
6,010 Å	53	8	9.6×10^{9} ergs/cm^2-sec-ster

Substitution of this data into Eq. 6 yields: $\alpha = 0.00191$

Temperature Measurement

The intensity ratios of the 13,589 Å line to the 6010 Å line were measured for the diode characteristics listed in Table II. Radiation from the entire length of the interelectrode gap was detected for those measurements, and the filament temperature was 1100°C. Here G 12 and G' 16, and the slit widths were equal (25 μ's).

TABLE II

Diode Characteristics V(Volts)	I(Amps)	$R_{13,589} = R$	$R_{6,010} = R'$	R/R'	I/I'	T (°K)
-0.2	0.4	17	29.5	0.576	48	2760
0.0	0.525	22	39.3	0.56	46.5	2770
0.2	0.6	26	45.0	0.577	48	2760
0.4	0.655	28.9	50.0	0.577	48	2760
0.6	0.70	31.7	53.8	0.59	49	2740
0.8	0.755	34.5	56.5	0.611	50.8	2720
1.0	.80	37.3	59.5	0.626	52	2720

The equation which relates the ratio of the line intensities is:

$$\frac{I}{I'} = \frac{\int_{\text{line}} I_\lambda \, d\lambda}{\int_{\text{line}} I'_\lambda \, d\lambda'} = \alpha^{-1} \frac{R}{R'} \frac{G}{G'}$$

$$\therefore \frac{I}{I'} = 82.7 \frac{R}{R'} \qquad (7)$$

Using Eq. 7 and Fig. 2, the temperatures were computed and listed in Table II.

Absolute Intensity Calibration

The absolute intensity of a line is determined by comparing its intensity with the intensity of the standard lamp at the same wavelength over a suitable wavelength interval. If the external geometries of the line source (plasma) and the continuous source (standard lamp) are the same, the relation between the line intensity and standard lamp intensities for a spectrometer whose exit slit width is wide enough to include the entire line (the spectrometer used satisfies these conditions) is:

$$I_{line} = \int I_\lambda \, d\lambda = \left(\frac{R_l}{R_{sl}}\right)\left(\frac{G_l}{G_{sl}}\right) \frac{h_{sl}}{h_l} \frac{(SW)_{sl}}{(SW)_l} (I_\lambda \Delta\lambda)_{sl} \qquad (8)$$

where h and SW are the height and width of the slit respectively, l refers to the line and sl to the standard lamp.

The data for the calibration are the following:

$h_{sl} = 1$ mm
$h_l = 2$ mm
$(SW)_{sl} = 50\mu$'s
$(SW)_l = 25\mu$'s
$G_{sl} = 13$
$G_l = 12$
$\Delta\lambda = 37$ Å
$I_\lambda = 2.1 \times 10^{11}$ ergs/cm^3-sec-ster
$R_{sl} = 64$

$\Delta\lambda$ is calculated in the following manner:

$\Delta\lambda$ at 6000 Å is 51.2 Å for 100μ exit slit width.

$$\Delta\lambda\,(13{,}589\text{ Å}) = \Delta\lambda\,(6000\text{ Å}) \frac{(\Delta\lambda/\Delta S)}{(\Delta\lambda/\Delta S)'} \frac{25\mu}{100}$$

or, $\Delta\lambda(13{,}589\text{ Å}) = 37$ Å for an exit slit width of 25μ's.

Therefore: $$\int I_\lambda d\lambda = 480\, R_l \text{ ergs/cm}^2\text{-sec-ster}. \qquad (9)$$

Electron Number Density Calculation

The number density of atoms in the ground state must be calculated to utilize the Saha equation for electron density evaluations. The intensity of radiation for an optically thin line is:[3]

$$\int I_\lambda d\lambda = I_{ul} = \frac{2\pi e^2 h \nu^3}{mc^3} \frac{g_l}{g_o} f_{lu} e^{-E_u/kT} N_{ol}$$

An evaluation of the constants and parameters for the 13,589 line yields:

$$\int I_\lambda d\lambda = N_o \frac{1.06 \times 10^{-5}}{\lambda^3} \frac{g_l}{g_o} f_{lu} e^{-\frac{E_u}{kT}} \text{ l ergs/cm}^2\text{-sec-ster}. \qquad (10)$$

and, where λ is in microns and l in cm.

$$\int_{13,589\,\text{Å}} I_\lambda \, d\lambda = N_o \, 7.18 \times 10^{-7} \; e^{\frac{-26,700}{T}} \; l \text{ ergs/cm}^2\text{-sec-ster} \tag{11}$$

The diameter of the cathode was 3 mm. Therefore, if the plasma is assumed to be uniform over this width, l equals 3 mm, so that:

$$\int_{13,589\,\text{Å}} I_\lambda \, d\lambda = N_o \, 2.15 \times 10^{-7} \; e^{\frac{-26,700}{T}} \text{ ergs/cm}^2\text{-sec-ster} \tag{12}$$

Substituting Eq. (12) into Eq. (9) yields:

$$N_o = \frac{480 \times 10^7}{2.15} \; e^{\frac{26,700}{T}} \; R_l \text{ atoms/cm}^3 = 2.23 \times 10^9 \; e^{\frac{26,700}{T}} \; R_l \text{ atoms/cm}^3 \tag{13}$$

Table III is a listing of the diode characteristics and temperature along with N_o and the values of SA(T) and N_e calculated using these data and Eq. (5). Since these values were determined from measurements of the radiation emanating from the entire interelectrode gap they must be considered average values for the plasma. (Filament temperature was 1100°C.)

TABLE III

Diode Characteristics V (volts)	I (amps)	T (°K)	N_o (atoms/cm^3)	SA(T) (°K)$^{3/2}$	N_e^2 (cm^{-6})	N_e (cm^{-3})	P (mm of Hg)
-0.2	0.40	2760	6.2×10^{14}	1.15×10^{-2}	1.72×10^{28}	1.31×10^{14}	0.075
0.0	0.525	2770	7.1×10^{14}	1.25×10^{-2}	2.14	1.46	0.085
0.2	0.60	2760	9.45×10^{14}	1.15×10^{-2}	2.62	1.62	0.101
0.4	0.655	2760	10.5×10^{14}	1.15×10^{-2}	2.91	1.71	0.11
0.6	0.70	2740	12.4×10^{14}	1.0×10^{-2}	3.0	1.73	0.12
0.8	0.755	2720	14.3×10^{14}	$.84 \times 10^{-2}$	2.9	1.71	0.13
1.0	0.80	2720	15.4×10^{14}	$.84 \times 10^{-2}$	3.12	1.77	0.135

Figure 5 is a plot of T_l N_e, and I as a function of voltage.

N_e was also determined roughly by counting the number of lines which appear in the sharp series (S-P series). This Inglis-Teller[4] method of determining the electron number yielded a value of N_e of $1.75 \pm 0.25 \times 10^{14}$ cm^{-3}. This number agrees with the electron number density calculated from the Saha equation.

Pressure Calculation

The cold spot temperature of the cesium bath was 195°C. This corresponds to a cesium vapor pressure of 6×10^{-2} mm of Hg. The pressure in the plasma should be:

$$P = 1.036 \times 10^{-19} \sum_i N_i \, T_i$$

where the i's are summed over the ions, electrons and neutral atoms. The ion and atom temperatures are assumed to be that of the bath (468°K) and the electron temperature to be the value of T measured.

Now, the total number of atoms, N_a is:

$$N_a = N_o \left[1 + \sum_{1}^{n'} \frac{g_n}{g_o} e^{-E_n/kT} \right]$$

$$\simeq N_o \quad , \text{ for } T = 2750°K$$

Therefore, $$P = (N_o + N_e) T_b + N_e T_e$$

With T_b = bath temperature and $T_e = T$

i.e. for the 0.4 volt - 0.655 amp data:

$$P = 1.036 \times 10^{19} \left[1.7 (2750) + 12 (468) \right] \times 10^{14}$$

$$= 1.036 \times 10^{-5} \left[4.67 \times 10^3 + 5.7 \times 10^3 \right]$$

$$= 0.11 \text{ mm of Hg.}$$

Table III lists the pressure as a function of the diode characteristics.

Conclusions

The electron number density measured from the Saha equation agrees with the value determined from the Inglis-Teller measurement. This agreement appears to substantiate the value. However, the increase in the atom number density with increasing voltage does not agree with a constant total pressure for the cesium atoms. However, a change in the bath temperature of only + 17°C would be enough to yield the higher values for atom number density and pressure. It is difficult to predict which values are incorrect: cold spot temperature or number density measurement. Certainly within the limits of accuracy of all of the data, the results agree satisfactorily.

References

1. M. Silverberg, Appendix H, PIC - CLE - TI 3/2 March 20, 1961
2. I. Langmuir and K. H. Kingdon, Science, 57, 58 (1923)
3. W. B. Nottingham, "General Theory of the Plasma Diode Energy Converter", TEECO 7002-5
4. R. J. Donohue and R. F. Majkowski, "Spectroscopic Measurements of Temperatures and Densities in a Cesium Plasma", J. Appl. Phys. 33, 1, (1962)
5. Studies being made by F. E. Jamerson.
6. R. J. Donohue, internal report
7. P. M. Stone, "Cesium Oscillator Strengths", (to be published)
8. Personal communication with Professor H. Griem
9. J. C. DeVos, Physica 20, 690 (1954); G. A. Rutgers and J. C. DeVos, Physica 20, 715 (1954)
10. R. J. Donohue, internal report

FIGURE 3

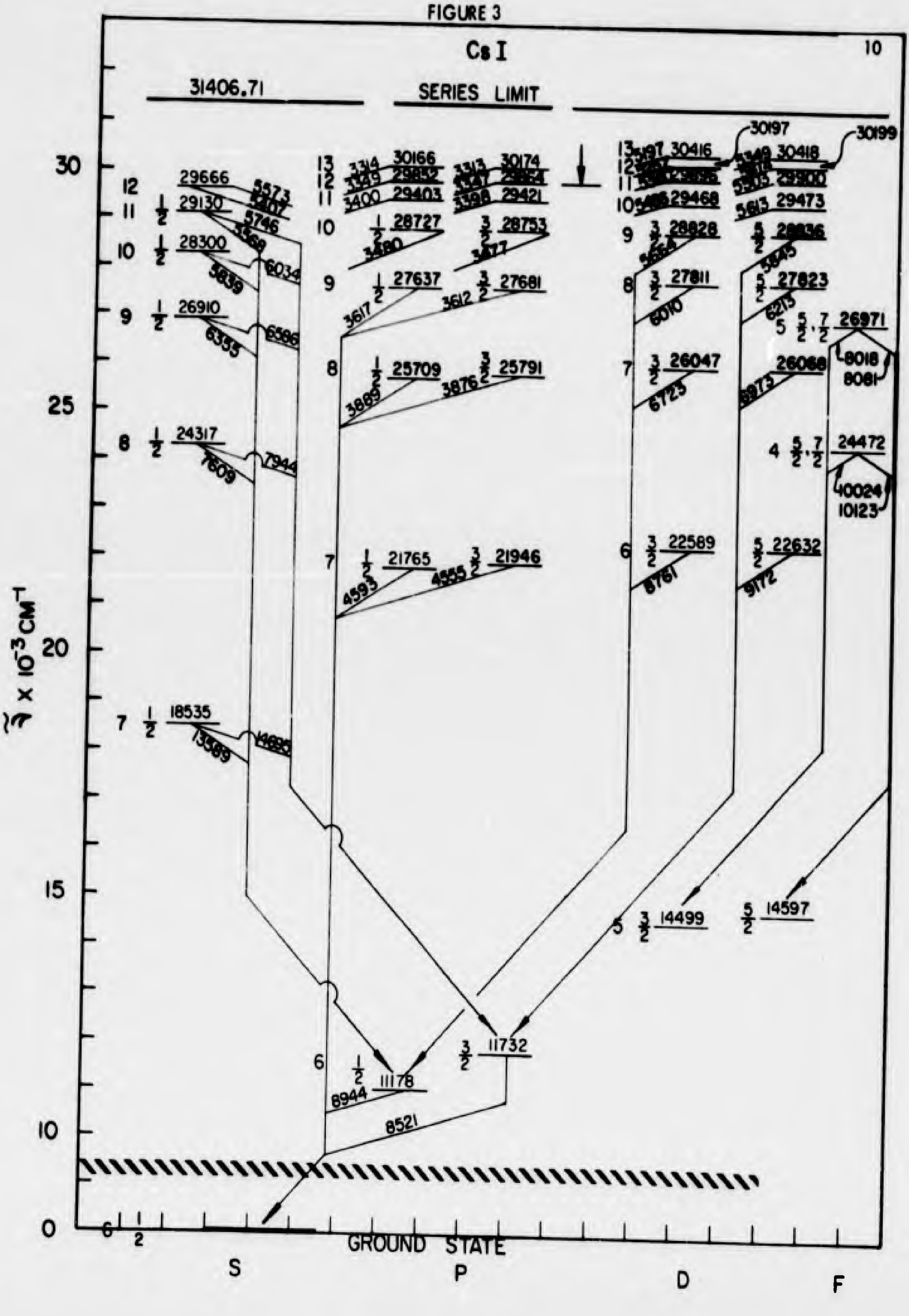
Cs I
10
31406.71
SERIES LIMIT
$\tilde{\nu} \times 10^{-3}$ CM^{-1}
GROUND STATE
S
P
D
F
11178
11732
14499
14597
8944
8521

FIGURE 4

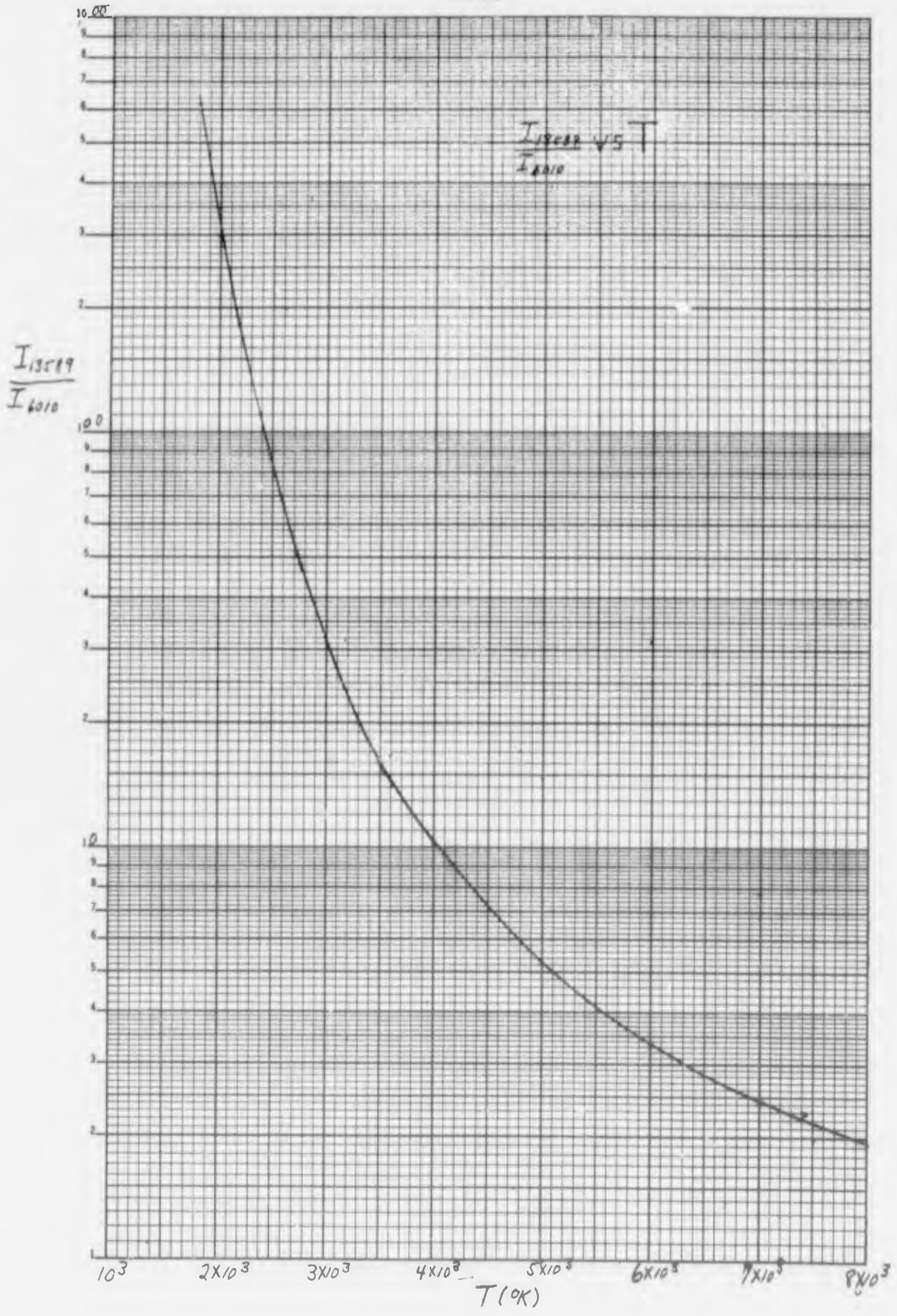
$\frac{I_{13599}}{I_{6010}}$ VS T
$\frac{I_{13599}}{I_{6010}}$
10.00
9
8
7
6
5
4
3
2
100
9
8
7
6
5
4
3
2
10
9
8
7
6
5
4
3
2
1
10^3
$2X10^3$
$3X10^3$
$4X10^3$
$5X10^3$
$6X10^3$
$7X10^3$
$8X10^3$
T(°K)

FIGURE 5

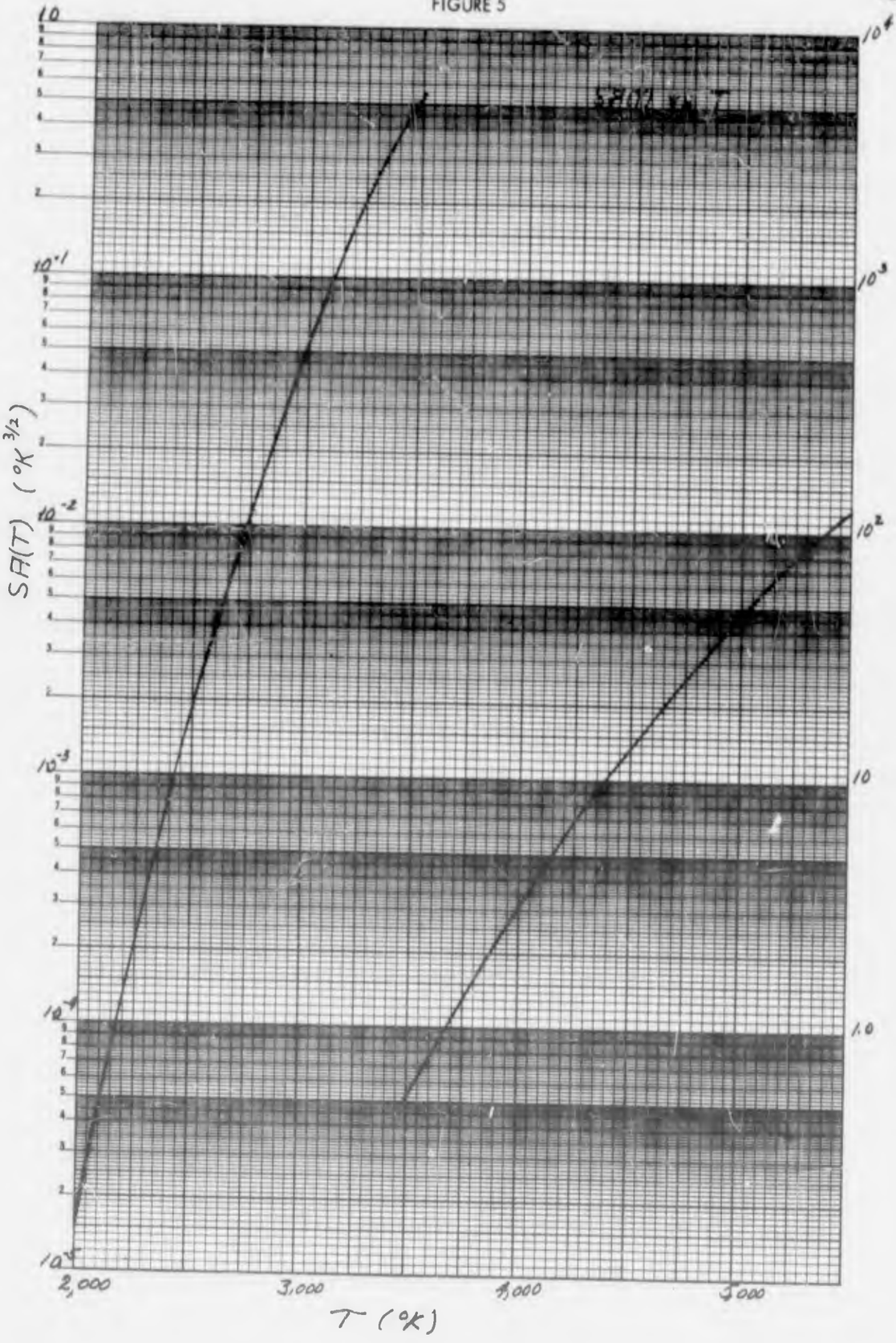

FIGURE 6

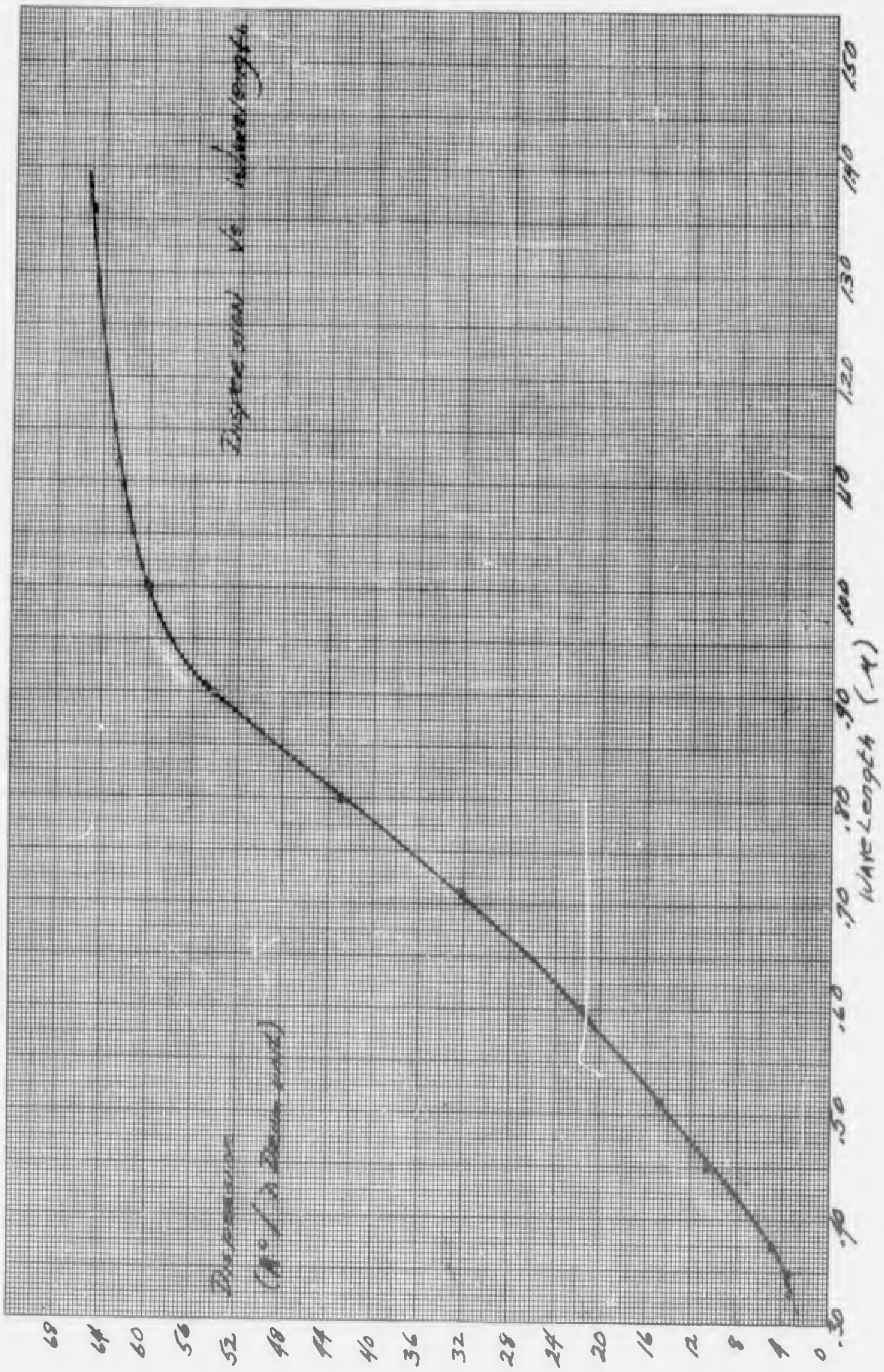
Dispersion vs wavelength
Wave Length (μ)
.30
.40
.50
.60
.70
.80
.90
1.00
1.10
1.20
1.30
1.40
1.50
0
4
8
12
16
20
24
28
32
36
40
44
48
52
56
60
64

FIGURE 7

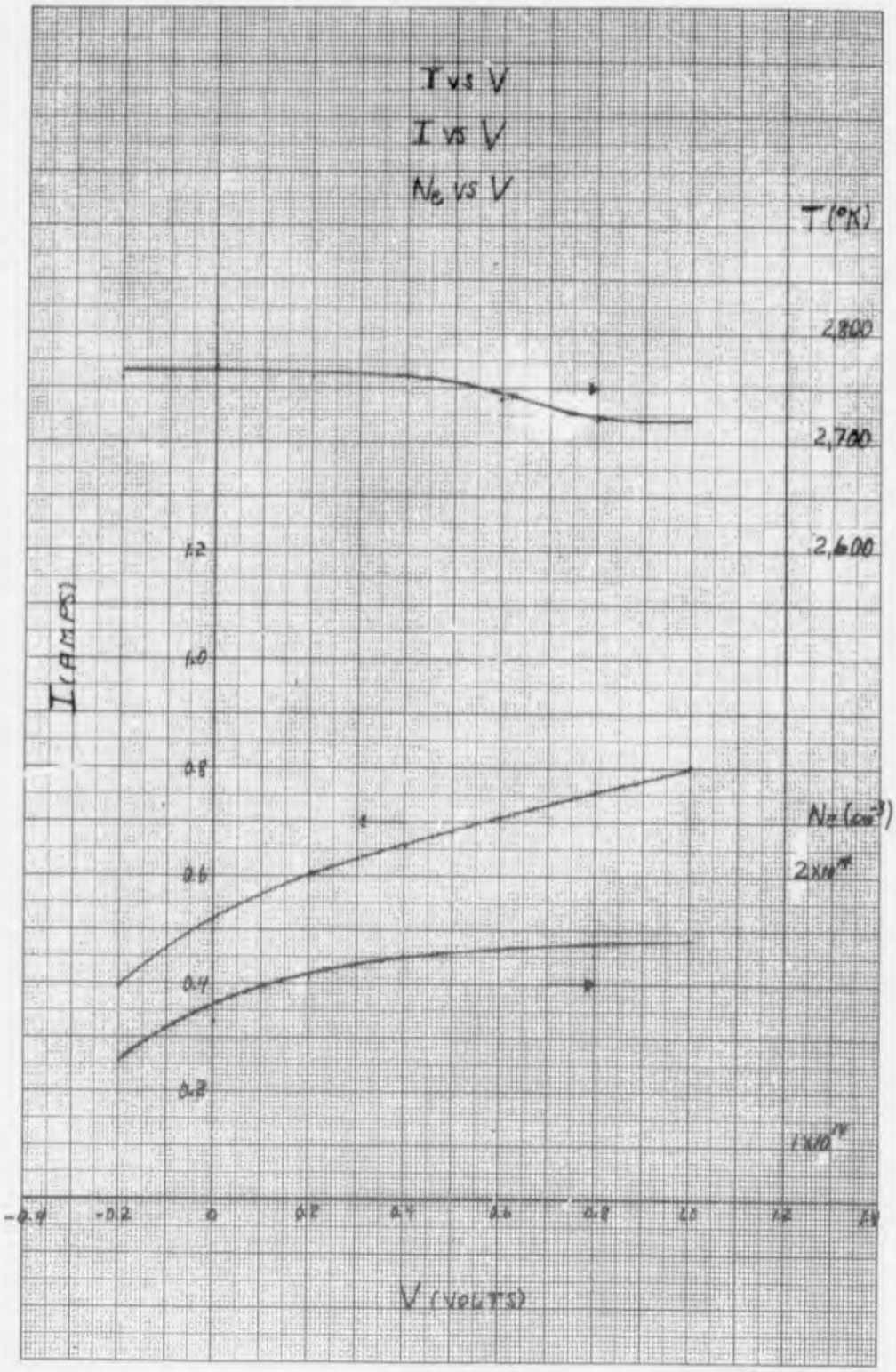
I vs V
I vs V
N_e vs V
T(°K)
2,800
2,700
2,600
I (AMPS)
1.2
1.0
0.8
0.6
0.4
0.2
N_e (cm^{-3})
2×10^{14}
1×10^{14}
-0.4
-0.2
0
0.2
0.4
0.6
0.8
1.0
1.2
V (VOLTS)

SECTION E

URANIUM CARBIDE-RHENIUM CERMET EMITTER

Robert F. Hill and Fay E. Gifford

Material Development - R. F. Hill

The development of uranium carbide emitter materials for use in the noble gas plasma diode thermionic converter has been completed and reported in a paper written during this report period.[1]

During the development program both ceramic and cermet type materials were investigated. The ceramic materials investigated were pure UC and the mixed carbide UC-ZrC. The cermet materials investigated contained 80 volume percent UC dispersed in either niobium, molybdenum, tungsten or rhenium. The reactivity of the metal matrix with the uranium carbide at 1700°C decreased in the following order: niobium, molybdenum, tungsten and rhenium. Thus a reference emitter material containing 80 v/o UC - 20 v/o Re was selected for use in the noble gas plasma diode.

A photograph of a completed emitter is shown in Figure 1. The emitter disk, containing a UC-Re core, was clad with niobium. A one mil tungsten foil diffusion barrier was placed between the core and cladding in order to prevent the diffusion of carbon from the uranium carbide particles into the niobium. If the carbon was allowed to diffuse from the core to the cladding the uranium carbide could eventually be reduced to metallic uranium which would be a liquid at the operating temperature of the emitter (1700°C).

The emitter disk was fabricated by the gas pressure-bonding process that was developed by Battelle Memorial Institute. This pressure-bonding process is a very suitable method for fabricating the clad cermet emitter structure since both bonding and densification can be accomplished in a one-step operation.

The photomicrograph insert in Figure 1 shows the UC-Re structure. The rhenium is shown as the massive white phase while the uranium carbide is shown as the dark phase. The presence of the white acicular phase in the uranium carbide is due to the formation of uranium dicarbide (UC_2) resulting from excess carbon in the emitter. Even though the rhenium does not form a stable carbide, carbon can diffuse through the rhenium quite readily. Thus the tungsten layer between the core and cladding is quite important in order to prevent the decarbonization of the core. Apart from the carbon diffusion, the UC-Re core has been shown to be quite stable at temperatures up to 1700°C.

Reference

1. R. F. Hill, "The Development of Emitter Materials for use in the Noble Gas Plasma Diode" presented at Symposium on Thermionic Power Conversion, at Colorado Springs, Colorado, May, 1962, and to be published in the Journal of Advanced Energy Conversion.

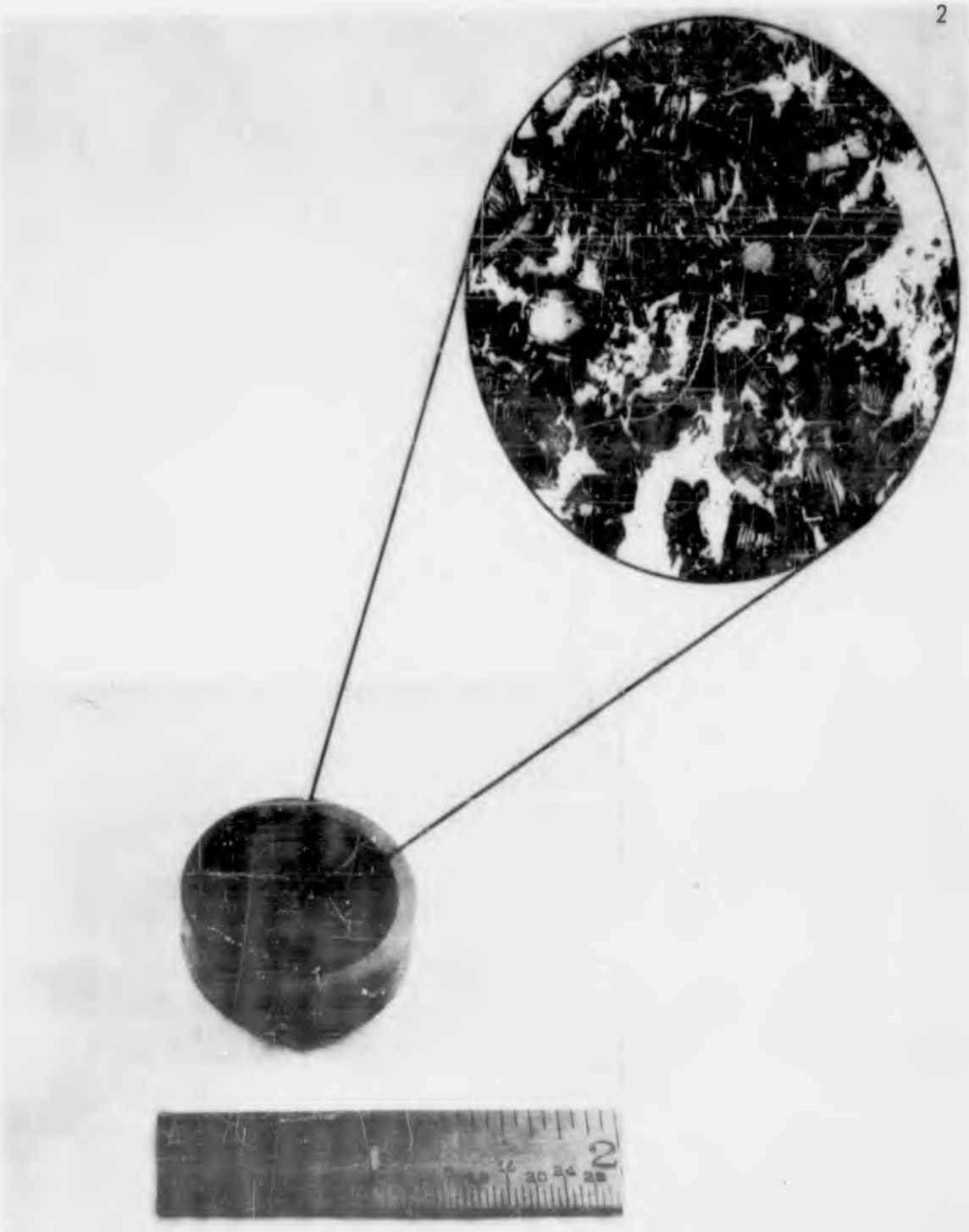

UC - Re EMITTER

Figure 1 -

Photograph showing the microstructure of a uranium carbide-rhenium emitter. The rhenium is shown as the massive white phase while the uranium carbide is shown as the dark phase. The presence of the white acicular phase in the uranium carbide is due to the formation of uranium dicarbide (UC_2) resulting from excess carbon in the emitter.

Thermionic Emission of UC-Re - F. E. Gifford

Measurements of the thermionic emission from UC-Re emitters have been conducted under vacuum and field conditions which allow making an estimate of the work function.

UC-Re emitter samples were employed that had a configuration as shown in Figure 2.

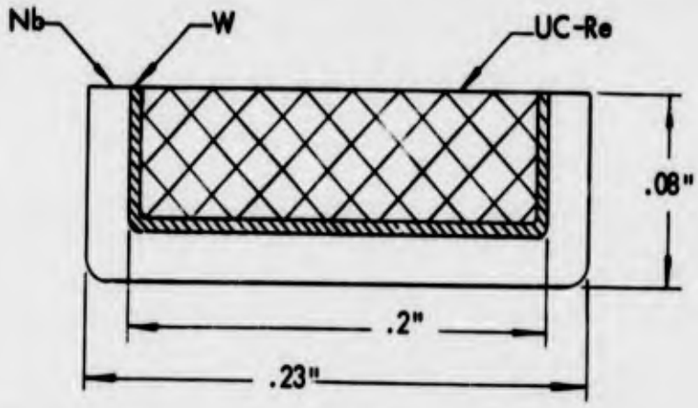

These samples were mounted on a tungsten plate and indirectly heated by electron bombardment from a thoriated tungsten filament. A tungsten collector with a large mass was located approximately 1 mm from the emitter. The large mass offered low thermal inertia to minimize any pressure rise due to electron bombardment heating of the collector.

The emitter, collector and heater were mounted in a vacuum bell jar in which the ultimate pressure realized was 10^{-6} Torr. During the time when the emitter was at high temperature the pressure rose to 5×10^{-4} Torr.

Thermal emissivity measurements were obtained on the UC-Re disc by means of a hohlraum in the emitter body. The hohlraum was made by an electrical discharge machining process and had a dimension of 0.010 in. diameter by 0.060 inch depth approximately. Figure 3 shows the emissivity values over a temperature range of 1000 to 1750° K. A value of 0.5 appears to be a reasonable number for the emissivity of UC-Re. This emissivity correction was applied to the observations of brightness temperature during the emission measurements on a solid UC-Re disc.

The saturated current density was extrapolated from the Schottky plot using a slope at the highest value of field corresponding to the observed temperature. This method has previously been employed for a UC-Nb emitter.[1] Leakage current from the heater and emitter support was taken into consideration. The saturated current density versus temperature is given in Figure 4 and compared to the data of Haas[2] on UC.

The Richardson plot of this data is given in Figure 5 and the data are best fit for a work function of 2.69 ev and an A value of 2.2 amps cm^{-2} $(°K)^{-2}$.

References

1. R. H. Abrams, Jr. and F. E. Jamerson, J. Appl. Phys. 32, 1783 (1961).
2. G. A. Haas, J. T. Jensen, Jr., J. Appl. Phys. 31, 1231 (1960).

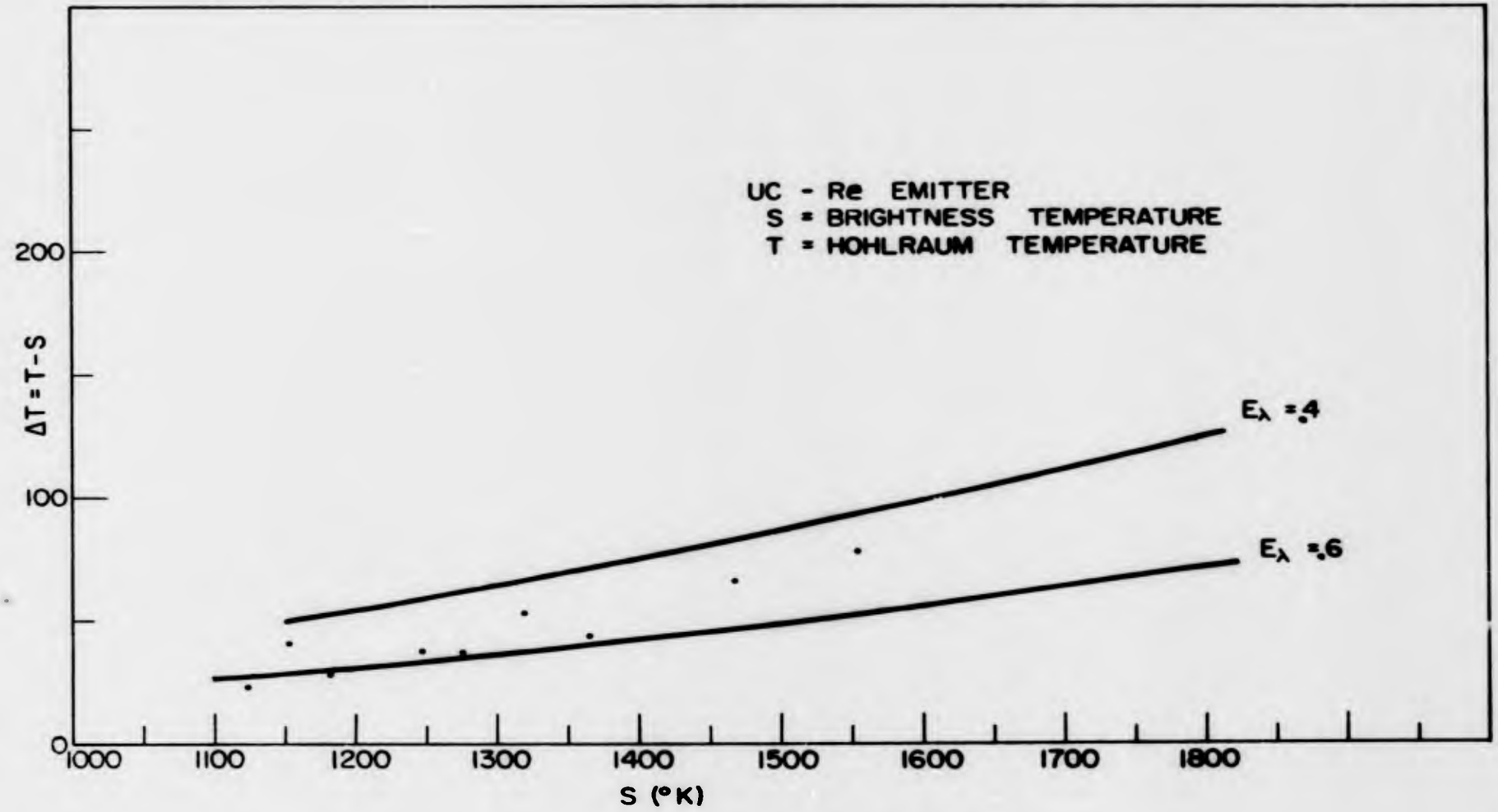

Figure 3 - Emissivity data for UC-Re.

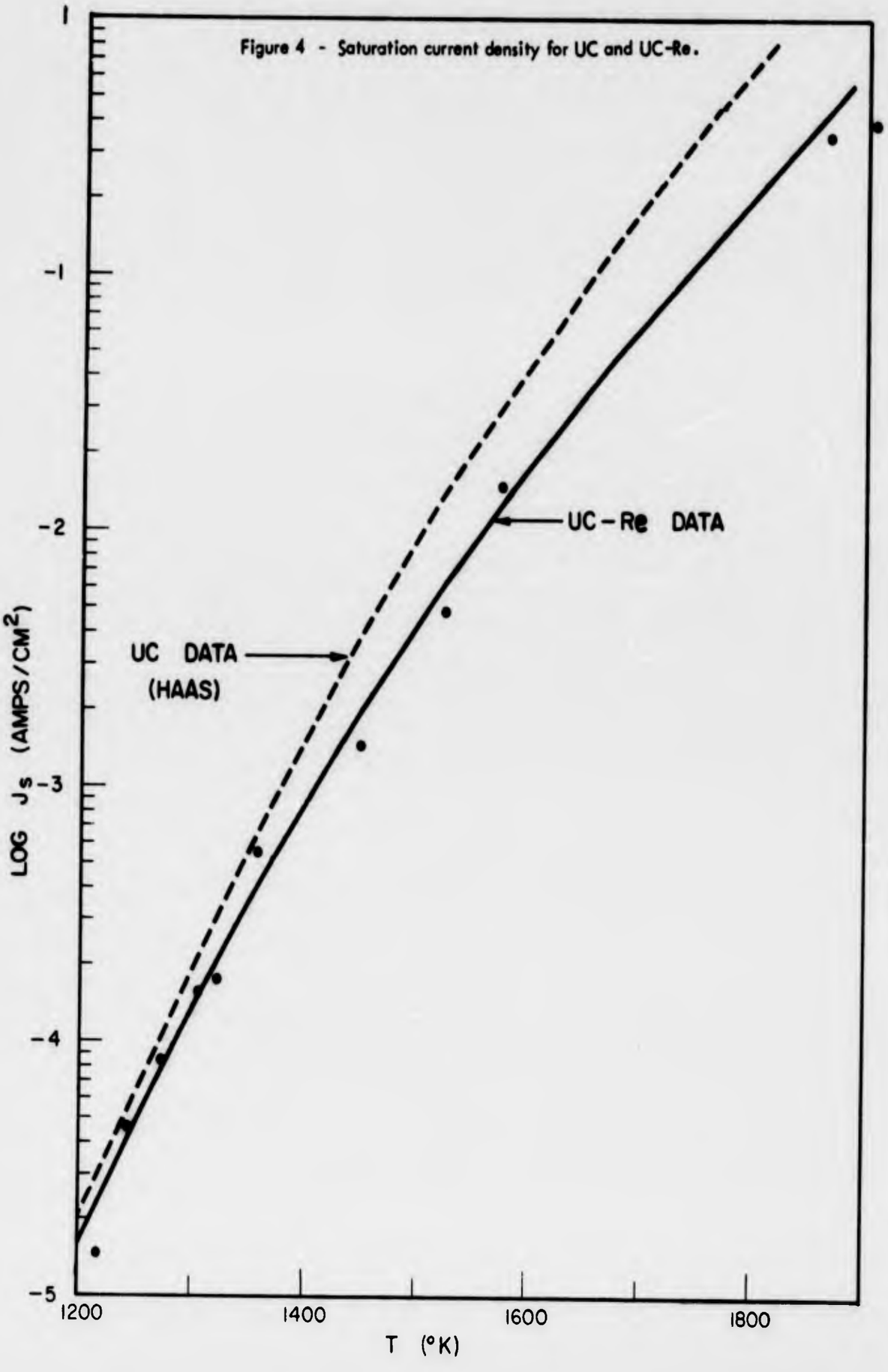

Figure 4 - Saturation current density for UC and UC-Re.

Figure 5 - Richardson plot for UC-Re.

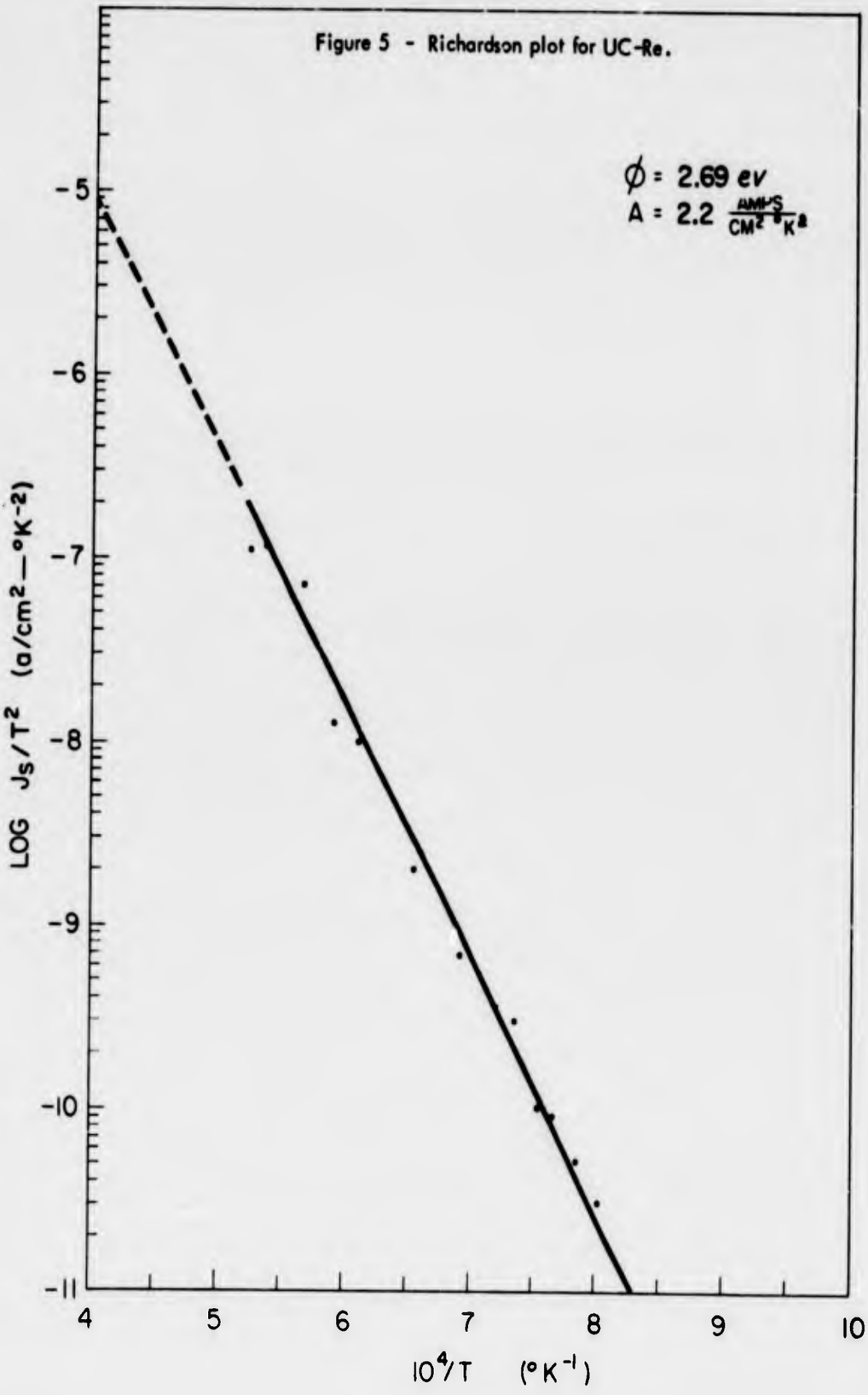

PUBLICATIONS

1. F. E. Jamerson, R. H. Abrams, Jr., C. B. Leffert, R. Silver, "Nuclear Generated Plasmas in Noble Gas Thermionic Converters", to be published in Journal of Advanced Energy Conversion.

2. C. B. Leffert, "A Plasma-Sheath Theory for Noble Gas Thermionic Converters", to be published in Journal of Advanced Energy Conversion.

3. R. F. Hill, "The Development of Emitter Materials for Use in the Noble Gas Plasma Diode", to be published in Journal of Advanced Energy Conversion.

4. R. F. Hill and S. R. Rouze, "Emission Characteristics of a Philips Impregnated Cathode", Journal of Applied Physics, Vol. 33, No. 4, April, 1962.

DISTRIBUTION

	No. Copies
Office of Naval Research Power Branch (Code 429) Department of the Navy Washington 25, D. C.	4
ONR Branch Office Chicago, Illinois Attn. M. A. Chaszeyka	1
U. S. Naval Research Laboratory Technical Information Division Washington 25, D. C.	6
U. S. Naval Research Laboratory Washington 25, D. C. Attn: Code 6430	1
Commanding Officer Office of Naval Research Branch Office Box 39 Navy #100 Fleet Post Office New York, New York	2
Office of Technical Services Department of Commerce Washington 25, D. C.	1
Armed Services Technical Information Agency Arlington Hall Station Arlington 12, Virginia	10
National Aeronautics and Space Administration 1520 H Street, N. W. Washington 25, D. C. Attn: James J. Lynch	1
National Aeronautics and Space Administration Lewis Research Center 2100 Brookpark Road Cleveland 35, Ohio	
Attn: Frank Rom	1
Roland Breitwieser	1
Bernard Lubarsky	1
Chief of Naval Operations (OP-07G) Department of the Navy Washington 25, D. C.	1

	No. Copies
Commandant, U. S. Marine Corps Code CSY-3 Headquarters, Marine Corps Washington 25, D. C.	1
Chief, Bureau of Ships Department of the Navy Washington 25, D. C.	
Attn: Code 342B	1
Code 1500, LCDR J. H. Weber	1
Code 350, LCDR F. Anders	1
Division of Reactor Development U. S. Atomic Energy Commission Washington 25, D. C.	
Attn: Auxiliary Power Branch	1
Direct Conversion Branch	1
Army Reaction and Water Systems Branch	1
Aeronautical Systems Division ASRMFP-2 Wright Patterson Air Force Base, Ohio	1
Air Force Cambridge Research Center (CRZAP) L. G. Hanscom Field Bedford, Massachusetts	1
Power Information Center University of Pennsylvania Moore School Building 200 South 33rd Street Philadelphia 4, Pennsylvania	1
Director of Special Projects (SP-001) Department of the Navy Washington 25, D. C.	10
Los Alamos Scientific Laboratory P. O. Box 1663 Los Alamos, New Mexico	
Attn: Dr. George M. Grover	1
Argonne National Laboratory 9700 South Cass Avenue Argonne, Illinois	
Att: Aaron J. Ulrich	1

	No. Copies
Director, Advanced Research Projects Agency The Pentagon Washington 25, D. C. Attn: Dr. John Huth	2
U. S. Army Signal R & D Laboratory Fort Monmouth, New Jersey Attn: Emil Kittil	1
Mr. A. F. Underwood Manager, General Motors Research Laboratories 12 Mile and Mound Roads Warren, Michigan	1
Atomics International P. O. Box 309 Canoga Park, California Attn: Dr. R. C. Allen	1
General Atomic P. O. Box 608 San Diego 12, California Attn: Dr. R. W. Pidd	1
Republic Aviation Framingdale Long Island, New York Attn: A. Schock	1
Allied Research Associates, Inc. 43 Leon Street Boston 15, Massachusetts Attn: Dr. P. Goodman	1
Ford Instrument Company 3110 Thomas Avenue Long Island City, New York Attn: T. Jarvis	1
Armour Research Foundation 10 West 35th Street Chicago 16, Illinois Attn: Dr. D. W. Levinson	1
Jet Propulsion Laboratory California Institute of Technology 4800 Oak Grove Drive Pasadena, California	1

	No. Copies
RCA Laboratories David Sarnoff Research Center Princeton, New Jersey Attn: Dr. P. Rappaport	1
The Martin Corporation Baltimore 3, Maryland Attn: Dr. M. Talaat	1
Thermo Electron Engineering Corporation 85 First Avenue Waltham 54, Massachusetts Attn: Dr. George Hatsopoulos	1
Hughes Research Laboratories 3011 Malibu Canyon Road Malibu, California Attn: Dr. R. C. Knechtli	1
Thomson Ramo Wooldridge, Inc. 7209 Platt Avenue Cleveland 4, Ohio Attn: Dr. Wm. J. Leovic	1
General Electric Research Laboratory Schenectady, New York Attn: Dr. V. C. Wilson	1
Westinghouse Electric Company Research Laboratories Beulak Road, Churchilboro Pittsburgh, Pennsylvania Attn: Dr. Max Gavbuny	1
Massachusetts Institute of Technology 77 Massachusetts Avenue Cambridge, Massachusetts Attn: D. White	1
The Marquardt Corporation ASTRO Division 16555 Saticoy Street Van Nuys, California Attn: A. N. Thomas	1
Texas Instruments, Inc. P. O. Box 5474 Dallas 22, Texas Attn: Dr. R. A. Chapman	1

	No. Copies
University of Denver Colorado Seminary Denver Research Institute Denver 10, Colorado Attn: Dr. Charles B. Magee	1
Radio Corporation of America Electron Tube Division Lancaster, Pennsylvania Attn: F. G. Block	1
Electro-Optical Systems Inc. 125 North Kinedo Avenue Pasadena, California Attn: A. Jensen	1
General Electric Company P. O. Box 846 Atomic Product Division Vallecitos Laboratory Pleasenton, California Attn: Robert Scott	1
General Electric Company Power Tube Division 1 River Road Schenectady 5, New York Attn: Mr. Wm. Miller	1

Abstract. Contract Nonr-3109(00)

General Motors Research Laboratories - "INVESTIGATIONS ON THE DIRECT CONVERSION OF NUCLEAR FISSION ENERGY TO ELECTRICAL ENERGY IN A PLASMA DIODE", F. E. Jamerson (Editor), Robert J. Donohue, Fay E. Gifford, Robert F. Hill, Charles B. Leffert, and Richard F. Majkowski. (121 pages).

Results of experimental and theoretical investigations are presented on the use of a nuclear generated plasma in a noble gas plasma diode thermionic converter. Related programs of emitter materials development and plasma measurements are described. These are presented in the following individual reports.

A. Inpile Ion Chamber Experiment - Theory and Tube Design.
B. Pulsed Noble Gas Plasma Diode Experiments.
C. Electron Mobility in Gases.
D. Spectroscopic Measurements in a Cesium Low Voltage Arc Converter.
E. Uranium Carbide-Rhenium Cermet Emitter.

Abstract. Contract Nonr-3109(00)

General Motors Research Laboratories - "INVESTIGATIONS ON THE DIRECT CONVERSION OF NUCLEAR FISSION ENERGY TO ELECTRICAL ENERGY IN A PLASMA DIODE", F. E. Jamerson (Editor), Robert J. Donohue, Fay E. Gifford, Robert F. Hill, Charles B. Leffert, and Richard F. Majkowski. (121 pages).

Results of experimental and theoretical investigations are presented on the use of a nuclear generated plasma in a noble gas plasma diode thermionic converter. Related programs of emitter materials development and plasma measurements are described. These are presented in the following individual reports.

A. Inpile Ion Chamber Experiment - Theory and Tube Design.
B. Pulsed Noble Gas Plasma Diode Experiments.
C. Electron Mobility in Gases.
D. Spectroscopic Measurements in a Cesium Low Voltage Arc Converter.
E. Uranium Carbide-Rhenium Cermet Emitter.

Abstract. Contract Nonr-3109(00)

General Motors Research Laboratories - "INVESTIGATIONS ON THE DIRECT CONVERSION OF NUCLEAR FISSION ENERGY TO ELECTRICAL ENERGY IN A PLASMA DIODE", F. E. Jamerson (Editor), Robert J. Donohue, Fay E. Gifford, Robert F. Hill, Charles B. Leffert, and Richard F. Majkowski. (121 pages).

Results of experimental and theoretical investigations are presented on the use of a nuclear generated plasma in a noble gas plasma diode thermionic converter. Related programs of emitter materials development and plasma measurements are described. These are presented in the following individual reports.

A. Inpile Ion Chamber Experiment - Theory and Tube Design.
B. Pulsed Noble Gas Plasma Diode Experiments.
C. Electron Mobility in Gases.
D. Spectroscopic Measurements in a Cesium Low Voltage Arc Converter.
E. Uranium Carbide-Rhenium Cermet Emitter.

Abstract. Contract Nonr-3109(00)

General Motors Research Laboratories - "INVESTIGATIONS ON THE DIRECT CONVERSION OF NUCLEAR FISSION ENERGY TO ELECTRICAL ENERGY IN A PLASMA DIODE", F. E. Jamerson (Editor), Robert J. Donohue, Fay E. Gifford, Robert F. Hill, Charles B. Leffert, and Richard F. Majkowski. (121 pages).

Results of experimental and theoretical investigations are presented on the use of a nuclear generated plasma in a noble gas plasma diode thermionic converter. Related programs of emitter materials development and plasma measurements are described. These are presented in the following individual reports.

A. Inpile Ion Chamber Experiment - Theory and Tube Design.
B. Pulsed Noble Gas Plasma Diode Experiments.
C. Electron Mobility in Gases.
D. Spectroscopic Measurements in a Cesium Low Voltage Arc Converter.
E. Uranium Carbide-Rhenium Cermet Emitter.

UNCLASSIFIED